


12-2018

# Epidermal growth factor receptor (EGFR) inhibition by polychlorinated biphenyls contributes to non-alcoholic fatty liver disease (NAFLD).

Josiah Hardesty  
*University of Louisville*

Follow this and additional works at: <https://ir.library.louisville.edu/etd>

 Part of the [Biochemical Phenomena, Metabolism, and Nutrition Commons](#), [Chemical and Pharmacologic Phenomena Commons](#), [Medical Biochemistry Commons](#), [Medical Toxicology Commons](#), and the [Nutritional and Metabolic Diseases Commons](#)

---

## Recommended Citation

Hardesty, Josiah, "Epidermal growth factor receptor (EGFR) inhibition by polychlorinated biphenyls contributes to non-alcoholic fatty liver disease (NAFLD)." (2018). *Electronic Theses and Dissertations*. Paper 3135.  
<https://doi.org/10.18297/etd/3135>

This Doctoral Dissertation is brought to you for free and open access by ThinkIR: The University of Louisville's Institutional Repository. It has been accepted for inclusion in Electronic Theses and Dissertations by an authorized administrator of ThinkIR: The University of Louisville's Institutional Repository. This title appears here courtesy of the author, who has retained all other copyrights. For more information, please contact [thinkir@louisville.edu](mailto:thinkir@louisville.edu).

EPIDERMAL GROWTH FACTOR RECEPTOR (EGFR) INHIBITION BY POLYCHLORINATED  
BIPHENYLS CONTRIBUTES TO NON-ALCOHOLIC FATTY LIVER DISEASE (NAFLD)

By

Josiah Hardesty  
B.S. University of Kentucky 2013  
M.S. University of Louisville 2016  
Ph.D. University of Louisville 2018

A Dissertation  
Submitted to the Faculty of the  
School of Medicine at the University of Louisville  
In Partial Fulfillment of the Requirements for the Degree of

Doctor of Philosophy in  
Biochemistry and Molecular Genetics

Department of Biochemistry and Molecular Genetics  
University of Louisville  
Louisville, Kentucky

December 2018



EPIDERMAL GROWTH FACTOR RECEPTOR (EGFR) INHIBITION BY POLYCHLORINATED  
BIPHENYLS CONTRIBUTES TO NON-ALCOHOLIC FATTY LIVER DISEASE (NAFLD)

By

Josiah Hardesty  
B.S. University of Kentucky 2013  
M.S. University of Louisville 2016  
Ph.D. University of Louisville 2018

A Dissertation Approved on

August 20<sup>th</sup> 2018

by the Following Dissertation Committee:

---

Matthew Cave, M.D.

---

Russell Prough, Ph.D.

---

Barbara Clark, Ph.D.

---

Carolyn Klinge, Ph.D.

---

Brian Ceresa, Ph.D.

## DEDICATION

This dissertation is dedicated to my wife Brittany Hardesty and my two sons  
Jalen Green-Hardesty, and Graeson Hardesty.

## ACKNOWLEDGEMENTS

I would like to thank my mentors Drs. Cave and Prough and my committee members Drs. Clark, Klinge, and Ceresa for their help and guidance in the start of my scientific journey. I would also like to thank all the lab members and collaborators that have contributed to the research presented in this dissertation. I would also like to thank my family for their sacrifices and support that allowed me the opportunity to pursue and obtain my Ph.D.

## ABSTRACT

### EPIDERMAL GROWTH FACTOR RECEPTOR (EGFR) INHIBITION BY POLYCHLORINATED BIPHENYLS CONTRIBUTES TO NON-ALCOHOLIC FATTY LIVER DISEASE (NAFLD)

Josiah E. Hardesty

August 20<sup>th</sup> 2018

This dissertation describes how poly-chlorinated biphenyls (PCBs) exacerbate the pathogenesis of non-alcoholic fatty liver disease (NAFLD). While PCBs were banned in 1979, they still persist in contaminated biota, including food, and are detected in human plasma and adipose. The body burden of PCBs is associated with elevation of liver enzymes and necrosis markers in humans, characteristic of NAFLD. PCB exposure in high-fat diet fed mice leads to steatohepatitis that recapitulate the findings seen in exposed humans. The global estimate of people diagnosed with NAFLD is up to 1 in 4 people, unrelated to dietary or genetic factors. The hepatic mechanisms most commonly associated with PCB exposures are xenobiotic nuclear receptor activation, followed by changes in xenobiotic metabolism. Other processes must be involved since highly chlorinated PCB congeners are not metabolized and are long-lived in the body.

A novel PCB target was elucidated and characterized, being the epidermal growth factor receptor (EGFR). New effectors downstream of EGFR, including NRF2 and HNF4 $\alpha$ , were identified and verified. The basic biology of EGFR signaling in the liver was observed, including regulation of glutathione synthesis, gluconeogenesis, and lipid metabolism. A novel therapy for NAFLD was elucidated in this dissertation, as well, which is therapeutically promising, since no available therapies for NAFLD exist.

I hypothesize that PCBs act through inhibition of EGFR action promoting NAFLD. The first finding in this work was that PCBs inhibit EGFR signaling in vivo and in vitro. Next PCBs and other chlorinated compounds were found to prevent EGF-EGFR endocytosis in cell-based assays. The third finding demonstrates that in PCB-mediated steatohepatitis, EGFR-NRF2 and EGFR-HNF4 $\alpha$  signaling pathways are downregulated, while fibrogenic pathways are upregulated. PCBs were shown to severely disrupt multiple signaling pathways in PCB-mediated liver disease including a loss of 25% of phospho-peptides involved in cellular regulation.

Epidermal growth factor (EGF) administration prevented PCB-mediated steatohepatitis and bridging fibrosis, two of the crucial stages of NAFLD. This dissertation is unique in that a mechanism of action for PCBs through EGFR inhibition was characterized biochemically, followed by evaluation of an effective therapeutic intervention that may impact human health interventions for NAFLD.



## TABLE OF CONTENTS

	PAGE
Acknowledgements.....	iv
Abstract.....	v
List of Tables.....	ix
List of Figures.....	x
Chapter 1: Introduction.....	1
Chapter 2: Polychlorinated biphenyls Disrupt Hepatic Epidermal Growth Factor Receptor Signaling.....	11
Introduction.....	11
Materials and Methods.....	14
Results.....	18
Discussion.....	33
Chapter 3: Epidermal Growth Factor Receptor Signaling Disruption by Endocrine and Metabolic Disrupting Chemicals.....	38
Introduction.....	38
Materials and Methods.....	40
Results.....	44
Discussion.....	58
Chapter 4: Proteomic Analysis Reveals Mechanisms by which Polychlorinated Biphenyls Sensitize the Liver to Dietary Steatohepatitis.....	62
Introduction.....	62
Materials and Methods.....	63
Results.....	67
Discussion.....	84

Chapter 5: PCBs are Signaling Disrupting Chemicals which Promote Secondary Necrosis in TASH.....	88
Introduction.....	88
Materials and Methods.....	89
Results.....	92
Discussion.....	104
Chapter 6: Therapeutic Efficacy of EGF Administration in PCB-mediated Steatohepatitis and Fibrosis.....	107
Introduction.....	107
Materials and Methods.....	107
Results.....	111
Discussion.....	120
Chapter7: Conclusion.....	123
References.....	125
Appendix I.....	139
Appendix II.....	144
Curriculum Vitae.....	146

## LIST OF TABLES

	PAGE
Table 1. <i>Trans</i> -Nonachlor, PCB-126, and PCB-153 Means Levels for NHANES 99-00, 01-02, and 03-04 (CDC, 2005).....	51
Table 2. Full list of pathways and processes significantly increased or decreased by a HFD.....	72
Table 3. Full list of pathways and processes significantly increased or decreased by a Aroclor exposure.....	73
Table 4. Full list of pathways and processes significantly increased or decreased by interaction.....	74
Table 5. Transcription factor analysis results.....	76
Table 6. Transcription factor analysis of HFD vs HFD+ (steatosis vs. steatohepatitis) peptide data.....	77
Table 7. MetaCore pathway, processes, and pathology analysis of peptides affected by a HFD, Aroclor, and their interaction.....	95

## LIST OF FIGURES

FIGURE	PAGE
1. The NAFLD Spectrum.....	2
2. Chemical structure of PCB-126 (dioxin like PCB) and PCB-180 (non-dioxin like PCB).....	5
3. Model of EGFR inhibition leading to indirect CAR activation.....	7
4. EGFR signaling pathway in the liver peaks in the inactive phase.....	9
5. Effects of Aroclor 1260 exposure on a DR4-luciferase reporter gene activity in HepG2 cells transfected with an expression vector for murine CAR.....	19
6. Decreased EGFR phosphorylation at multiple sites <i>in vitro</i> with Aroclor 1260 exposure.....	21
7. Effects of Aroclor 1260 exposure on mouse hepatic EGFR phosphorylation.....	23
8. Effects of Aroclor 1260 exposure to mice for 12 weeks on hepatic Akt and mTOR phosphorylation.....	25
9. Effects of PCB exposure and high fat-diet for 12 weeks on mouse hepatic protein expression of downstream targets of EGFR and ERK activity.....	27
10. Decreased EGFR phosphorylation at multiple tyrosines in HepG2 cells with Aroclor 1260 exposure.....	29
11. PCB congeners 3, 6, 8, 9, 126, 151, 153, 170, and 180 elicit the greatest decrease in EGFR phosphorylation in HepG2 cells.....	31
12. Proposed PCB-mediated EGFR hypo-phosphorylation Model.....	32
13. Selected compounds do not appear to be direct agonists of CAR, but <i>trans</i> -nonachlor, chlordane and atrazine inhibit EGF stimulated Y1173 phosphorylation of EGFR.....	46
14. Chlordane, <i>trans</i> -nonachlor, PCB-126, PCB-153, and atrazine prevent EGF endocytosis in A-431 cells.....	49

15. Chlordane, <i>trans</i> -nonachlor, PCB-126, PCB-153, and atrazine prevent EGF-mediated phosphorylation at the IC <sub>50</sub> value from the EGF endocytosis assay.....	53
16. <i>Trans</i> -nonachlor, chlordane PCB-126, and PCB-153, but not atrazine, displace EGF from the EGF ligand binding domain of the EGFR.....	55
17. Predicted binding sites for <i>trans</i> -nonachlor, PCB-126, PCB-153, and atrazine with the EGFR.....	57
18. Liver proteomic analysis identifies proteomic alterations due to HFD, Aroclor 1260, and their interaction in a steatohepatitis mouse model.....	68
19. Linear relationship of peptide expression between biological replicates in LC/MS/MS..	69
20. Pathway analysis of proteins altered by either a HFD, Aroclor exposure or their interaction.....	71
21. Aroclor 1260 reduced HNF4 $\alpha$ protein expression and activity, and HNF4 $\alpha$ is a downstream phosphorylation target of the EGFR.....	79
22. Aroclor 1260 reduced NRF2 protein/mRNA expression and glutathione levels, and NRF2 is an EGF-sensitive target.....	81
23. Aroclor exposure activates HSCs through hepatocyte-derived TGF- $\beta$ .....	83
24. Phosphoproteomic analysis identifies phosphorylated substrates altered by Aroclor 1260 exposure, a HFD, and their interaction.....	93
25. PhosphoScanSite 3 analysis of the significant phosphopeptide demonstrates that many kinases are downregulated with Aroclor exposure and the Aroclor and HFD interaction.	97
26. PP2A and PTP1b were not significantly upregulated with Aroclor exposure suggesting the cumulative loss phosphoprotein signaling is due to loss of phosphorylation.....	99
27. Aroclor exposure diminishes CK2 activity and reduces expression of the $\alpha$ and $\beta$ subunits but increases the expression of the $\alpha'$ subunit.....	101
28. Aroclor exposure promotes secondary necrosis in TASH.....	103
29. EGF rescues hepatic EGFR signaling in PCB-exposed mice and downregulates CAR activation .....	112

30. EGF promotes hepatic gluconeogenesis and reduces insulin sensitivity but does not affect glucose uptake.....	114
31. EGF promotes lipid redistribution to adipose tissue in Aroclor exposed mice.....	116
32. EGF reduces PCB-induced steatohepatitis and bridging fibrosis.....	118
33. EGF promotes hepatic lipid packaging and export while preventing PCB-mediated steatohepatitis and fibrosis.....	119
34. PCBs act through EGFR inhibition in the pathogenesis of NAFLD.....	125
35. Lindane, Dieldrin, DDT, DDE, Alachlor are not potent EGFR antagonists.....	141
36. Pre-clearing compounds in 10% serum media does not alter EGF endocytosis in A-431 cells.....	142
37. Cytotoxicity of <i>trans</i> -nonachlor, chlordane, atrazine, PCB-126, PCB-153, dieldrin, alachlor, lindane, DDE, and DDT in HepG2 and A-431 cells.....	143

## CHAPTER 1

### INTRODUCTION

NAFLD is a spectrum of diseases ranging from simple steatosis (lipid accumulation) which can progress to steatohepatitis (chronic inflammation). This can progress further to liver fibrosis and ultimately liver failure or hepatocarcinoma. Currently 25% of the global population fall somewhere on the spectrum of NAFLD (Figure 1). While obesity is a global epidemic it does not fully explain the 25% prevalence of NAFLD worldwide (1). Obesity would primarily explain hepatic steatosis, but many patients progress to later stages of NAFLD without a direct explanation. Steatosis is the result of an imbalance of lipid uptake vs. oxidation resulting in hepatic lipid droplet formation and accumulation. Steatohepatitis is a state of chronic inflammation in the liver where immune cells are responsive but cannot efficiently clear the abundant dead hepatocytes leading to secondary necrosis (2). Chronic steatohepatitis can activate hepatic stellate cells (HSCs) which deposit collagen leading to scarring or cirrhosis. Late stage NAFLD can end in liver failure or hepatocellular carcinoma (HCC). Non-alcoholic steatohepatitis (NASH) is a subset of NAFLD that is not due to alcohol (alcoholic steatohepatitis/ASH) or chemicals exposure (toxicant associated steatohepatitis/TASH). NASH has been shown to be exacerbated by loss of gut barrier function leading to endotoxemia, and dietary stress such as a high fat diet (HFD). No matter the subset of NAFLD a majority of animal models are built upon a two-hit hypothesis for NAFLD. Where one stressor alone will not promote NAFLD but requires two such as alcohol and lipopolysaccharide (LPS). For TASH models a HFD in combination with the chemical exposure is required to elicit progression from steatosis to steatohepatitis (3). The HFD alone has been shown to promote insulin resistance and promote steatosis. Chemicals such as PCBs can in turn promote hepatic necrosis in combination with a HFD and has been coined TASH (4, 5).

## Non-alcoholic fatty liver disease (NAFLD) Spectrum

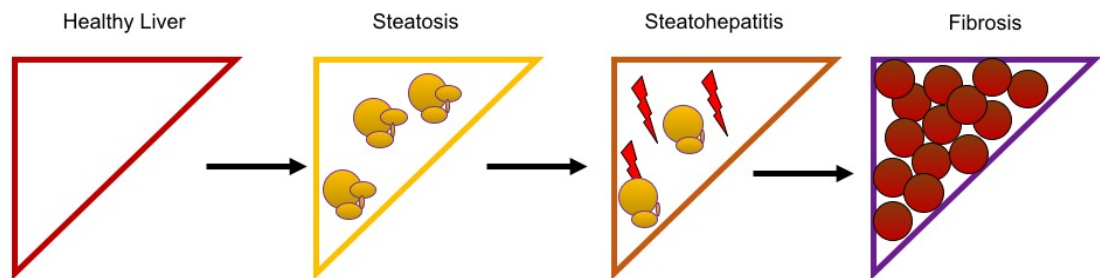


**Figure 1. The NAFLD spectrum**

Figure 1 illustrates the stages of NAFLD ranging from left to right simple steatosis, NASH, cirrhosis, and HCC. Figure 1B demonstrates the histological changes at each stage of NAFLD from top to bottom steatosis, NASH, and cirrhosis. This figure is adapted from Cohen *et al* 2011(6).



PCBs were mass produced as highly chlorinated mixtures under the brand name Aroclor from 1930 to 1977 by Monsanto in the US. PCBs, like most chemicals, were developed solely for their chemical properties. PCBs have a high thermostability and were used to insulate transformers and electrical equipment as they maintain their structure and chemical properties under high electrical current. The chlorine carbon bonds give PCBs a high thermal stability and in turn make these chemicals hydrophobic. PCBs were ultimately banned from production in the US in the 1970s due to their carcinogenic effects in rodents (7). Although they have been banned from production for many years they still persist in the environment and are detected in humans due to propagation by consumption of contaminated biota (8). There are 209 theoretical PCB congeners that are chlorinated biphenyls with varying amounts of chlorination based on the congener (9). The chlorine positions alter the structure of the PCB leading to two major classes of PCBs. PCBs fit into either non-dioxin like PCBs which are noncoplanar or the dioxin-like PCBs which are coplanar (Figure 2). There have been many adverse effects associated with PCB exposures over the years, but metabolic diseases are a growing concern. Environmental chemical exposures are often overlooked and unfortunately the last factor considered as contributing to a patient's disease phenotype. This is somewhat disturbing since 100% of National Health and Nutrition Examination Survey (NHANES) participants that had polychlorinated biphenyls (PCBs) measured in serum had detectable levels (10). In the NHANES population increasing body burdens of PCBs are associated with elevated ALTs which is a proxy marker for NAFLD (10). It is important to note that these participants are randomly selected and are not a highly exposed cohort such as the Anniston, AL cohort who reside where PCBs were manufactured in the US. Other human exposures to PCBs outside of the US have occurred as well including the Yusho (Japan 1968) and Yu-Cheng (Taiwan 1979) PCB poisonings where rice oil was contaminated with PCBs. Follow-up studies of these cohorts have demonstrated increased mortality to liver disease and increased incidence of diabetes relative to non-exposed populations (11, 12). Within the Anniston cohort there is a strong association with elevated PCB body burden and elevated liver necrosis biomarker cytokeratin-18 (CK-18), suggestive of steatohepatitis (13). PCB exposure within these two genetically distinct populations have been associated with NAFLD (10, 12, 14). While there is strong evidence

demonstrating that PCB exposures in humans can promote NAFLD the mechanisms remain ill-defined.



**Figure 2. Chemical structure of PCB-126 (dioxin like PCB) and PCB-180 (non-dioxin like PCB):** Figure 2 illustrates the chemical structure of PCB-126 (left) and PCB-180 (right). PCB-126 is co-planar and considered a dioxin-like PCB whereas PCB-180 is non-co-planar and considered a non-dioxin like PCB. Both PCBs have a carbon biphenyl ring structure (gray) with varying numbers of chlorine (green) and in various positions. The biphenyl rings for PCB-126 are in the same plane (coplanar) but PCB-153 have the biphenyl rings in different planes (non-coplanar) due to the positioning of the chlorine atoms.

Primary studies of PCBs effects on gene transcription demonstrated two key responses that can be explained by the congener type. Dioxin-like (DL) congeners elicit an aryl hydrocarbon receptor (AhR) mediated response while non-dioxin like (NDL) PCBs give rise to a constitutive androstane receptor (CAR) or pregnane x receptor (PXR) mediated responses (9). Both of these responses are a part of xenobiotic metabolism and thus activation of these pathways does not explain how they would cause progressive hepatic necrosis and NAFLD. In fact, activation of xenobiotic metabolism would be considered positive for clearance of PCBs but unfortunately there are no endogenous enzymes to metabolize certain PCBs and some highly chlorinated congeners have 18 year half-lives (15). In fact, direct activation of CAR can ameliorate diet induced NAFLD (16, 17). PCBs increase hepatic CAR target gene expression in rodents robustly but even in the absence of CAR animals still develop steatohepatitis upon a HFD and PCB exposure (18). This would suggest that PCBs do more than just activate xenobiotic receptors such as CAR. Previous studies with Phenobarbital demonstrate that CAR can be indirectly activated by epidermal growth factor receptor inhibition (19) (Figure 3). Phenobarbital and NDL PCBs have been shown to elicit similar hepatic responses and could both be acting through EGFR inhibition (20-22).

**Model for indirect CAR activation through EGFR inhibition by phenobarbital**

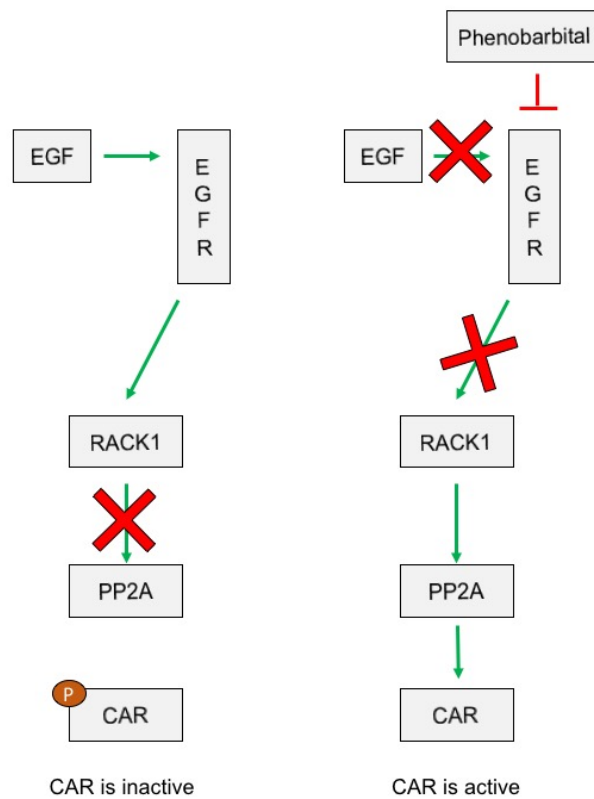


**Figure 3. Model of EGFR inhibition leading to indirect CAR activation:** Figure 3 illustrates a mechanism for phenobarbital and potentially PCBs to indirectly activate CAR through inhibition of EGFR leading to loss of protein phosphorylation and CAR activation. This figure is adapted from Negishi 2017(23).

EGFR is a receptor tyrosine kinase that is highly expressed in the liver. Upon ligand binding the EGFR will dimerize and autophosphorylate leading to downstream activation or inactivation of kinases, enzymes, and transcription factors through protein phosphorylation (24, 25). Upon autophosphorylation the active EGFR complex will undergo endocytosis and eventually the signal will be attenuated, and the receptor recycled. Some downstream kinases of EGFR include PI3K, ERK, AKT, and mTOR which are implicated in regulation metabolism through enzyme phosphorylation (24). EGFR has been shown to have many roles in development and tissue homeostasis such as in skin and gastrointestinal tract tissue homeostasis (26). EGFR signaling maintains tissues with high cellular turnover through growth and proliferation mediated pathways. EGFR is most heavily implicated in cancer where EGFR mutations can promote more aggressive cancers (27). Many EGFR inhibitors have been manufactured and used as effective cancer therapeutics. There are many studies demonstrating EGFR's role in pathological disease states like cancer but very few that study the physiological role of EGFR in adult metabolism. Recently EGFR has been implicated in adult liver homeostasis (28). While EGFR is highly expressed in the liver and 60% of labeled EGF traffics to the liver little is known about its role in liver function and homeostasis (29). Recently EGFR signaling has been shown to peak in the inactive phase in murine liver suggesting it may be integral for fasting responses in the liver (28) (Figure 4). Some data demonstrate that attenuation of EGFR signaling can promote NAFLD (30, 31). Research in alcoholic liver disease models suggest that EGF administration can prevent inflammation (32). Previous work has demonstrated that placenta EGFR phosphorylation is downregulated in pregnant mothers exposed to PCBs relative to non-exposed mothers following the Yu-Cheng poisoning (33). While this is mechanistic evidence for PCB-mediated inhibition of placenta EGFR and not hepatic EGFR follow-up studies of this cohort demonstrate increased mortality due to liver disease (11, 12).

**Hepatic EGFR Signaling peaks in Inactive Phase while INSR Signaling Peaks in active Phase**

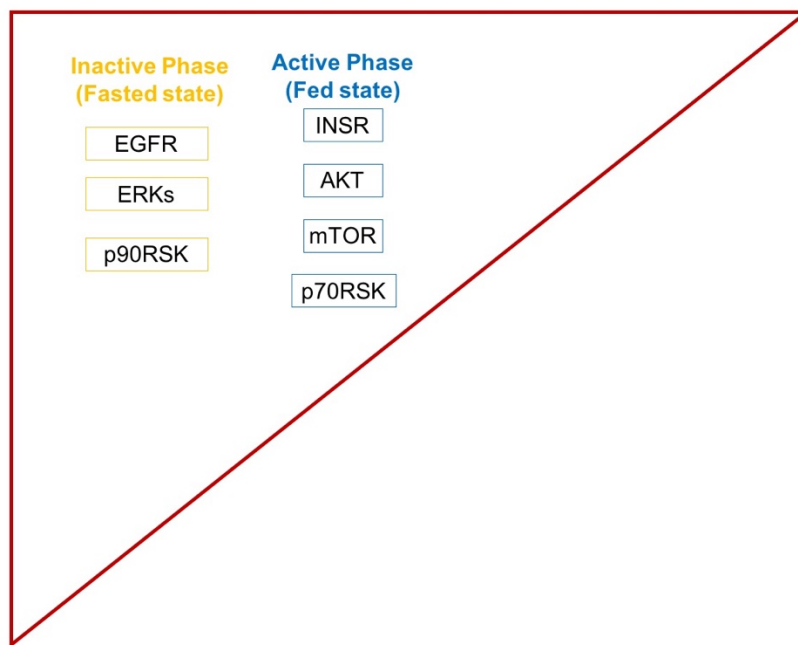


**Figure 4. EGFR signaling pathway in the liver peaks in the inactive phase:** Figure 4 illustrates the circadian phosphoproteome in murine liver. EGFR regulated phospho-sites peak during the inactive phase (yellow) whereas insulin receptor (IR) regulated sites peak during the active phase (blue). This data suggests that EGFR signaling may be critical for many hepatic functions during the inactive phase in organisms. This figure was adapted from the original figure that is attributed to Robles *et al* 2017(28).

These human and animal findings demonstrate the necessity to determine how environmental PCB exposures progress NAFLD in combination with hypercaloric intake. Since PCB exposures are extensive and can progress steatosis to steatohepatitis in mice it may be a critical factor in the rising rates of NAFLD worldwide. While the association between PCB exposures, diet, and NAFLD progression are heavily intertwined no real mechanism has been elucidated to explain the disease phenotype. With the following taken into consideration; 1) strong association with NAFLD and PCB exposure, 2) CAR-null mice still develop TASH with PCB exposure, and 3) PCBs prevent placenta EGFR phosphorylation I aimed to investigate 1) whether PCBs act through EGFR inhibition to promote NAFLD, 2) characterize the PCB disrupted proteome and phosphoproteome, and 3) determine if epidermal growth factor (EGF) administration ameliorates PCB-mediated steatohepatitis.



CHAPTER 2  
POLYCHLORINATED BIPHENYLS DISRUPT HEPATIC EPIDERMAL GROWTH FACTOR  
RECEPTOR SIGNALING

**INTRODUCTION**

Polychlorinated biphenyls (PCBs) are lipid-soluble, persistent organic pollutants that preferentially accumulate in visceral adipose tissue and liver (34). Previously, PCBs were used in industrial applications such as heat exchangers and electrical capacitors. PCBs were manufactured as mixtures based on chlorine content, rather than as individual congeners. The PCB mixture, Aroclor 1260 (Monsanto Company, US), contains 60% chlorine by weight, and its composition is similar to human adipose bioaccumulation patterns (35, 36). Daily human PCB consumption is estimated to be 30 ng/day (37), but is likely to be greater in people eating highly contaminated foods, such as fish from polluted waterways. Higher chlorinated PCB congeners such as PCB-180 have a half-life of 11.5 years and thus could chronically alter signaling pathways involved in metabolic disorders (15). As a result, 100% of US adult participants in the National Health and Nutrition Examination Survey (NHANES) had detectable levels of PCBs in serum (10). In humans, PCBs have been associated with metabolic diseases including nonalcoholic fatty liver disease (NAFLD) (10, 38-40), obesity (41), hypertension (42), diabetes (11, 43, 44), and dyslipidemia (45). Animal models document the development of NAFLD and its more severe form, nonalcoholic steatohepatitis (NASH), following PCB treatment (3). In fact, PCBs were among the most potent environmental chemicals associated with NAFLD in rodents (46). Determining mechanisms by

which PCBs may contribute to NAFLD pathogenesis is the overall objective of this dissertation. Historically, PCB congeners have been classified by structure-activity relationships based on their observed effects on hepatic xenobiotic metabolism (9). “Dioxin-like” PCBs increase ethoxyresorufin O-deethylase activity (47), while “phenobarbital-like” PCBs increase pentoxyresorufin O-dealkylase activity. PCBs were subsequently noted to activate xenobiotic receptors including the aryl hydrocarbon receptor (AhR), the pregnane X receptor (PXR), and the constitutive androstane receptor (CAR) leading to the induction of specific cytochrome P450 enzymes including CYP1A, CYP3A, and CYP2B, respectively (3, 48). While PCB-nuclear receptor interactions influenced intermediary metabolism in an animal model of NASH (18), exposure to PCBs alone was insufficient to cause NASH, but rather served as a ‘second hit’ in the transition of diet-induced steatosis to steatohepatitis (3). Aroclor 1260 treated *Car*<sup>-/-</sup> mice fed a high fat diet (HFD) had increased activity, decreased food consumption, and increased insulin sensitivity compared to wild type mice also fed HFD (18). However, NASH pathology did not improve concordantly with these favorable metabolic changes in *Car*<sup>-/-</sup>. This suggests that while PCB-*Car* interactions are important in metabolic syndrome, other mechanisms must also be important for PCB-related NAFLD.

CAR may be activated either directly or indirectly by xenobiotics. The mechanism of CAR activation may be important, because indirect CAR activation could be associated with additional ‘off target’ effects influencing NAFLD. I observed that PCBs directly activated human CAR (hCAR) splice variants 2-3 but not hCAR1 (36). Although mouse CAR (mCAR) is homologous to hCAR1, mice treated with PCBs displayed increased *Cyp2b10* expression (3). The reasons for the varied responses observed by these homologous proteins is most likely due to splice variants 2 and 3 having slightly larger ligand binding pockets allowing for additional space for ligand binding. Phenobarbital is a prototypical *Cyp2b10* inducer, and the indirect mechanism by which phenobarbital activates CAR has recently been discovered (19). Phenobarbital prevented epidermal growth factor (EGF) binding to its receptor (EGFR) inhibiting the phosphorylation cascade leading to an increased abundance of dephosphorylated, active CAR.

EGFR is a transmembrane receptor tyrosine kinase that is ligand-activated by the epidermal growth factor (EGF) and other similar growth factors. Upon ligand binding, EGFR dimerizes with itself or other family members. This induces activation of the receptor's intrinsic kinase activity, resulting in transphosphorylation of tyrosine residues on its receptor pair. These newly formed phosphotyrosine residues serve as docking sites for downstream signaling proteins (effectors) that act to modulate metabolic gene expression. Normal EGFR signaling is essential in development and metabolism (49). In addition to CAR, downstream targets include the phosphoinositol 3-kinase/serine/threonine kinase 1 or PKB/mechanistic target of rapamycin (PI3K/Akt/mTOR) pathway, signal transducer and activator of transcription 3 (STAT3), serine and threonine kinase (c-Raf) and extracellular signal-regulated kinase (ERK). Akt and mTOR are effector kinases downstream of EGFR that regulate lipid metabolism, and glycogen synthesis (50, 51). Decreased EGFR signaling has been implicated in metabolic diseases such as type II diabetes (52, 53) and NASH (25, 30-32, 54), both of which have been associated with PCB exposures (3, 10, 12, 14, 18, 55). Thus, I hypothesized that if PCBs antagonized EGFR like phenobarbital, this effect could account for indirect CAR activation and the associated 'off target' effects contributing to PCB-related NASH. Understanding how PCBs disrupt these pathways could provide mechanistic insight into how PCBs mediate metabolic syndrome and liver disease (3, 56, 57). In this dissertation I determine: (i) if PCB-mediated indirect CAR activation in mice is mediated by inhibition of EGFR phosphorylation; (ii) if PCB effects on EGFR phosphorylation in mice are modified by diet; (iii) if PCB-mediated hypophosphorylation of EGFR in mice impact additional downstream phosphoprotein targets (including Akt and mTOR); and (iv) if PCBs also inhibit human EGFR phosphorylation. I conclude from our studies that PCBs decrease phosphorylation of EGFR and its downstream effector kinases.

## MATERIALS AND METHODS

### Chemicals

1,4-Bis(3,5-dichloro-2-pyridyloxy)benzene (TCPOBOP) and androstanol were obtained from Sigma Chemical Co., St. Louis, MO. Aroclor 1260, Aroclor 1254, and PCB congeners, PCB 3, PCB 6, PCB 8, PCB 9, PCB 126, PCB 138, PCB 149, PCB 151, PCB 153, PCB 170, PCB 174, PCB 180, PCB 187, were obtained from AccuStandard, Inc., New Haven, CT. Epidermal growth factor (EGF) and EGFR inhibitor (EI, Cyclopropanecarboxylic acid-(3-(6-(3-trifluoromethyl-phenylamino)-pyrimidin-4-ylamino)-phenyl)-amide) were purchased from Millipore (Norwood, OH). The following antibodies were used for Western blotting proteins from HepG2 and AML-12 cells: EGFR (Santa Cruz, Santa Cruz, CA), P-EGFR Y1173 (abcam, Cambridge, MA), P-EGFR Y845 (abcam, Cambridge, MA), and P-EGFR Y1068, P-EGFR Y845, mouse liver EGFR, mTOR, P-mTOR, AKT, P-AKT, STAT3, cRaf, ERK, P-ERK,  $\beta$ -actin, GAPDH (CST, Danvers, MA).

### Cell culture

Alpha mouse liver 12 (AML-12) cells of male origin obtained from ATCC (Mannassas, VA), were seeded at  $1 \times 10^4$  per well in 12-well plates and grown to confluence for 24 hours in DMEM/F12 (GE Healthcare, Pittsburgh, PA) media supplemented with 10% fetal bovine serum, and 1% antimyotic/antibiotic solution. The cells incubated in a 5% carbon dioxide atmosphere at 95% humidity and 37°C were sub-cultured every 2-3 days. Cells were treated for 30 minutes with either 20 ng/mL of epidermal growth factor (EGF) (Fisher Scientific, Pittsburgh, PA) as a positive control, 20 ng/mL of EGF and 20  $\mu$ g/mL EGFR inhibitor (EI) (CAS 879127-07-8) (Millipore, Norwood, OH) as a negative control, or 20 ng/mL EGF and 20  $\mu$ g/mL Aroclor 1260 (A1260). Aroclor 1260 concentration was used based on previous work demonstrating that *in vitro* concentrations higher than 20  $\mu$ g/ml were cytotoxic (Toxicity threshold =  $26.7 \pm 3.7$   $\mu$ g/mL in HepG2s)(36). The concentration of EGF was optimal to induce EGFR phosphorylation, and EGFR inhibitor was used at its IC<sub>50</sub> concentration for EGFR dephosphorization. The 30-minute treatment was used as that still produced robust EGFR phosphorylation but had no effect on PCB-mediated inhibition of EGFR

phosphorylation. The positive and negative controls were used to establish phosphorylated EGFR's dynamic range. Media was removed by aspiration and the cells were washed with PBS. Cells were lysed in modified radioimmunoprecipitation assay (RIPA) buffer (20 mM Tris, 150 mM NaCl, 1 mM EDTA/EGTA/ $\beta$ -glycerophosphate/ $\text{Na}_3\text{VO}_4$ , and 1% Triton X-100) supplemented with protease and phosphatase inhibitors (Sigma-Aldrich, St. Louis, MO).

The human male hepatoma-derived (HepG2) cell line (male origin) obtained from American Type Culture Collection (ATCC, Manassas, MD) were plated  $3 \times 10^5$  cells per well in 12-well plates and grown to confluence in DMEM High Glucose media (GE Healthcare, Pittsburgh, PA) supplemented with 10% fetal bovine serum (FBS) and 1% antimycotic/antibiotic solution (Mediatech, Manassas, VA). HepG2 cells were treated and collected in a similar manner as the AML-12 cells. The Aroclor 1260 concentration-dependence assay was conducted in AML-12s and HepG2s similarly to aforementioned experiments with varied concentrations of Aroclor 1260 ranging from (0, 0.38, 0.94, 1.88, 5, 10, 15, 20  $\mu\text{g}/\text{mL}$ ) at constant EGF concentration. Aroclor 1254 was used at a concentration of 20  $\mu\text{g}/\text{mL}$  similarly to the Aroclor 1260 experiments in HepG2s. The experiments with individual PCB congeners (PCB 3, PCB 6, PCB 8, PCB 9, PCB 138, PCB 149, PCB 151, PCB 153, PCB 170, PCB 174, PCB 180, and PCB 187) were performed with HepG2 cells at congener concentrations of 10  $\mu\text{M}$ .

### **Preparation of Expression vectors**

A mCAR-active luciferase reporter containing two AGGTCA repeats separated by 4 base pairs was generated as an expression construct for this receptor (36). Murine CAR cDNA was generously provided by T.H Rushmore (Merck, Westpoint, PA). The expression vector used was a modified version of pcDNA3.1 (Thermo Scientific, Waltham, MA) in which the CMV promoter was replaced with a weaker promoter, the minimal promoter from the rat glutathione S-transferase A2 gene (58) which produces lower expression levels of CAR.

### **Transient Transfection Assays**

HepG2 cells were plated in Nunc 24-well plates (Thermo Scientific, Waltham, MA) and transfected at 40–60% confluence. Unless otherwise specified, the transfection mix per well contained 150 ng  $\beta$ -galactosidase expression plasmid pCMV- $\beta$ , (Stratagene, San Diego, CA) as a transfection control, 50 ng receptor expression plasmid, and 150 ng luciferase reporter plasmid. All cells were transfected using lipofectamine reagent (Thermo Scientific, Waltham, MA) according to the manufacturer's instructions and Opti-MEM (Thermo Scientific, Waltham, MA) as the transfecting medium. After a 4-hour incubation, the medium was changed to the growth media, DMEM (Thermo Scientific, Waltham, MA) supplemented with 10% FBS and 1% antimycotic/antibiotic solution and 24 hours after transfection, cells were treated with either Aroclor 1260 (0-20  $\mu$ g/mL), androstanol (10  $\mu$ M) or 1,4-Bis(3,5-dichloro-2-pyridyloxy)benzene (TCPOBOP, 10 $\mu$ M) either alone or in combination. After another 24 hours the cells were harvested using cell lysis buffer (Promega, Fitchburg, WI) and the  $\beta$ -galactosidase activity determined spectrophotometrically on a Biotek Synergy plate reader using chlorophenol red  $\beta$ -D-galactopyranoside as substrate. The luciferase activity was determined using a Berthold (Bad Wildbad, Germany) plate reading luminometer using the luciferase assay kit from Promega, (Fitchburg, WI) according to the manufacturer's instructions. All data are presented as normalized luciferase activity/ $\beta$ -galactoside activity from 4 independent experiments and all comparisons were made to the untreated group.

### **Exposure of mice to Aroclor 1260**

The mouse liver samples used in this study were obtained from archived (-80°C) tissues obtained during a previous study (3). The treatment protocol was approved by the University of Louisville Institutional Animal Care and Use Committee. Male C57Bl/6J mice (8 weeks old; The Jackson Laboratory, Bar Harbor, ME, USA) were divided into 4 study groups (n = 10) based on diet and Aroclor 1260 exposure in this 12-week study utilizing a 2  $\times$  2 design. Mice were fed either a control diet (CD, 10.2% kCal from fat; TD.06416 Harlan Teklad, Indianapolis, IN) or a HFD (42% kCal from fat; TD.88137 Harlan Teklad, Indianapolis, IN). Aroclor 1260 (AccuStandard, CT, USA) was administered in corn oil by oral gavage (vs. corn oil alone) at a dose of 20 mg/kg early in week 1,

at a dose similar to the maximum human PCB exposures seen in the Anniston cohort (10). Mice were housed in a temperature- and light controlled-room (12 h light; 12 h dark) with food and water *ad libitum*. The animals were euthanized at the end of week 12 using ketamine/xylazine, 100/20 mg/kg body weight, i.p., respectively), followed by exsanguination to minimize blood in the liver sample. The mice fed a HFD and treated with Aroclor 1260 developed steatohepatitis as demonstrated by CAE and H&E staining. Aroclor 1260 treatment was associated with induction of *Cyp2b10* consistent with *Car* activation (3).

### **Western Blot Analysis**

Mouse liver samples and cell culture lysates were homogenized in RIPA Buffer (100 mg tissue/0.5 mL RIPA supplemented with protease, and phosphatase inhibitors 1  $\mu$ l/mL, (Sigma-Aldrich, St. Louis, MO). The protein concentration was determined by bicinchoninic acid protein assay (Sigma-Aldrich, St. Louis, MO). Protein (15  $\mu$ g) was separated on 7.5% SDS Gel (BioRad, Hercules, CA), transferred to polyvinylidene difluoride membranes and blocked in Phosphate Buffered Saline (PBS), pH 7.5 containing 1% Tween 20 (PBS-T) and 5% fat free Milk for 1 hour at room temperature. Membranes were incubated at 4° C overnight with primary antibody at 1:1000 dilution in 5% bovine serum albumin in PBS-T, then washed 4 times with PBS-T for 5 minutes followed by incubation with secondary antibody 1:2000 in 5% Milk in PBS-T (Cell Signaling Technology, Danvers, MA). After 4 PBS-T washes the membranes were incubated with ECL (Thermo Scientific, Waltham, MA) and luminescent signals were captured with BioRad Chemidoc Imaging System (Hercules, CA). Western blot protein bands were quantified using BioRad Image Software. For detection of phosphoproteins, the phospho-antibody blots were stripped for 15 minutes (Thermo Scientific, Waltham, MA) then re-probed using primary antibody against total protein overnight in 5% FF Milk in PBS-T. For phospho-Akt detection in mouse liver, duplicate protein samples were analyzed in parallel under identical conditions. One blot was probed for phosphoprotein and the other total protein and then both were re-probed for the loading control  $\beta$ -actin. Then the

quantitation of band density was normalized to  $\beta$ -actin and then to total protein. This strategy was necessary due to the inability to strip the phospho antibodies for Akt.

### **Statistical Analysis**

Western blot densitometry values were statistically analyzed using Graphpad Prism Version 6 for Macintosh (San Diego, CA). The data are expressed as mean  $\pm$  standard error of the mean. All *in vitro* datasets were compared using one-way ANOVA.  $p < 0.05$  was considered statistically significant. *In vivo* data sets were compared using two-way ANOVA and  $p < 0.05$  was considered statistically significant. The concentration dependence curves and  $IC_{50}$  values were generated by fitting data to a 4-parameter logistic equation using SigmaPlot (Systat Software Inc. San Jose, CA).

## **RESULTS**

**Aroclor 1260 did not counter the inhibitory effect of the direct CAR antagonist, androstanol, *in vitro*.** To establish whether PCBs can directly activate mCAR, HepG2 cells transfected with mCAR and a DR4 luciferase reporter gene were incubated with varied concentrations of Aroclor 1260 (0-20  $\mu$ g/mL) and compared to control HepG2 cells treated with direct mCAR agonist, TCPOBOP with or without androstanol exposure, as shown in Figure 5. As anticipated, treatment with 10  $\mu$ M androstanol reduced luciferase activity by 45%. The CAR ligand, TCPOBOP did not significantly increase luciferase expression above control, consistent with the concept that CAR is constitutively active when over-expressed in HepG2 cells. TCPOBOP treatment did, however, completely reverse the inhibitory effect of androstanol in TCPOBOP-treated cells; cells treated with both TCPOBOP and androstanol had the same activity as TCPOBOP-treated cells alone. In contrast, Aroclor 1260-treated cells failed to show reversal of the inhibitory effects of androstanol at any concentration of Aroclor 1260 tested (from 0-20  $\mu$ g/mL). In fact, Aroclor 1260 exposure decreased luciferase activity either itself or in combination with androstanol. Because the negative androstanol effect was observed at even the highest concentrations of Aroclor 1260 exposure, Aroclor 1260 cannot counter androstanol's inhibition of CAR, therefore is unlikely to be a direct murine CAR ligand. Direct binding assays are required to conclude that PCBs cannot directly bind to murine CAR.



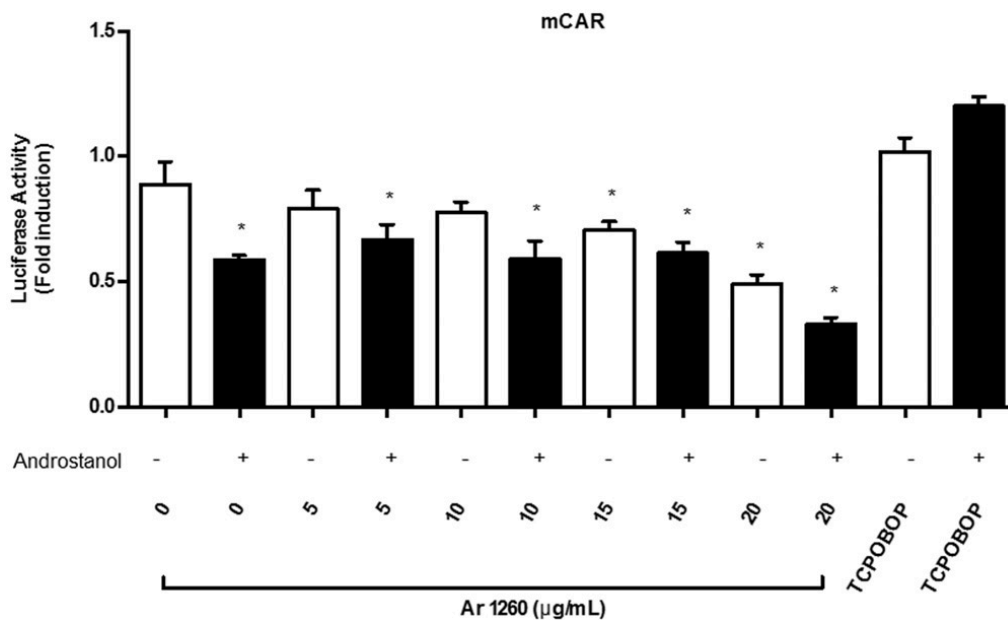


**Figure 5. Effects of Aroclor 1260 exposure on a DR4-luciferase reporter gene activity in HepG2 cells transfected with an expression vector for murine CAR:** Cells were grown and after transfection with expression vector for mCAR and luciferase reporter DR4 luciferase treated with either androstanol, TCPOBP, or increasing amounts of Aroclor 1260 (0-20 µg/mL). The results as presented represent an n = 4 separate experiments. A One-way ANOVA statistical test was utilized to compare experimental data to non-treated cells. \* = p < 0.05

**Aroclor 1260 exposure decreased murine hepatic EGFR phosphorylation *in vitro*.** To determine if Aroclor 1260 exposure could cause an indirect activation of CAR, the phosphorylation status of EGFR was examined in AML-12 cells, a murine cell line that expresses normal functioning EGFR. EGFR has multiple tyrosine residues within the receptor tyrosine kinase (RTK) domain that have specific downstream effects when autophosphorylated upon homo or heterodimerization. EGFR phosphorylation status was measured at Y1173, Y1068, and Y845 due to their specific downstream effects. Y1173 phosphorylation regulates Akt, Y1068 phosphorylation regulates STAT3, cRaf, and ERK, while Y845 phosphorylation has been shown to regulate CAR (19). In AML-12 cells, EGFR phosphorylation at Y1173 was diminished by co-exposure to EGF and Aroclor 1260 for 30 min (Figure 6a), relative to EGF alone. EGFR inhibitor also decreased phosphorylation at Y1173. EGFR phosphorylation at Y1173 was decreased 48% by Aroclor 1260 and EGF co-exposure as compared to EGF alone ( $p = 0.006$ ) (EGF  $0.87 \pm 0.09$  vs. A1260  $0.45 \pm 0.1$ ), while EGFR inhibitor in the presence of EGF caused a 45% reduction in EGFR ( $0.39 \pm 0.03$ ) phosphorylation. Phosphorylation at Y1068 was also decreased with EGF and Aroclor 1260 co-exposure as shown in Figure 6b. In a similar manner, Y1068 EGFR phosphorylation was decreased 45% with Aroclor 1260 and EGF co-exposure for 30 min as compared to EGF alone ( $p = 0.003$ ) (EGF  $0.92 \pm 0.04$  vs. A1260  $0.51 \pm 0.08$  vs. EGFR inhibitor  $0.32 \pm 0.02$ ). Y845 phosphorylation also decreased in AML-12 cells with Aroclor 1260 and EGF co-exposure (Figure 6c). At Y845, EGFR phosphorylation was decreased 43% with Aroclor 1260 and EGF exposure as compared to EGF alone ( $p = 0.005$ ) (EGF  $0.61 \pm 0.05$  vs. A1260  $0.35 \pm 0.03$  vs. EGFR inhibitor  $0.12 \pm 0.02$ ). In the AML-12 cells, the concentration-dependence of the inhibition of EGFR Y1173 phosphorylation by Aroclor 1260 is shown in Figure 6d. The  $IC_{50}$  value obtained was  $1.2 \pm 0.3 \mu\text{g/mL}$  and the Hill slope coefficient is  $1.4 \pm 0.5$  indicating one binding site at EGFR. These findings demonstrate that not only can PCBs diminish EGFR phosphorylation contributing to increased CAR activity (Y845) previously reported, but they may also affect many other downstream targets independent of CAR (Y1068, Y1173) based on the decreased phosphorylation of the EGFR tyrosine residues and the specific downstream targets.

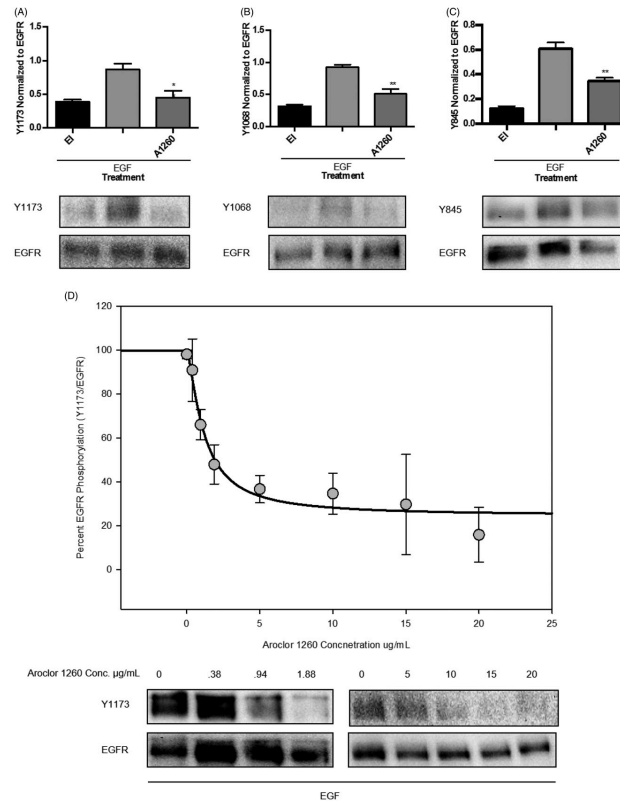


**Figure 6. Decreased EGFR phosphorylation at multiple sites *in vitro* with Aroclor 1260 exposure:** AML-12 cells treated with EGF and either EGFR inhibitor (EI), or Aroclor 1260 (A1260) for 30 minutes were lysed for western blot analysis as described in the Materials and Methods. **A.** EGFR phosphorylation at Y1173 in AML-12 cells was decreased by Aroclor 1260 and EGF co-exposure as compared to EGF alone ( $p = 0.006$ ). **B.** EGFR phosphorylation at Y1068 was decreased with Aroclor 1260 and EGF co-exposure as compared to EGF alone ( $p = 0.003$ ). **C.** EGFR phosphorylation at Y845 was decreased with Aroclor 1260 exposure as compared to EGF alone ( $p = 0.005$ ). **D.** Aroclor 1260 displayed an  $\text{IC}_{50}$  of  $1.18 \pm 0.32 \mu\text{g/mL}$  for EGFR hypophosphorylation in AML-12 cells. The Hill slope coefficient was  $1.39 \pm 0.5$ . A representative blot of the effect was shown in each panel and the graph represents quantitation of normalized protein relative to EGF alone. The results are presented as mean  $\pm$  SEM and represent an  $n = 3$  experiments. A One-way ANOVA statistical test was utilized to compare experimental data to the positive control data (EGF exposure alone),  $p < 0.05$  was considered significant. \*  $p < 0.05$ , \*\*  $p < 0.01$

**Aroclor 1260 exposure diminished murine hepatic EGFR phosphorylation *in vivo*.** To validate the effect of Aroclor 1260 on hepatic EGFR phosphorylation, hepatic EGFR Y1173 phosphorylation was measured in liver tissue from mice exposed to 20 mg/kg Aroclor 1260 in a diet-induced obesity model of our previous study (3). Mice were fed either a control diet which contained 10.2% of its calories as fat or a high fat diet which contained 43% of its calories as fat for 12 weeks and treated with Aroclor 1260 (20 mg/kg by gavage) or vehicle control early in week 1. Mice treated with Aroclor 1260 plus a high fat diet developed NASH (3). As shown in Figure 7, Panel A, Aroclor 1260 exposure resulted in a 43% and 48% decrease in hepatic EGFR phosphorylation at Y1173 in the control diet (CD  $0.67 \pm 0.12$  vs. CD+  $0.39 \pm 0.08$ ) and high-fat diet (HFD  $0.64 \pm 0.12$  vs. HFD+  $0.34 \pm 0.1$ ) groups, respectively ( $p = 0.02$ ). In Figure 7, Panel B, Aroclor 1260 exposure resulted in a 60% and 41% decrease in hepatic EGFR phosphorylation at Y1068 in the control diet (CD  $0.48 \pm 0.14$  vs. CD+  $0.19 \pm 0.05$ ) and high-fat diet (HFD  $0.36 \pm 0.07$  vs. HFD+  $0.21 \pm 0.06$ ) groups respectively ( $p = 0.03$ ). In Figure 7 Panel C, Aroclor 1260 exposure resulted in a 46% and 49% decrease in hepatic EGFR phosphorylation at Y845 in the control diet (CD  $0.64 \pm 0.16$  vs. CD+  $0.35 \pm 0.08$ ) and high-fat diet (HFD  $0.53 \pm 0.16$  vs. HFD+  $0.27 \pm 0.02$ ) groups respectively ( $p = 0.04$ )

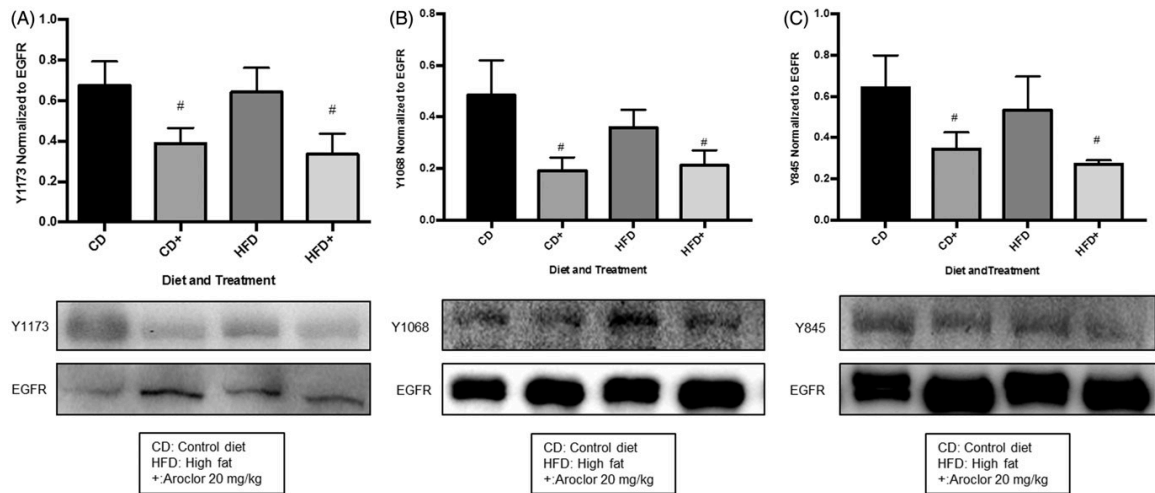


**Figure 7. Effects of Aroclor 1260 exposure on mouse hepatic EGFR phosphorylation:** Mice were treated with Aroclor 1260 and placed on either a control (10.2% fat) or high fat-diet (43% fat) for 12 weeks. Aroclor 1260 (20  $\mu\text{g}/\text{kg}$ ) was administered *per os* early in week 1. Phosphorylation was determined at Y1173, Y1068, and Y845 of EGFR by Western blot analysis as described in Methods and Materials. **3a:** Hepatic Y1173 EGFR phosphorylation was diminished in mice independent of diet by Aroclor 1260 exposure ( $p = 0.015$ ). **3b:** EGFR phosphorylation at Y1068 was diminished in mice independent of diet with Aroclor 1260 exposure ( $p = 0.03$ ). **3c:** EGFR phosphorylation at Y845 was diminished in mice independent of diet with Aroclor 1260 exposure ( $p = 0.04$ ). A Two-way ANOVA statistical test was utilized to determine significant variation due to diet or Aroclor 1260 exposure. # denotes significance due to Aroclor 1260 exposure,  $p < 0.05$ . Displayed is a representative blot of the effect and the graph is a representation of the densitometry results from  $n = 5$  mice in each group.

**Aroclor 1260 exposure decreased phosphorylation of the downstream effectors of hepatic EGFR signaling, Akt and mTOR *in vivo*.** The EGFR-AKT-mTOR pathway regulates hepatic regeneration and energy metabolism. Aroclor 1260 exposure was associated with decreased hepatic Akt and mTOR phosphorylation, independent of diet as shown in Figure 8 Panels A & B. In the control diet (CD  $0.79 \pm 0.11$  vs. CD+  $0.32 \pm 0.11$ ) and high-fat diet (HFD  $0.53 \pm 0.1$  vs. HFD+  $0.23 \pm 0.07$ ) groups, there was a 60% and 57% decrease in Akt phosphorylation due to Aroclor 1260 exposure, respectively ( $p = 0.002$ ). For mTOR phosphorylation, there was a 70% and 25% decrease in the control diet (CD  $0.65 \pm 0.15$  vs. CD+  $0.19 \pm 0.05$ ) and high-fat diet (HFD  $0.6 \pm 0.21$  vs. HFD+  $0.45 \pm 0.11$ ) groups with Aroclor 1260 exposure, respectively ( $p = 0.04$ ).

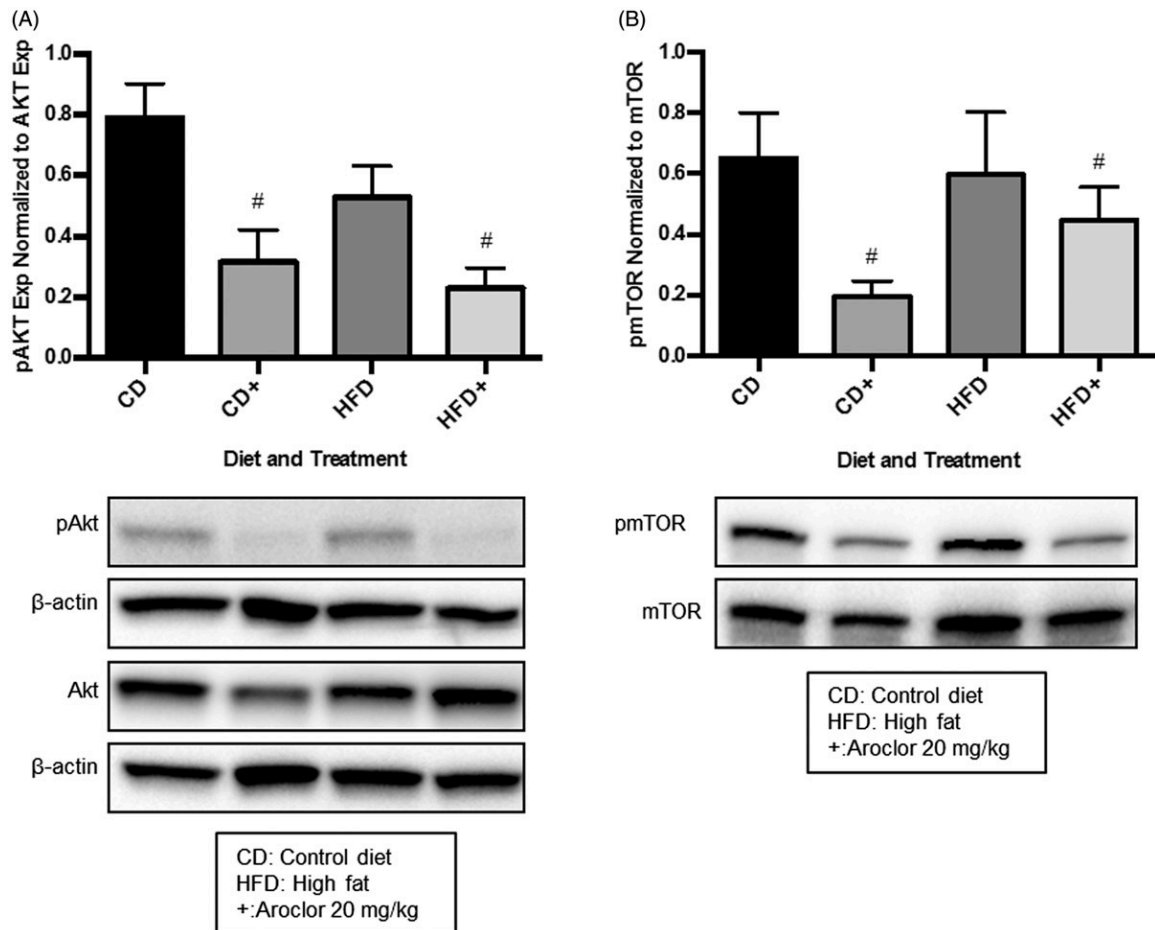


**Figure 8. Effects of Aroclor 1260 exposure to mice for 12 weeks on hepatic Akt and mTOR phosphorylation:** Mice were treated early in week 1 with Aroclor 1260 (20  $\mu\text{g}/\text{kg}$  *per os.*) and western blot analysis of mouse liver conducted as previously described in Figure 7 and Materials and Methods. **A.** Hepatic Akt phosphorylation was diminished in mice with Aroclor 1260 exposure independent of diet ( $p = 0.002$ ). **B.** Hepatic mTOR phosphorylation was decreased in mice with Aroclor 1260 exposure independent of diet ( $p = 0.04$ ). A Two-way ANOVA statistical test was utilized to determine significant variation due to diet or Aroclor 1260 exposure. # denotes significance due to Aroclor 1260 exposure,  $p < 0.05$ . A representative blot of the effect is displayed in each panel and the graph is a representation of the results from  $n = 5$  mice in each group.

**Aroclor 1260 exposure decreased hepatic protein expression of c-Raf and STAT3 while ERK activity was reduced by high-fat diet *in vivo*.** Hepatic protein expression of STAT3 and cRaf were decreased in an Aroclor 1260-dependent manner as shown in Figure 9 Panels A & B, respectively. STAT3 expression was decreased 84% and 66% with Aroclor 1260 exposure in the control diet (CD  $0.57 \pm 0.18$  vs. CD+  $0.09 \pm 0.06$ ) and high-fat diet (HFD  $0.31 \pm 0.06$  vs. HFD+  $0.11 \pm 0.04$ ) groups, respectively ( $p = 0.007$ ). c-Raf expression is decreased 56% and 77% with Aroclor 1260 exposure in the control diet (CD  $0.57 \pm 0.18$  vs. CD+  $0.09 \pm 0.06$ ) and high-fat diet (HFD  $0.31 \pm 0.06$  vs. HFD+  $0.11 \pm 0.04$ ) groups ( $p = 0.0014$ ). Due to unanticipated low expression of STAT3 and cRaf with Aroclor 1260 exposure, it was not possible to evaluate potential differences in the phosphorylation status of these proteins. ERK activity was decreased slightly in a high fat-diet dependent manner as shown in Figure 9c. Mice fed a high fat diet had a 29% decrease in ERK phosphorylation compared to the untreated group (CD  $0.26 \pm 0.08$  vs. HFD  $0.19 \pm 0.05$ ) and a 78% decrease in ERK phosphorylation in the Aroclor 1260 treated group (CD+  $0.61 \pm 0.24$  vs. HFD+  $0.13 \pm 0.02$ ) ( $p = 0.04$ ). While ERK phosphorylation is increased with Aroclor 1260 exposure in the control diet group, the increase did not attain statistical significance ( $p = 0.22$ ). Quantitation for ERK1 phosphorylation is shown but similar findings were demonstrated in the quantitation of ERK2 phosphorylation as well. In summary, hepatic c-Raf and STAT3 protein expression was decreased in a PCB-dependent manner *in vivo*, while ERK activity was decreased in a high fat diet-dependent manner.



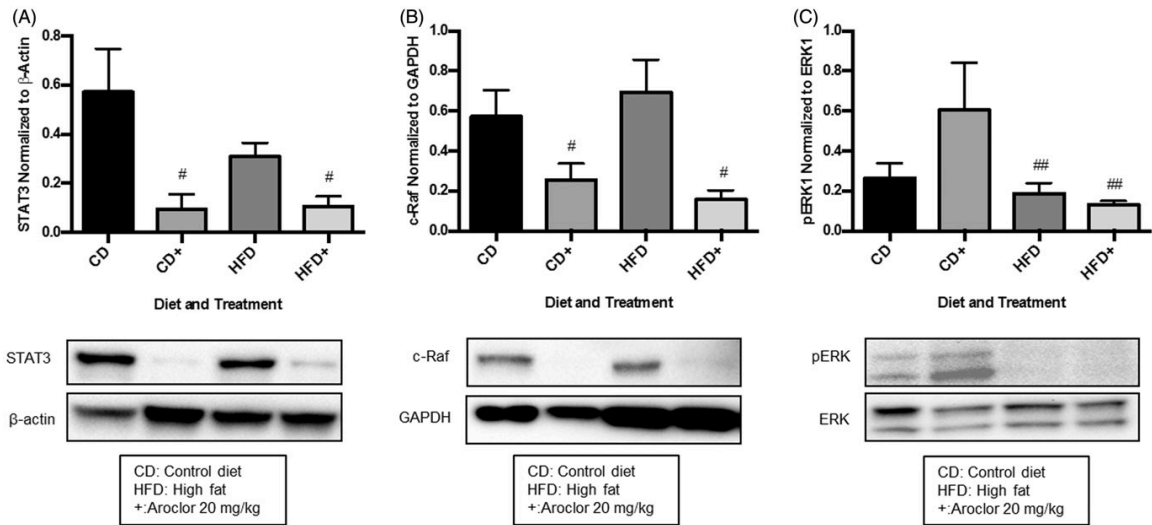


**Figure 9. Effects of PCB exposure and high fat-diet for 12 weeks on mouse hepatic protein expression of downstream targets of EGFR and ERK activity:** Mice were treated for 12 weeks as described above and western blot analysis conducted as previously described in Materials and Methods. **5a:** STAT3 protein expression was decreased in an Aroclor 1260-dependent manner independent of diet ( $p = 0.007$ ). **5b:** cRaf protein expression was decreased with Aroclor 1260 exposure independent of diet ( $p = 0.0014$ ). **5c:** Phosphorylated ERK was decreased in a high fat diet-dependent manner ( $p = 0.04$ ). A Two-way ANOVA statistical test was utilized to determine significant variation due to diet or Aroclor 1260 exposure. **#** = significant effect of Aroclor 1260 exposure  $p < 0.05$ , **##** = significant effect of high fat diet  $p < 0.05$ . A representative blot of the effect is displayed in each panel and the graph is a representation of the results from  $n=5$  mice in each group.

**Aroclor 1260 exposure decreased hepatic EGFR phosphorylation in a human *in vitro* model.**

We previously demonstrated that PCBs directly activated hCAR2 and hCAR3 (36), however, this does not exclude simultaneous indirect CAR activation through inhibition of EGFR signaling. In HepG2 cells, EGFR phosphorylation at Y1173, Y1068, and Y845 all decreased with EGF and Aroclor 1260 co-exposure for 30 min. as shown in Figure 10 Panels A-C. Y1173 phosphorylation was decreased 61% with Aroclor 1260 and EGF co-exposure as compared to EGF alone ( $p = 0.01$ ) (EGF  $0.67 \pm 0.13$  vs. A1260  $0.26 \pm 0.02$ ); EGFR inhibitor also suppressed phosphorylation of EGFR ( $0.12 \pm 0.02$ ). EGFR phosphorylation at Y1068 was decreased 38% with Aroclor 1260 and EGF co-exposure as compared to EGF alone, ( $p = 0.04$ ) (EGF  $0.95 \pm 0.05$  vs. A1260  $0.59 \pm 0.18$  vs. EGFR inhibitor  $0.13 \pm 0.025$ ). EGFR phosphorylation at Y845 was decreased 40% with Aroclor 1260 and EGF co-exposure as compared to EGF alone ( $p = 0.005$ ), (EGF  $0.81 \pm 0.07$  vs. A1260  $0.49 \pm 0.04$  vs. EGFR inhibitor  $0.36 \pm 0.06$ ). The concentration-dependence of the inhibition of EGFR phosphorylation at Y1173 is shown in Figure 10d. The  $IC_{50}$  value was  $4.0 \pm 1.5 \mu\text{g/mL}$  for EGFR hypo-phosphorylation by Aroclor 1260. The Hill slope coefficient is  $1.37 \pm 0.6$ .

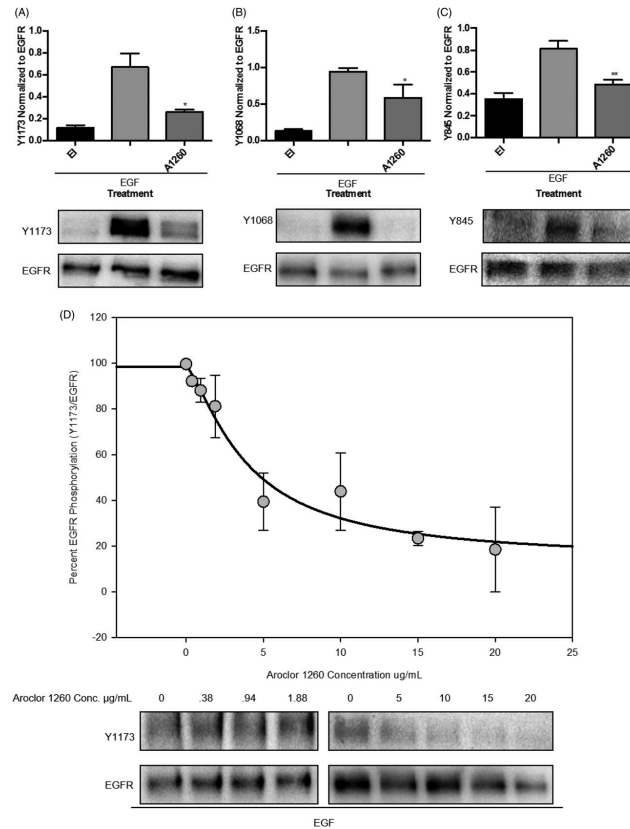


**Figure 10. Decreased EGFR phosphorylation at multiple tyrosines in HepG2 cells with Aroclor 1260 exposure:** HepG2 cells were grown, treated with EGF and either EGFR inhibitor (EI) or Aroclor 1260 (A1260) for 30 min, and lysed for western blot analysis as described in the materials and methods. **A.** EGFR phosphorylation at Y1173 was decreased by Aroclor 1260 and EGF co-exposure as compared to EGF alone ( $p = 0.011$ ). **B** EGFR phosphorylation at Y1068 was decreased by Aroclor 1260 and EGF exposure as compared to EGF alone ( $p = 0.04$ ). **C.** EGFR phosphorylation at Y845 was decreased by Aroclor 1260 and EGF co-exposure as compared to EGF alone ( $p = 0.005$ ). **D.** the  $IC_{50}$  value for EGFR hypo-phosphorylation in HepG2 cells was  $4.0 \pm 1.5 \mu\text{g/mL}$ . The hill slope coefficient was  $1.37 \pm 0.6$  indicative of one binding site. A representative blot of the effect is shown in each panel and the graph represents the mean  $\pm$  SEM for  $n = 3$  experiments for Y068, Y845, and 6 experiments for Y1173. The  $IC_{50}$  value for Aroclor inhibition of phosphorylation was determined from 3 experiments for Y1173. A One-way ANOVA statistical test was used to compare experimental data to the positive control data. \*  $p < 0.05$ , \*\*  $p < 0.01$ .

**Specific PCB congeners decreased hepatic EGFR phosphorylation in a human *in vitro* model.** Different PCB congeners in Aroclor 1260 had varied effects on EGFR phosphorylation in HepG2 cells as shown in (Figure 11 A & B). The “non-dioxin like” PCBs 151, 153, 170, 180, and the “dioxin-like” PCBs 3, 6, 8, 9, 126 reduced EGFR phosphorylation. The PCBs 138, 149, 187, and 174 had no significant effect. With PCB 180 and EGF co-exposure for 30 min, EGFR phosphorylation decreased 54% ( $p = 0.012$ ) in contrast to EGF alone (EGF  $0.95 \pm 0.05$  vs. PCB 180  $0.43 \pm 0.14$  vs. negative EGF control  $0.17 \pm 0.1$ ). PCB 170 exposure decreased EGFR phosphorylation 51% ( $p = 0.027$ ) (PCB 170  $0.46 \pm 0.12$ ). PCB 153 decreased EGFR phosphorylation 49% ( $p = 0.036$ ) (PCB 153  $0.49 \pm 0.14$ ). PCB 151 exposure decreased EGFR phosphorylation 57%, ( $p = 0.016$ ) (PCB 151  $0.41 \pm 0.12$ ). PCB 126 decreased EGFR phosphorylation 68% ( $p = 0.004$ ) (PCB 126  $0.3 \pm 0.01$ ). PCB 3 decreased EGFR phosphorylation 50% ( $p = 0.0015$ ) in contrast to EGF alone (EGF  $0.9 \pm 0.06$  vs. PCB 3  $0.48 \pm 0.07$  vs. negative EGF control  $0.16 \pm 0.07$ ). PCB 6 decreased EGFR phosphorylation 46% ( $p = 0.0032$ ) (PCB 6  $0.49 \pm 0.1$ ). PCB 8 decreased EGFR phosphorylation 46% ( $p = 0.003$ ) (PCB 8  $0.48 \pm 0.07$ ). PCB 9 decreased EGFR phosphorylation 52% ( $p = 0.001$ ) (PCB 9  $0.43 \pm 0.05$ ). These results demonstrate that treatment with individual PCBs found in Aroclor 1260 and some not found in the mixture (PCB 3, 9) all blunt EGFR Y1173 phosphorylation, suggesting that this may be a phenomenon caused by many PCB congeners.

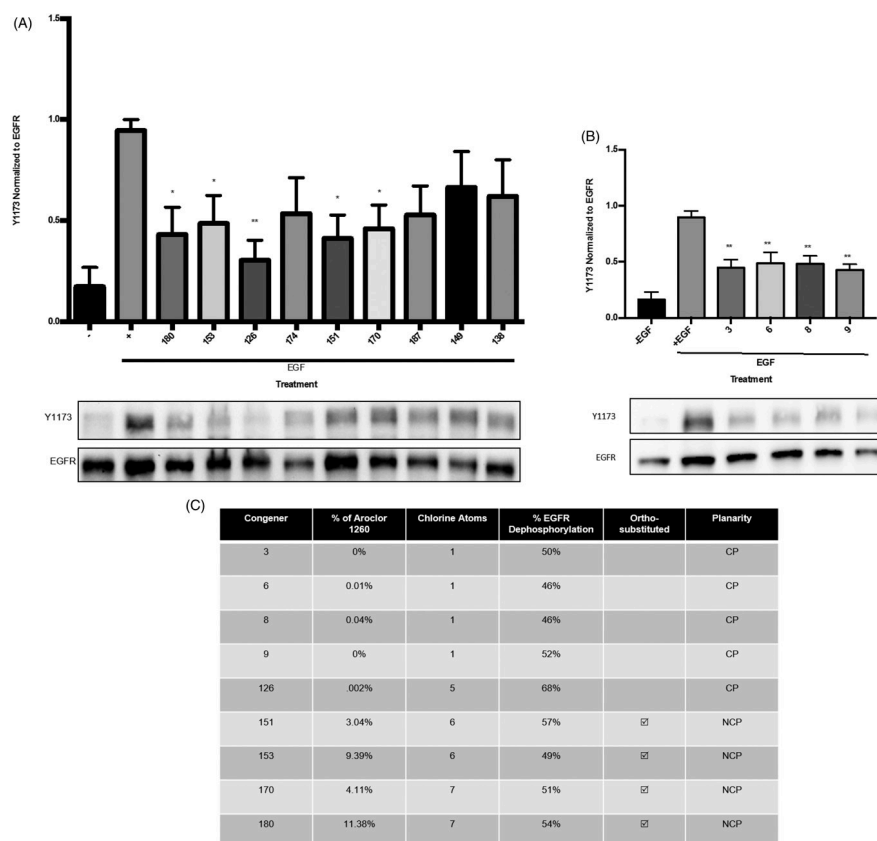


**Figure 11. PCB congeners 3, 6, 8, 9, 126, 151, 153, 170, and 180 elicit the greatest decrease in EGFR phosphorylation in HepG2 cells:** HepG2 cells were treated with EGF and various PCB congeners for 30 min, and subsequently lysed for western blot analysis as described in the materials and methods. **A.** Co-exposure with PCB 180 and EGF decreased EGFR phosphorylation at Y1173 as compared to EGF alone ( $p = 0.02$ ), PCB 170 ( $p = 0.03$ ), PCB 153 ( $p = 0.04$ ), PCB 151 ( $p = 0.016$ ), PCB 126 ( $p = 0.004$ ). A representative blot representation of the results of the effect is shown with the graph. The results are presented as mean  $\pm$  SEM and represent the average intensities from 3 experiments. **B.** Co-exposure with PCB 3 and EGF decreased EGFR phosphorylation at Y1173 as compared to EGF alone ( $p = 0.0015$ ), PCB 6 ( $p = 0.0032$ ), PCB 8 ( $p = 0.003$ ), and PCB 9 ( $p = 0.001$ ). **C.** Table comparing PCB congeners characteristics and EGFR hypo-phosphorylation percentage as compared to EGF alone control. CP denotes co-planar; NCP; non-co-planar. A One-way ANOVA statistical test was utilized to compare experimental data to the positive control data \*  $p < 0.05$ , \*\*  $p < 0.01$ .

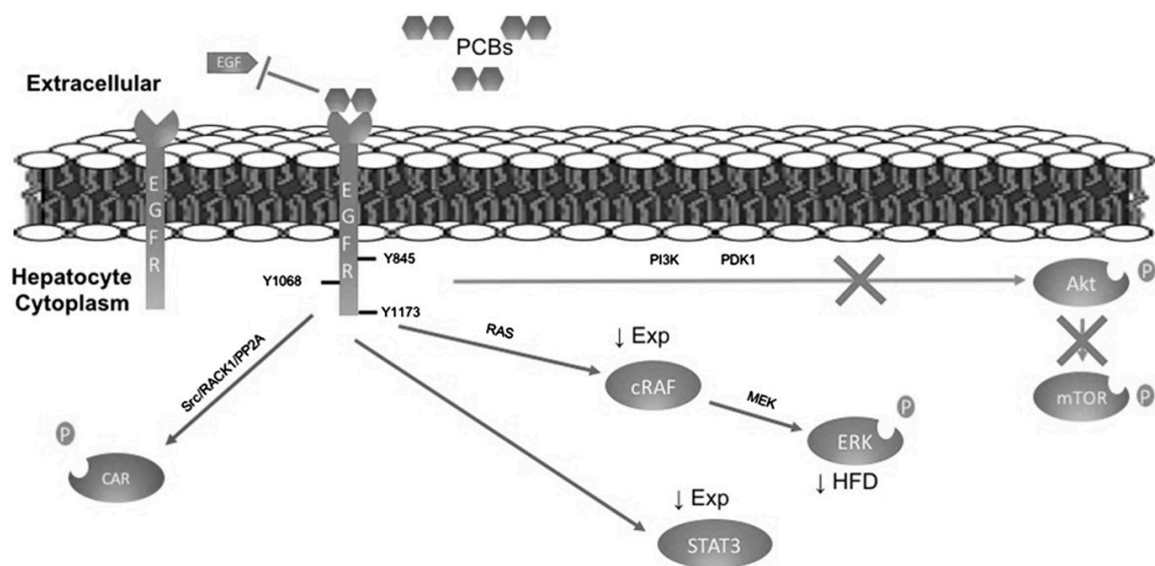


**Figure 12. Proposed PCB-mediated EGFR hypo-phosphorylation Model:** Figure 12 represents the hypothesis that PCBs bind to EGFR preventing EGF binding, thereby preventing phosphorylation. Decreased EGF binding to EGFR leads to decreased Akt and mTOR phosphorylation downstream of EGFR. STAT3, cRaf, and ERK are downstream targets of EGFR. Chronic hypo-phosphorylation of STAT3 and cRaf leads to diminished expression either through transcription regulation or protein ubiquitination. ERK activity was decreased on a high fat diet. Phenobarbital was recently found to activate CAR through EGFR-RACK1 and PP2A (19) and Aroclor 1260 acts in a similar manner leading to increased xenobiotic metabolism. HFD denotes high fat diet; Ind denotes independent.

## DISCUSSION

In this study, Aroclor 1260 exposure did not counter androstanol's inhibitory effect on activation of mCAR in transient transfection assays. Unlike humans, mice do not express multiple splice variants of CAR but rather produce a single transcript (59). Humans express at least three splice variants, and we have previously shown that only some of these splice variants (CAR2 and CAR3) were directly activated by PCB congeners in cell-based assays (36). Murine CAR is homologous to human CAR1, which apparently is not directly activated by PCBs in cell-based transactivation assays (36). Thus, PCB-induced mCAR activation must occur solely by indirect mechanisms. Furthermore, the concept that PCBs act as indirect CAR activators would explain how PCBs elicit a CAR activation response *in vivo* but cannot lessen androstanol's inhibitory effect *in vitro*. This may explain why PCBs worsened NAFLD in mice (18), while the direct CAR activator, TCPOBOP, improved NAFLD in a diet-induced obesity co-exposure animal model (60).

To study the effects of PCBs on EGFR phosphorylation, I modeled our experimental design on Negishi's approach to investigate mechanisms of phenobarbital-induced indirect CAR activation (19). In that study, EGFR phosphorylation was maximal 30 minutes after EGF treatment *in vitro*, and phenobarbital inhibited EGF binding leading to downstream CAR activation. Likewise, I determined the effects of PCBs by adding EGF and either EGFR inhibitor or PCB co-treatments. EGFR phosphorylation was determined 30 minutes post-exposure in mouse and human hepatocyte *in vitro* models as I found this time was optimum to induce robust EGFR phosphorylation similarly to Negishi's findings. Aroclor 1260 and specific PCBs including the classically described 'phenobarbital-like' congener, PCB 153, reduced EGFR phosphorylation just like phenobarbital (19). The 30-minute time course and the Hill slopes for the concentration dependence curves were consistent with PCBs being simple EGFR antagonists, again similar to phenobarbital (19). It is important to note that human PCB poisonings from the Yucheng incident were previously linked to decreased placental EGF-stimulated EGFR phosphorylation and low birth weights associated with exposures to PCBs 153 and 170 (33). Preliminary radiolabeled EGF binding kinetic studies indicated possible competition for a low affinity EGF binding site in PCB-

exposed Yucheng vs. unexposed placentas (33). Also, within the Yucheng cohort there is a substantial increase in the mortality due to chronic liver disease and diabetes in both the 13 and 30 year follow up (12, 14). These proof of concept data document the potential human relevance of our findings.

The IC<sub>50</sub> for PCB-mediated EGFR Y1173 hypophosphorylation occurred at 1.2±0.3 µg/ml in the murine AML-12 cell line and 3.9±1.9 µg/mL in the human derived HepG2 cell line. These PCB concentrations were similar to those that directly activated hCAR2 and hCAR3 as determined by a luciferase reporter construct in transient transfection assays (36). These exposures were also similar to the hepatic PCB levels achieved when rodents were exposed to PCB 153 at an environmentally relevant cumulative dose of 20 mg/kg (3.7 µg/g) (61). However, because PCBs are lipophilic, they may concentrate in a cultured cell monolayer leading to significantly higher cellular PCB concentrations than in the surrounding media. Because AML-12 cells were 3.25-fold more sensitive to EGFR inhibition by PCBs than HepG2 cells, it is also possible that PCBs are stronger indirect CAR activators in mice than in humans. In the 12-week mouse study, Aroclor 1260 (20 mg/kg) robustly induced *Cyp2b10* in mice fed control diet (1000-fold) but was a much weaker inducer of *Cyp2b10* in mice fed a high fat diet (4-fold) (3). However, basal expression of *Cyp2b10* was increased in livers of mice fed high fat diet. Our results show that the decrease in EGFR phosphorylation associated with Aroclor 1260 treatment was not diet-dependent, and other factors must regulate the basal and inducible CAR expression in the mouse liver. However, the *in vivo* EGFR phosphorylation results are consistent with the *in vitro* findings. While PCBs appear to simultaneously activate hCAR by both direct and indirect mechanisms; PCBs activate mCAR only indirectly. To fully characterize the observed EGFR inhibition, ligand-binding studies with PCB congeners and the extracellular domain of EGFR should be performed in the future.

In cell culture experiments, reduction of EGFR phosphorylation occurred with Aroclor 1260, the dioxin-like congener, PCB 126, and the non-dioxin-like PCB congeners 151, 153, 170 and 180. While all the PCB congeners tested diminished EGFR phosphorylation, the most significant were among the higher chlorinated, non-coplanar congeners tested. The congener specific effect on



EGFR phosphorylation is most likely due to the differences in binding affinity between these congeners to EGFR which will be evaluated in future studies. PCBs have similar structures to phenobarbital which may explain their similar modes of action through EGFR. While Aroclor 1260 also reduced EGFR phosphorylation *in vivo*, it did not increase expression of *Cyp1a2* (3), suggesting that AhR was not activated at the level of Aroclor exposure in this model. While the related persistent organic pollutant, 2,3,7,8-tetrachlorodibenzodioxin (TCDD), reduced EGFR phosphorylation in an AhR-dependent manner (62), this process required 12-14 hours to reach maximal effect *in vitro*. In contrast, our cell culture experiments employed a shorter 30-minute study, making a receptor-dependent transcriptional response unlikely. These, and other data, (19, 33) suggest that AhR activation is not required to reduce EGFR phosphorylation. However, this does not exclude the possibility that AhR-dependent pathways could also exist for PCBs, as they do for TCDD. In fact, among tested PCB congeners, the strongest observed effect occurred for PCB 126, a potent AhR activator. Previously PCB 104 was shown to activate EGFR demonstrating that there are varied effects on EGFR based on the congener used (63). Also PCB 104 is not present in Aroclor 1260 and was not used due to only being detected in the serum of 1 of 26 industrial workers (64).

Loss of EGFR activity has been implicated in both the progression of liver disease and diabetes (25, 52). 39.6% of chemotherapy patients on gefitinib, a small molecule EGFR inhibitor, developed abnormal liver function (65). In humans and mice loss of EGFR function has been implicated in the development of steatosis (30, 54). EGFR is hepatoprotective against chemical-induced liver injury and EGF supplementation attenuated alcohol-induced liver disease (31, 32). Loss of EGFR function has also been implicated in diabetes as it diminishes insulin production, islet cell mass, and proliferation (52, 53). Together these studies and our findings suggest that future studies should be performed to elucidate the potential role of PCB-induced EGFR inhibition in NAFLD and diabetes. In addition to EGFR, activity of downstream targets including the PI3K/AKT/mTOR pathway were diminished as well. Decreased PI3K/AKT/mTOR signaling was also associated with type-II diabetes (66) and increased gluconeogenesis, a common feature in NASH. Our results show that PCB exposure decreased Akt and mTOR phosphorylation which is

consistent with the observation that EGFR is directly involved in PI3K phosphorylation, independent of insulin receptor signaling. The diabetes and steatohepatitis associated with Aroclor 1260-HFD co-exposures were recently characterized in mice (18). mTOR is an energy sensor kinase that is critical in regulating hepatic energy homeostasis. PI3K/Akt have been recently implicated in lipid efflux in the development of steatosis (67). It now appears possible that alterations in the Akt/mTOR pathway, independent of CAR and PXR, may contribute to the abnormal hepatic glucose and lipid metabolism associated with steatohepatitis, and this mechanism requires further investigation.

STAT3 and cRaf are other downstream targets of EGFR that were impacted by PCB treatments in the animal model. The phosphorylation status of these targets could not be determined as their expression was decreased significantly by PCBs through yet unknown mechanisms. STAT3, a critical second messenger in interleukin 6 and leptin signaling, also regulates hepatic intermediary metabolism and the mitogenic response during liver regeneration. The STAT3 pathway is activated in human NAFLD and worsens insulin resistance while protecting against lipotoxicity by increasing autophagy and decreasing endoplasmic stress (68). STAT3 polymorphisms have been associated with human NAFLD (69). In our HFD-fed mice, Aroclor 1260 increased interleukin 6, while leptin was increased regardless of PCB exposure (3). However, decreased STAT3 levels may have induced adipocytokine resistance due to disrupted intracellular signaling. This warrants further study because IL-6 deficient mice fed HFD displayed worsened NASH (70), while leptin resistance is implicated in the pathogenesis of obesity and metabolic syndrome.

While cRaf protein levels were reduced by PCB exposure, phosphorylation of its downstream target, ERK, was reduced by HFD. This is a novel nutrient-toxicant interaction. In the literature, this pathway has been linked to liver regeneration and carcinogenesis, but more recently it has been found to regulate lipid metabolism through sterol regulatory element binding protein-1 (SREBP-1) phosphorylation (71). PCBs have been demonstrated to induce oxidative stress in rats and ERK activity is increased in response to oxidative stress (72, 73). I demonstrate that hepatic ERK activity is diminished on a HFD demonstrating that with PCB exposure and a HFD, the liver

cannot properly respond to oxidative stress potentially promoting steatohepatitis. In rats exposed to high dose of PCB 153 for 5 days, Akt and ERK activity increased which is characteristic of hepatocellular carcinoma (74), while with a low exposure to Aroclor 1260 in mice for 12 weeks, I observed decreased Akt activity. More research is required to understand the possible congener dose, time and species-specific responses of Akt, mTOR, and ERK to PCB treatments. Furthermore, while I identified new pathways beyond hepatic nuclear receptors by which PCBs can impact hepatic cell signaling, future studies are required to demonstrate if PCB-mediated EGFR inhibition promotes NAFLD and diabetes. Likewise, the precise mechanism by which PCBs inhibit EGFR activation requires elucidation which are a part of future studies ongoing in our laboratory.

In conclusion, polychlorinated biphenyls diminish epidermal growth factor receptor signaling in both humans and mice, leading to dysregulation of critical effector kinases and transcription factors implicated in hepatic xenobiotic, glucose, and lipid metabolism (Figure 12).

## CHAPTER 3

### EPIDERMAL GROWTH FACTOR RECEPTOR SIGNALING DISRUPTION BY ENDOCRINE AND METABOLIC DISRUPTING CHEMICALS

#### INTRODUCTION

Exposures to environmental chemicals occurs primarily through oral, inhalation, and transdermal routes. Subsets of chemicals or their metabolites bio-accumulate as demonstrated from population-based studies (10, 75, 76). Endocrine and metabolic disrupting chemicals (EDCs/MDCs) include pesticides, herbicides, dioxins, and poly-chlorinated biphenyls (PCBs) (10, 77-80). EDCs disrupt hormonal and growth factor signaling thus contributing to adverse outcomes in sex organs and metabolic organs. These metabolic aberrations due to chemical exposures are concerning due to the inexplicable rising rates of metabolic disorders (80). These classes of chemicals have been linked to many adverse outcomes such as hepatotoxicity, skin rash, developmental disorders, pancreatic dysfunction, and diabetes in humans and animal models (7, 78, 81-86). Recently chemical exposures have been found to promote a distinct type of fatty liver disease termed toxicant associated fatty liver disease (TAFLD) (5, 87, 88). TAFLD is perhaps the newest disease associated with EDC/MDC exposures (80).

The Environmental Protection Agency (EPA) has established the ToxCastDB database to prioritize, screen, and catalog high-priority chemicals using high throughput receptor activation assays in part to address issues of endocrine disruption (89). The ten EDCs/MDCs included in the ToxCastDB characterized in this study include atrazine, alachlor, lindane, dieldrin, dichlorodiphenylchloroethane (DDT), dichlorodiphenyldichloroethylene (DDE), *trans*-nonachlor, chlordane, PCB-153, and PCB-126. These chemicals have previously been characterized as inducers of constitutive androstane receptor (CAR) dependent gene expression (9, 22, 90-92).

These pesticides, herbicides, and PCBs all overlap in their abilities to activate CAR-dependent gene expression, while also exerting adverse effects primarily in the liver, pancreas, , and development (21, 93-95). *Cyp2b10* induction is an indicator of constitutive androstane receptor (CAR) activation. Direct CAR activation has been shown to be hepatoprotective in NAFLD animal models (16, 17, 60). Recent investigation of CAR activation has elucidated indirect activation by xenobiotics through epidermal growth factor receptor (EGFR) inhibition leading to CAR dephosphorylation and thus activation (19, 96). If the mode of action for environmental chemicals is indirect through EGFR inhibition, multiple signaling pathways would be disrupted potentially countering the protective effects of CAR activation as seen with direct ligand activation (16, 17). These observations add to the complexity of how these compounds elicit their effects while providing some explanation as to why they are hepatotoxic. If these compounds act through EGFR inhibition, this could disrupt a vast signaling cascade essential for hepatic function (25, 28, 30, 31, 54, 96, 97).

Dermal rashes upon exposure to pharmaceutical EGFR inhibitors, dioxins, PCBs, chlorinated pesticides and herbicides are well-documented adverse effects common between these classes of compounds (83-86, 94, 103-108). Loss of EGFR function in mice leads to skin inflammation suggesting the importance of EGFR function for skin homeostasis and wound healing (105, 106, 109, 110). PCB exposure in pregnant women has been shown to diminish placental EGFR phosphorylation which correlated with lower birth weights (33). EGFR is instrumental in development and homozygous EGFR-null mice do not survive past postnatal day 20 (majority die on postnatal day 1) and have severe abnormalities (111-113). These previous studies serve to illustrate the multiple adverse effects due to inhibition of EGFR signaling in the liver,  $\beta$ -islets of the pancreas, skin, and during development. With the literature demonstrating that the selected EDCs/MDCs are CAR activators, their mode of action has not been firmly established. Therefore, compounds in this study were investigated to determine if they directly activate CAR or act through EGFR inhibition. Should the selected pollutants inhibit EGFR function at environmentally relevant concentrations, then the impact of their signaling disruption on human health and disease could be evaluated in future studies.

## MATERIALS AND METHODS

### Compound Selection:

A set of 10 MDCs/EDCs known to activate CAR were selected from high priority chemicals identified in NHANES or ToxCastDB. These chemicals included *trans*-nonachlor, chlordane, DDE, DDT, dieldrin, alachlor, atrazine, lindane, PCB-153, and PCB-126. *Trans*-nonachlor and DDE were purchased from SUPELCO (Bellefonte, PA). Lindane and DDT were purchased from CHEM Service (West Chester, PA). Dieldrin, chlordane, atrazine and alachlor were purchased from Sigma Aldrich (St. Louis, MO). PCB-153, a non-dioxin like PCB (NDL) and PCB-126, a dioxin-like PCB (DL PCB) were purchased from AccuStandard (New Haven, CT).

### Plasmid construction:

mCAR cDNA was a generous gift from Tom Rushmore (Merck Research Laboratories, West Point, PA) which was subcloned into a modified version of pGL3-basic (58, 96). Mice lack CAR splice variants found in humans but the mCAR is 89% homologous to hCAR1. Restriction endonucleases and T4 DNA ligase were purchased from New England BioLabs (Ipswich, MA). Dimethyl sulfoxide (DMSO) was purchased from Fisher BioReagents (Thermo Fisher Scientific, Pittsburg, PA). Lipofectamine and Opti-MEM were acquired from Life Technologies Inc. (Carlsbad, CA). Oligonucleotides were purchased from Integrated DNA Technologies (Coralville, IA).

### Cell culture:

A-431 Cells: The human epidermoid carcinoma cell line derived from a female patient was obtained from American Type Culture Collection (ATCC, Manassas, MD). Cells were grown in Dulbecco's modified Eagle's medium (DMEM) (VWR, Radnor, PA) supplemented with 10% fetal bovine serum and 1% antimycotic/antibiotic solution (Mediatech, Manassas, VA). The cells were incubated in a 5% carbon dioxide atmosphere and 95% humidity at 37° and sub-cultured every 2 days. HepG2 cells were used as previously described in chapter 2.

**Transfection:**

HepG2 cells were plated in Thermo Scientific Nunc 24-well plates and transfected at 40-60% confluency. The transfection mix per well contained 150 ng  $\beta$ -galactosidase expression plasmid (pCMV- $\beta$ , Stratagene, CA) as a transfection control, 50 ng receptor expression plasmid (pGL3-mCAR), and 150 ng reporter plasmid (pGL<sub>3</sub>-DR4-Luc) if not otherwise specified. The artificial DR4 construct consists of two AGGCTA repeats separated by 4 base pairs and has been described previously (36, 96). All cells were co-transfected by lipofection using Lipofectamine reagent according to the manufacturer's instructions (Thermo-Scientific, Waltham, MA) and Opti-MEM (reduced serum medium) was used for the transfection medium. After 4 hours of incubation, the medium was changed to DMEM supplemented with 10% FBS and 1% antimycotic/antibiotic solution and cells were left overnight to recover. Compounds of interest were then added to the cells and incubated for 24 hours. DMSO was used as a vehicle for all compounds (final concentration 0.1%). 1,4-Bis-[2-(3,5-dichloropyridyloxy)] benzene, 3,3',5,5'-Tetrachloro-1,4-bis(pyridyloxy)benzene (TCPOBOP) (Sigma-Aldrich, St Louis MO) was used as a positive control as it is a murine CAR direct agonist.

**Luciferase Reporter assay:**

Cells were washed twice with phosphate buffered saline (PBS 1X), harvested using 50  $\mu$ L cell lysis buffer (Promega, Madison, WI) and subjected to a single freeze-thaw event. For  $\beta$ -galactosidase assays, cell extracts (5  $\mu$ L), were incubated with chlorophenol red  $\beta$ -galactopyranoside (CPRG, Sigma-Aldrich, St Louis MO) at 37°C for 30-60 minutes. The enzyme activity was measured spectrophotometrically at 595 nm using the Bio-Tek Synergy HT multi-mode micro plate reader. Luciferase activity assays were performed on cell extracts (5  $\mu$ L) using the Luciferase Assay System (Promega, Madison, WI). Luminescence was measured using the Orion L micro plate luminometer (Berthold Detection Systems, Pforzheim, Germany) over a 10 second period. Receptor activation was measured by luciferase activity and results were normalized to the amount of  $\beta$ -galactosidase expressed.

**EGF Assay in HepG2 cells:**

Cells were pre-treated with 10  $\mu$ M (this concentration was found to not be cytotoxic in MTT assays, (Figure 37, Appendix I) (or 4.1  $\mu$ g/mL for the chlordane mixture) of the compound of interest for 10 minutes followed by 30 minutes with 20 ng/mL of epidermal growth factor (EGF) (Fisher Scientific, Pittsburgh, PA). EGF alone for 30 minutes was used as a positive control, and 30-minute treatment with 0.1% DMSO was used as a negative control. The 30-minute treatment was used as that was the peak time for EGFR phosphorylation (96). The positive and negative controls were used to establish phosphorylated EGFR's dynamic range. Media was removed by aspiration and the cells were washed with PBS. Cells were lysed in modified radioimmunoprecipitation assay (RIPA) buffer (20 mM Tris, 150 mM NaCl, 1 mM EDTA/EGTA/ $\beta$ -glycerophosphate/ $\text{Na}_3\text{VO}_4$ , and 1% Triton X-100) supplemented with protease and phosphatase inhibitors (Sigma-Aldrich, St. Louis, MO).

**EGF Endocytosis Assay in A-431 Cells:**

This assay was modified from a previously described method (114). A-431 cells were used as they express  $2.6 \times 10^6$  epidermal growth factor receptors per cell (115). Alexa Fluor 555 labeled EGF was purchased from Thermo Scientific, (Philadelphia, PA) and was used at 20 ng/100  $\mu$ L. After a 3-hour serum starvation, A-431 cells were exposed to varying concentrations of the compounds ( $10^{-19}$  -  $10^{-3}$  M) for 10 minutes. Since chlordane is a mixture it was administered at the following concentrations  $0.41 \times 10^{-16}$  to 41  $\mu$ g/100  $\mu$ L. The chlordane competition curve is in the logarithmic scale for ease of comparison. Positive control cells were treated with 0.1% DMSO and negative control cells were treated with 20 ng/100  $\mu$ L of unlabeled EGF purchased from Millipore (Norwood, OH). This served as a negative since the EGF receptors would be saturated and endocytosed preventing fluorescently labeled EGF from binding thus preventing any signal. Cells were then treated with 20 ng/100  $\mu$ L of Alexa Fluor 555 labeled EGF for 30 minutes. This was followed by 3 washes with pre-warmed PBS and incubation with 3.7% formaldehyde for 15 minutes. Cell nuclei were then stained with Hoechst 33342 purchased from Thermo Scientific (Philadelphia, PA) at 1  $\mu$ g/100  $\mu$ L for 15 minutes. Images and data were obtained *via* an ArrayScan HCS 4.0 Reader. Filter sets specific for Hoechst labeled nuclei and the Alexa Fluor 555-EGF were used for detection. A



20X microscope objective was used for imaging and the SpotDetector bioapplication was used to acquire and analyze images. Approximately 500 cells from randomized fields were analyzed for each well. The equation used to normalize 555-EGF count/nuclei values is listed below.

$$\text{Alexa Fluor 555 EGF Endocytosis} = \left(1 - \frac{\text{Exp-DMSO}}{\text{EGF-DMSO}}\right) * 100$$

To determine if these compounds could displace 555-EGF from the ligand binding domain of EGFR cells were pre-treated with 20 ng/100 $\mu$ L of Alexa Fluor 555-EGF for 2.5 minutes on ice to prevent endocytosis. Cells were then exposed to 1pM of (PCB-126, PCB-153, *trans*-nonachlor) 0.041 pg/100 $\mu$ L of chlordane and 100 pM of atrazine for 2.5 minutes on ice. The plated cells were incubated at 37° C for 25 minutes and the assay was continued as previously described. The relative effect potencies (REPs) were calculated from the normalized IC<sub>50</sub> values from the EGF endocytosis assay for the compounds tested (normalized to *trans*-nonachlor, most potent).

#### **Western Blot Analysis:**

Cell culture lysates from HepG2 and A-431 cells were homogenized in RIPA Buffer (150  $\mu$ L RIPA supplemented with protease, and phosphatase inhibitors 10  $\mu$ L/mL, (Sigma-Aldrich, St. Louis, MO). The antibodies for p-EGFR Y1173 were obtained from Abcam (Cambridge, MA). The antibody for EGFR was purchased from Santa Cruz (Santa Cruz, CA). Antibodies for p-ERK1/2 and ERK1/2 were purchased from Cell Signaling Technology (Danvers, MA). Full methods for western blot analysis can be found in chapter 2.

#### **Molecular Modeling and Docking Simulation:**

The inactive EGFR structure (INQL) and select chemicals from PubChem were prepared using Chimera (116-118). Docking simulations were conducted using AutoDock Vina and the predicted sites with the best scores were further analyzed. The top two ligand positions were selected based on their root-mean-square deviation (RMSD) lower and upper bound metrics. The EGFR tyrosine kinase structure (4HJO) was used for docking simulations for atrazine (119). The structures for the

ligands were obtained from PubChem; PCB-153 (CID:37034), PCB-126 (CID: 63090), *trans*-nonachlor (CID: 19520), atrazine (CID: 2256) (117).

### **NHANES 1999-2004 and Population Analysis**

University of Louisville Institutional Review Board determined that the use of the publicly available de-identified 1999-2004 NHANES data (64) was not considered human subjects research and did not require IRB approval. The methods used to acquire NHANES samples and determine the chemical concentrations were described previously (64). The NHANES (1999-2004) wet weight and lipid adjusted means of *trans*-nonachlor, PCB-153, and PCB-126 were used to for comparison with the calculated IC<sub>50</sub> values.

### **Statistical analysis**

All statistical analyses were performed using GraphPad Prism version 7 for Macintosh (GraphPad Software Inc., La Jolla, CA, USA). Data are expressed as mean ± SEM. Multiple group data were compared using One Way ANOVA followed by Bonferroni's post-hoc test for parametric data for all pairwise comparisons. P <0.05 was considered statistically significant. Competitive binding curves and IC<sub>50</sub> values were calculated with Graphpad Prism 7 using two sites – Fit logIC<sub>50</sub>. Two group comparisons were made using a two-tailed unpaired t-test and a P<0.05 was considered statistically significant.

## **RESULTS**

### **Selected compounds do not appear to be direct agonists of CAR, but *trans*-nonachlor, chlordane and atrazine inhibit EGF stimulated Y1173 phosphorylation of EGFR**

To determine whether previously characterized CAR activators were direct CAR activators, a DR4-luciferase reporter in HepG2 cells co-transfected with mCAR was used. The assay was performed for the following compounds: atrazine, dieldrin, *trans*-nonachlor, lindane, alachlor, chlordane, DDT and DDE, at 10 µM to evaluate their ability to directly activate CAR. PCB-126 and PCB-153 were not used for this assay as the results have already been published and both were found to ablate

EGF-mediated EGFR phosphorylation (96). If the compounds act as direct activators of mCAR then they should increase luciferase activity similarly to TCPOBOP (Fig. 9a). As anticipated, TCPOBOP increased reporter signal by 2.6-fold, which is in good agreement with our previous work and others (96, 120). None of the compounds significantly increased the reporter expression even though *in vivo* studies demonstrate that they induce *Cyp2b10*.

CAR has been shown to be indirectly activated through inhibition of EGFR signaling (19). In Fig. 9b compounds that can prevent EGF stimulation of EGFR in HepG2 cells were identified. The EGF assay in HepG2 cells was performed with the same chemicals previously used at 10  $\mu$ M concentration for 10 minutes followed by EGF at 20 ng/mL for 30 minutes. Compared to EGF alone, atrazine, chlordane, and *trans*-nonachlor all substantially diminished EGF stimulation of EGFR phosphorylation: 73% for atrazine ( $p < 0.02$ ) and 82% for *trans*-nonachlor ( $p < 0.01$ ) and chlordane ( $p < 0.01$ ). DDE, DDT, dieldrin, alachlor, or lindane did not significantly alter EGFR phosphorylation in the presence of EGF (Fig. 9b). Indirect CAR activation by these compounds may occur through uncharacterized EGFR-independent mechanisms. These experiments suggested that chlordane, *trans*-nonachlor, and atrazine were indirect CAR activators possibly acting through EGFR inhibition. Chlordane, *trans*-nonachlor, and atrazine were chosen to investigate further along with previously characterized EGFR signaling disruptors PCB-126 and PCB-153 (96)

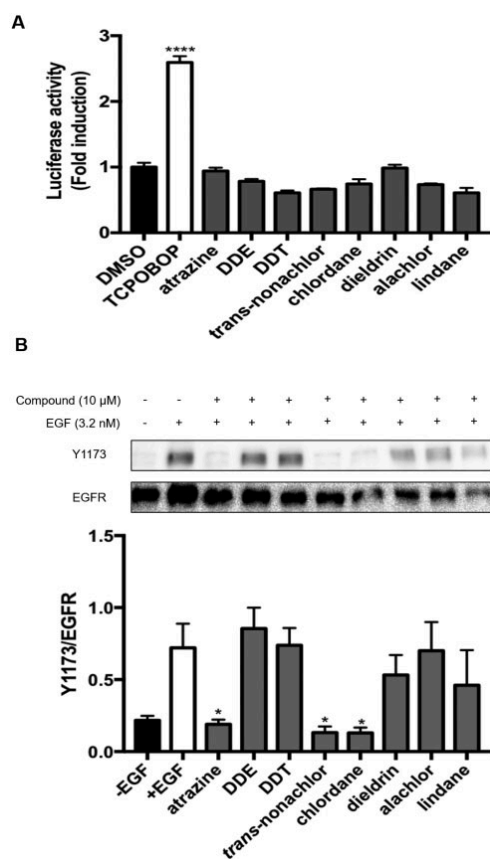


**Figure 13. Selected compounds do not appear to be direct agonists of CAR, but *trans*-nonachlor, chlordane and atrazine inhibit EGF stimulated Y1173 phosphorylation of EGFR:**

**A.** HepG2 cells were co-transfected with pCMV $\beta$ , mCAR and pGL<sub>3</sub>-DR4-Luc constructs and exposed to each compound at 10  $\mu$ M, 0.1 % DMSO was used as a negative control, and TCPOBOP (direct mCAR agonist) was used as positive control. The data are presented as mean  $\pm$  SEM and a n = 4 was used, A \* denotes a P<0.05. **B.** HepG2 cells were pre-exposed to the select compounds at 10  $\mu$ M for 10 minutes before EGF administration at 20 ng/mL for the experimental groups for 30 minutes. 0.1% DMSO and EGF treated cells served as the negative and positive controls, respectively. EGFR phosphorylation at Y1173 was measured *via* western blot analysis and was normalized to total EGFR. An n = 4 was used and the values are represented as mean  $\pm$  SEM for Fig 13a-b. Experimental values were compared to EGF alone values by a one-way ANOVA for Fig 13b. A \* denotes a P<0.05, and \*\*\*\* denotes a P<0.0001 and are considered statistically significant.

***Trans*-nonachlor, chlordane, PCB 126, PCB-153, and atrazine prevent EGF endocytosis in A-431 cells**

To determine whether select compounds prevent EGF endocytosis, a competition assay in human A-431 cells using Alexa Fluor 555-EGF (20 ng/100  $\mu$ L or 32 nM) and increasing concentrations of the select compounds and non-labeled EGF ( $10^{-19}$  -  $10^{-3}$  M) was conducted. Fluorescently labeled EGF in the absence of an inhibiting compound will bind the EGFR leading to dimerization and endocytosis. The amount of fluorescent signal per cell is a measure of EGF-EGFR endocytosis, and EGF binding in the presence of varied concentrations of these compounds. If fluorescently labeled EGF is incapable of binding the EGFR, there will be no to low fluorescent signal per cell indicating a lack of EGF binding and / or dimerization and endocytosis. This concentration of Alexa Fluor 555-EGF was used as it was previously shown to give robust signal in the Cellomics assay (114). The EGFR has two conformational states that have different affinities for EGF (33, 121, 122). The lower affinity state is most likely the unliganded monomer, while the high affinity state is probably unliganded, pre-formed dimers and/or tetramers (122, 123). Thus, the biphasic competition curves likely reflect these two affinity states where the first  $IC_{50}$  value is the low affinity state (EGFR monomer) and the second  $IC_{50}$  is the high affinity state (pre-formed EGFR dimers or tetramers) of the EGFR. Figure 14a shows non-labeled EGF's ability in preventing fluorescent EGF endocytosis and EGF's  $IC_{50}$  value was  $\log -15.4 \pm 0.31$  M for the high affinity site and  $\log -8.99 \pm 0.6$  M for the low affinity site. Fig 14b shows that the  $IC_{50}$  value for prevention of EGF endocytosis by chlordane was  $\log -16.49 \pm 0.33$  M (0.0013 fg/100 $\mu$ L) for the high affinity site and  $\log -4.0 \pm 0.54$  M (4.1  $\mu$ g/100  $\mu$ L) for the low affinity site. Fig 14c shows the  $IC_{50}$  value for loss of EGF endocytosis due to *trans*-nonachlor of  $\log -16.6 \pm 0.23$  M for the high affinity site and  $\log -3.88 \pm 0.72$  M for the low affinity site. Fig 14d shows  $IC_{50}$  values for loss of EGF endocytosis due to PCB-126 to be  $\log -16.07 \pm 0.31$  M for the high affinity site and  $\log -8.38 \pm 0.24$  M for the low affinity site. Fig 14e shows the  $IC_{50}$  values for PCB 153 of the loss of EGF endocytosis being  $\log -12.4 \pm 0.2$  M for the high affinity site and  $\log -5.26 \pm 0.49$  M for the low affinity site. Atrazine's  $IC_{50}$  value for loss of EGF endocytosis was  $\log -10.42 \pm 0.34$  M for the high affinity site and  $\log -3.51 \pm 0.95$  M for the low

affinity site (Fig 14f). These findings suggest that chlordane, *trans*-nonachlor, PCB-126, PCB-153, and atrazine are potent EGFR antagonists that prevent EGF endocytosis.

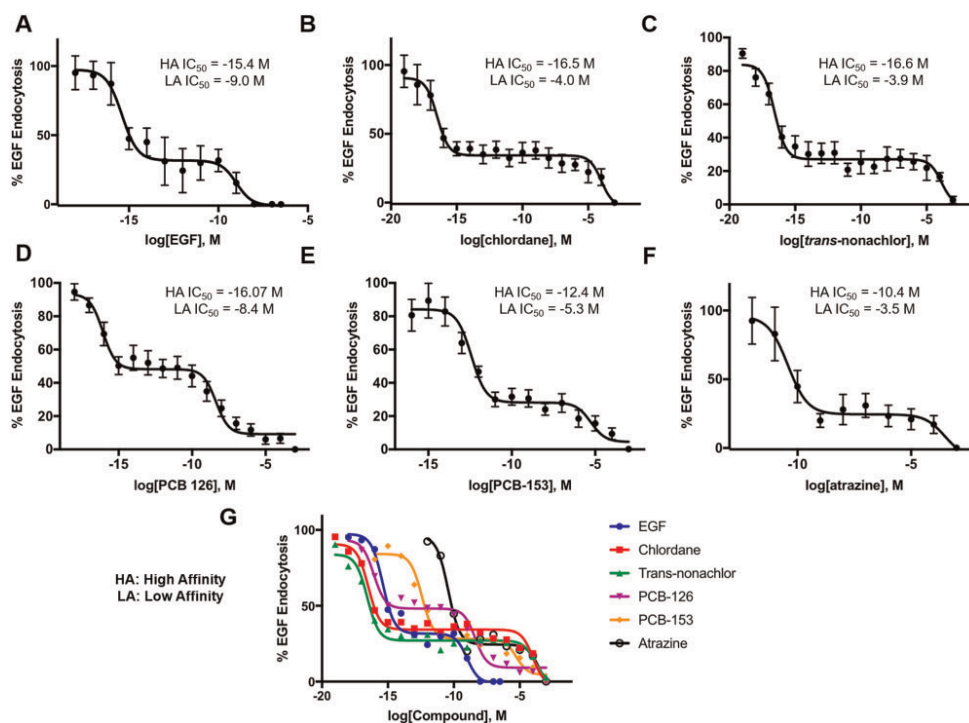


**Figure 14. Chlordane, *trans*-nonachlor, PCB-126, PCB-153, and atrazine prevent EGF endocytosis in A-431 cells: A-G.** A-431 cells were serum starved for 3 hours before pre-treating cells for 10 minutes with varying concentrations of the select compounds. Cells were then treated with 20 ng/100  $\mu$ L of Alexa Fluor 555 conjugated EGF for 30 minutes. Fluorescent EGF spots per stained cell nuclei were the measure for this assay. 0.1% DMSO pre-treated cells served as the positive control, and cells pre-treated with 20 ng/100 $\mu$ L of unlabeled EGF served as the negative control for this experiment. An n = 3 (3 96-well plates) was used and there were 8 technical replicates for each concentration for each individual plate. Values were normalized between the positive and negative controls of the plate with the equation described in methods. Curves were fitted by nonlinear regression with GraphPad 7 Prism software and a two site logIC<sub>50</sub> curve fit for the data for the potent compounds and non-labeled EGF.

**Relative effect potencies and NHANES serum concentrations for *trans*-nonachlor, PCB-126, and PCB-153**

In this study, the data gathered was used to develop relative effect potencies (REPs) for EGFR inhibiting compounds. REPs are used to rank chemicals based on their potency to activate or inhibit a receptor and in turn that value is used for risk assessment based on the individual's additive body burden of multiple chemicals. (Table 1) REPs were calculated by normalizing the high affinity site IC<sub>50</sub> values to the most potent *trans*-nonachlor. In descending order of REP values *Trans*-nonachlor had a REP of 1, PCB-126 had a REP of 0.33, PCB-153 had a REP of  $8.3 \times 10^{-4}$ , and atrazine's REP was  $7.9 \times 10^{-6}$ .



	Population Lipid-Adjusted Mean 95% CI (ng/g)	Wet Weight Mean 95% CI (ng/g)
<b>Trans-Nonachlor</b>		
99-00, n = 1933	(99-00) 18.3 (16.7–20.0) (41 nM)	(99-00) 0.11 (0.1–0.12) (248 pM)
01-02, n = 2286	(01-02) 17.0 (15.2–18.9) (38 nM)	(01-02) 0.104 (0.093–0.12) (234 pM)
03-04, n = 1955	(03-04) 14.7 (13.1–16.5) (33 nM)	(03-04) 0.09 (0.08–0.1) (203 pM)
<b>PCB-126</b>		
01-02, n = 1226	(01-02) 0.023 (0.021–0.025) (71 pM)	(01-02) 0.00015 (0.00014–0.00016) (460 fM)
03-04, n = 1860	(03-04) 0.016 (0.0149–0.0179) (50 pM)	(03-04) 0.0001 (0.0009–0.00011) (307 fM)
<b>PCB-153</b>		
01-02, n = 2306	(01-02) 27.2 (24.7–30.1) (75 nM)	(01-02) 0.17 (0.15–0.19) (471 pM)
03-04, n = 1896	(03-04) 19.8 (18.8–20.9) (55 nM)	(03-04) 0.12 (0.114–0.13) (332 pM)

Abbreviations: CI, confidence interval.

**Table 1. *Trans*-Nonachlor, PCB-126, and PCB-153 Means Levels for NHANES 99-00, 01-02, and 03-04 (CDC, 2005)(64):** The mean lipid adjusted and wet weight serum concentrations for *trans*-nonachlor, PCB-126, and PCB-153 in NHANES 1999-2004 participants are given in Table 1. The mean *trans*-nonachlor lipid adjusted concentrations ranged from 18.3 – 14.7 ng/g (41 – 31 nM) and decreased over time. The *trans*-nonachlor wet weight means ranged from 0.11 – 0.09 ng/g (248 – 203 pM) and were higher than the IC<sub>50</sub> for EGFR inhibition (0.03 fM). PCB-126 mean lipid adjusted concentrations varied from 0.023 – 0.016 ng/g (71 – 50 pM) and decreased over time. The PCB-126 wet weight mean varied between 0.00015 – 0.0001 ng/g (460 – 307 fM) and was higher than the IC<sub>50</sub> for EGFR inhibition (0.09 fM). The PCB-153 mean lipid adjusted concentration was 27.2 – 19.8 ng/g (75 - 55 nM) and decreased over time. The PCB-153 wet weight mean ranged from 0.17 – 0.12 ng/g (471 – 332 pM) and was greater than the IC<sub>50</sub> for EGFR inhibition (363 fM). These data demonstrate that the levels measured in humans may be relevant for future investigation of adverse effects due to EGFR inhibition by these chemicals.

***Trans*-nonachlor, chlordane, PCB-126, PCB-153, and atrazine prevent EGF-mediated EGFR and ERK phosphorylation in A-431 cells at the IC<sub>50</sub> concentration**

To determine if exposure to the respective IC<sub>50</sub> values for these compounds would diminish EGFR phosphorylation and downstream signaling EGFR Y1173 and ERK phosphorylation were measured at the IC<sub>50</sub> concentrations previously determined by the EGF endocytosis assay. A-431 cells were pre-treated with compounds at the respective IC<sub>50</sub> values followed by a 30-minute treatment with EGF at 20 ng/mL. Protein was then extracted, and western blot analysis was conducted to measure phosphorylation of EGFR and effector kinase ERK1/2 (Fig 15a-b). Chlordane (p<0.02, p<0.02), *trans*-nonachlor (p<0.019, p<0.05), PCB-126 (p<0.02, p<0.05), PCB-153 (p<0.03, p<0.03), and atrazine (p<0.03, p<0.05) exposure significantly diminished EGFR and ERK phosphorylation respectively, at their respective IC<sub>50</sub> values. These results demonstrate that these compounds can prevent EGF mediated EGFR phosphorylation and downstream signaling.

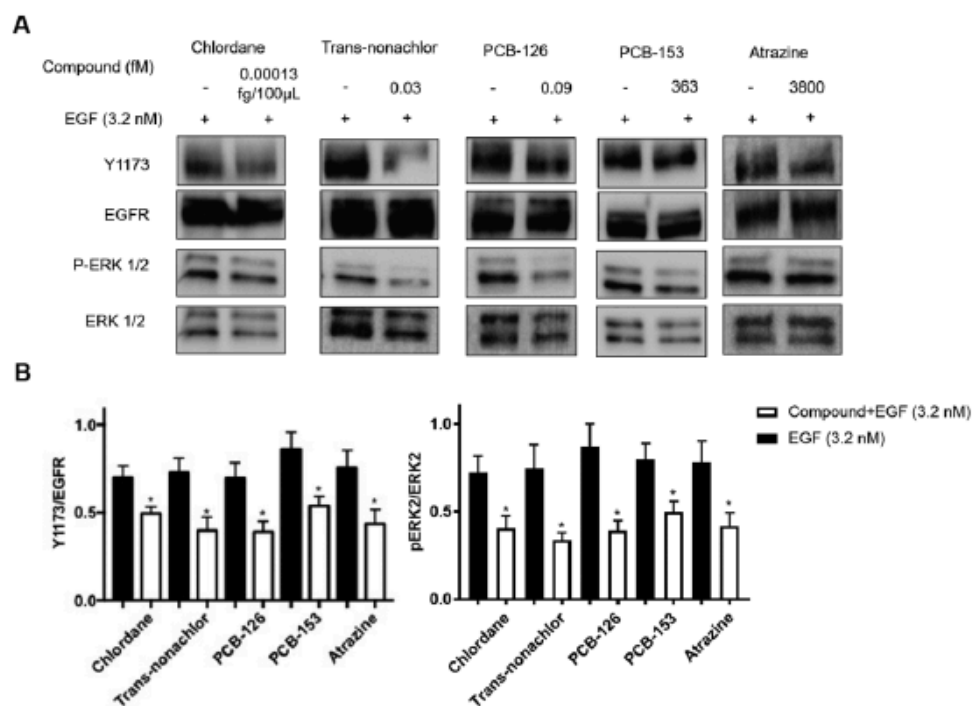


**Figure 15. Chlordane, *trans*-nonachlor, PCB-126, PCB-153, and atrazine prevent EGF-mediated phosphorylation at the IC<sub>50</sub> value from the EGF endocytosis assay: A-B.** To test whether EGFR Y1173 and ERK phosphorylation was diminished concordantly at the measured IC<sub>50</sub> for loss of EGF endocytosis, A-431 cells were exposed to the IC<sub>50</sub> concentration for the respective compounds and EGFR Y1173 and ERK phosphorylation were measured *via* western blot analysis after EGF treatment. An n = 4 was used and values are represented as mean ± SEM. Quantitated band densities were statistically compared to the EGF positive control values by an unpaired, two-tailed t-test. A \* denotes P<0.05 which is considered statistically significant.

***Trans*-nonachlor, chlordane, PCB-126, and PCB-153 can displace bound 555-EGF from the EGFR but not atrazine**

Next, to determine if these compounds act as competitive inhibitors that can displace bound fluorescent EGF from the ligand-binding domain of the EGFR a competition assay with fluorescent EGF administration before the chemical was conducted. A-431 cells on ice were treated with 20 ng/100  $\mu$ L of Alexa-Fluor 555-EGF for 2.5 minutes and then exposed to 1  $\mu$ M of either PCB-126, PCB-153, *trans*-nonachlor, chlordane (0.041 pg/100  $\mu$ L), or 100  $\mu$ M of atrazine for 2.5 minutes. Cells were then incubated at 37° C for 25 minutes to continue the endocytosis reaction (Fig 16). Chlordane ( $p < 0.0002$ ), *trans*-nonachlor ( $p < 0.0001$ ), PCB-126 ( $p < 0.0001$ ), and PCB-153 ( $p < 0.0008$ ) were all able to significantly displace fluorescent EGF from interaction with EGFR similarly to non-labeled EGF. Atrazine ( $p < 0.94$ ) was unable to displace fluorescent EGF from its interaction with the EGFR and had similar signal intensity as seen with the DMSO positive control. These findings would suggest that chlordane, *trans*-nonachlor, PCB-126 and PCB-153 are competitive antagonists, while atrazine appears to be an EGFR antagonist that cannot prevent EGF endocytosis once already bound.

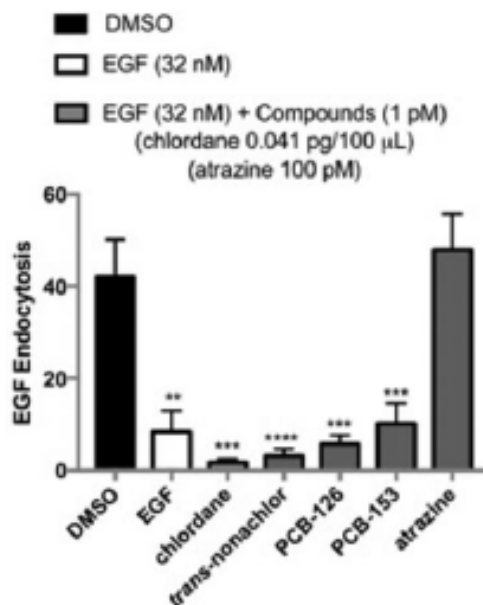


**Figure 16. *Trans*-nonachlor, chlordane PCB-126, and PCB-153, but not atrazine, displace EGF from the EGF ligand binding domain of the EGFR:** A-431 cells were treated with 20 ng/100  $\mu$ L of fluorescent EGF for 2.5 minutes on ice to allow EGFR binding but to prevent endocytosis. Cells were then exposed to 1 pM of *trans*-nonachlor, PCB-153, PCB-126, 0.041 pg/100  $\mu$ L of chlordane, and 100 pM of atrazine for 2.5 minutes while on ice. The cells were then put in the incubator at 37° C for 25 minutes. Then cells were fixed and stained and EGF spots per nuclei were measured as previously described. An n = 16 was used and the data are represented as mean  $\pm$  SEM. Experimental groups were statistically compared to positive control cells (0.1% DMSO) by one-way ANOVA. A \* denotes P < 0.05, \*\* P < 0.01, \*\*\* P < 0.001, and \*\*\*\* P < 0.0001 was considered statistically significant.

***Trans*-nonachlor, PCB-153, and PCB-126 are predicted to bind within the extracellular domain of EGFR, while atrazine is predicted to bind to the ATP-binding pocket of the tyrosine kinase domain**

At this stage, chlordane, *trans*-nonachlor, PCB-126, PCB-153, and atrazine were demonstrated to ablate EGF endocytosis, and EGF signaling with two measures in two human cell lines. Next, to elucidate where these compounds are predicted to bind EGFR, protein-ligand docking simulations were performed. Since there are currently no available protein structures for pre-formed unliganded dimers or tetramers of EGFR, an inactive EGFR monomer structure (1NQL) and an EGFR tyrosine kinase structure (4HJO) were used for the docking simulations (116, 119). This allowed for the identification of where the various chemicals are predicted to bind in the single monomer state of the EGFR. As seen in Fig 17a, *trans*-nonachlor was predicted to bind within a hydrophobic pocket between domains II and IV (red) and domain IV (blue) of EGFR with an affinity of -5.8 kcal/mol for both sites. PCB-126 was predicted to bind within a hydrophobic pocket of domain III (red) and domain II (blue) with an affinity of -6.1 and -5.9 kcal/mol respectively (Fig 17b). PCB-153 was predicted to bind within a hydrophobic pocket between domain II and IV (red) of and domain IV (blue) of EGFR with an affinity of -5.9 and -6.1 kcal/mol respectively (Fig 17c). In striking contrast, atrazine was predicted to interact within the tyrosine kinase domain in the ATP binding pocket with an affinity of -5.6 kcal/mol (red) and at another site within the TK domain at -5.5 kcal/mol (blue) (Fig 17d).

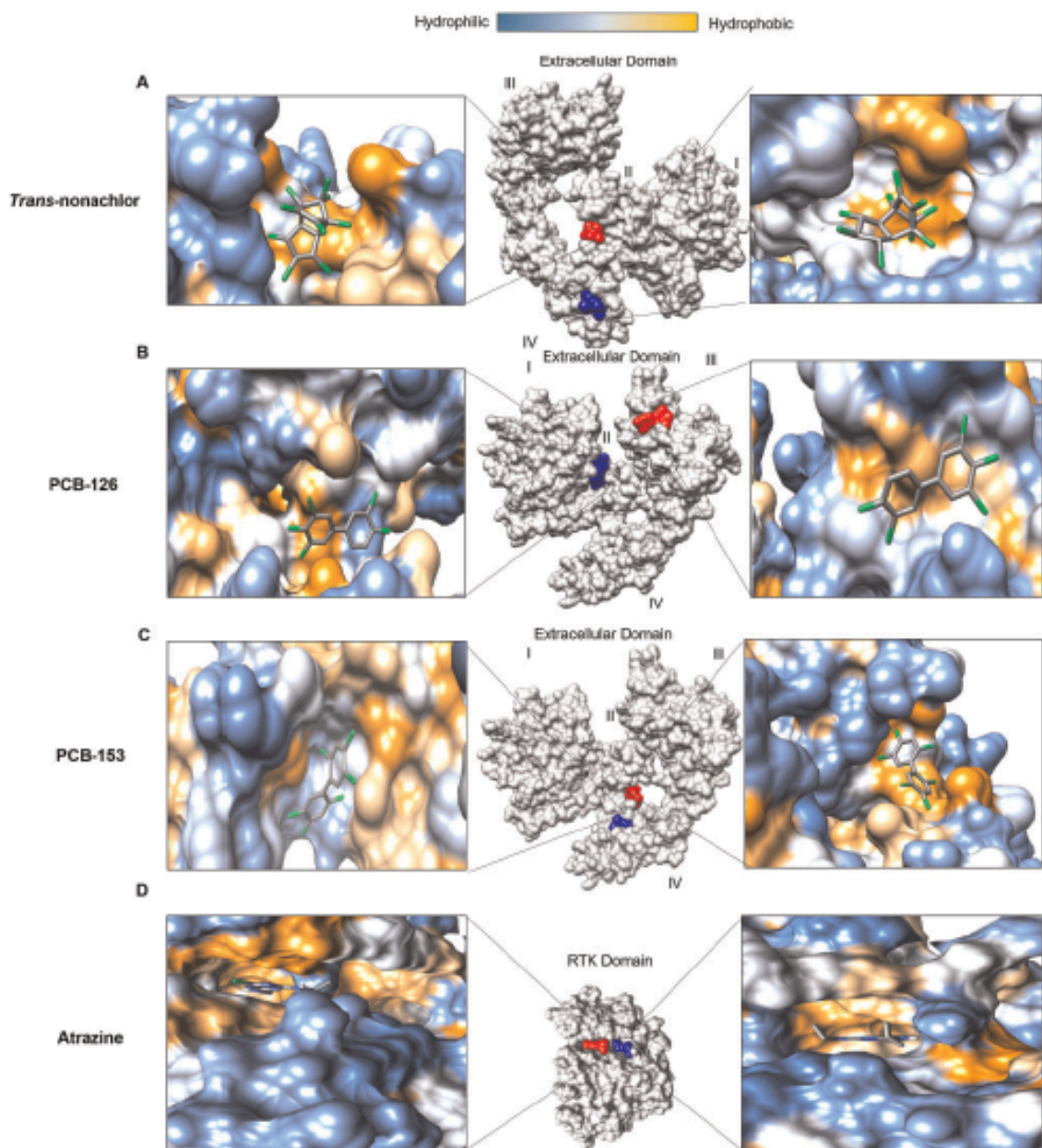


**Figure 17. Predicted binding sites for *trans*-nonachlor, PCB-126, PCB-153, and atrazine with the EGFR:** Small molecule docking simulations with the compounds (**A.** *trans*-nonachlor, **B.** PCB-126, **C.** PCB-153) (structures obtained from PubChem, PubChem IDs found within methods) and the extracellular domain of EGFR (INQL). **D.** Atrazine was modeled with the inactive EGFR RTK domain (4HJO). The EGFR structure and compounds were prepared in Chimera and docking simulations were conducted using AutoDock Vina software. The models show the two most energetically favorable sites and the hydrophobicity of the amino acids within those predicted sites.

## DISCUSSION

Initially the well-characterized CAR-activating chlorinated compounds were determined to not directly activate mCAR relative to the direct mCAR ligand, TCPOBOP in cell culture. This led to the evaluation of their potential roles as EGFR inhibitors that possibly indirectly activate CAR through phosphorylation as has been previously demonstrated for phenobarbital and PCBs (19, 96). Interestingly *trans*-nonachlor, chlordane, and atrazine all had a significant effect in preventing EGF-mediated EGFR phosphorylation in HepG2 cells. At this stage, these compounds were investigated further to understand how they act on the EGFR.

The EGFR has 4 sequential and highly regulated steps for activation including I) EGF binding to an inactive EGFR monomer generating an active monomer, II) homo or heterodimerization of ligand bound monomers, III) autophosphorylation by the tyrosine kinase domain, and IV) endocytosis (124, 125). Using these regulatory steps of EGFR activation, the experimental design was developed to investigate at what step these chemicals are eliciting their inhibitory effects. The fluorescent EGF assay was used to measure EGF-EGFR endocytosis in the presence of the chemicals tested. Subsequently, the effect of these chemicals on EGFR phosphorylation was determined by western blot analysis. These assays paired with the structural modeling was used to determine how these chemicals ablate EGFR signaling.

Previously published studies in cell-based competition assays have determined that there are low and high affinity sites for EGF binding (33, 121, 122). Currently it is hypothesized that roughly 10% of EGF receptors are in the high affinity conformation which are either pre-formed non-liganded dimers or potentially tetramers (123, 126). The other 90% of EGF receptors are hypothesized to be in the single monomer conformation or the low affinity state. This is an important concept as the concentration curves from the fluorescent EGF assay demonstrate two-site binding which may be representative of a low affinity and high affinity conformation of the EGFR. The data presented suggest that the amount of high affinity receptors may have been previously underestimated at 10%. Collectively the data suggest that the amount of high affinity receptors in the A-431 cells may be as high as 30% of the total receptors. The low affinity site seems more



sensitive to EGF than in previous studies. This may be due to differences in the EGF label (fluorescent vs. radiolabeled) and the reaction temperature (37 °C vs. 4 °C) (127).

While *trans*-nonachlor, PCB 126, PCB 153, and atrazine were potent at preventing EGF endocytosis, confirmation that the phosphorylation cascade was disrupted was necessary to validate these compounds as EGFR signaling disrupting chemicals. At the respective concentrations of the IC<sub>50</sub> values for the chemicals, both EGFR phosphorylation and ERK1/2 phosphorylation were reduced. This demonstrated that multiple steps of the EGFR activation mechanism were prevented by exposure to these compounds.

The EGF displacement assay demonstrated that *trans*-nonachlor, PCB-126, PCB-153, and chlordane can apparently displace bound fluorescent EGF from interacting with the EGFR. This suggests that these compounds are competitive antagonists that interact with the extracellular domain of the EGFR. Further ligand-receptor docking studies found that *trans*-nonachlor, PCB-126, and PCB-153 interact with hydrophobic residues within the extracellular domain of EGFR. Interestingly, atrazine could not compete off bound EGF from EGFR, and thus it may bind within the ATP pocket of the tyrosine kinase domain of EGFR and not at the hydrophobic pocket between domains II and IV of EGFR. Since these compounds are structurally diverse and EGFR has multiple regulatory activation steps, it seems logical that environmental chemicals could differ in their method of EGFR inhibition. Atrazine appeared to act as a tyrosine kinase inhibitor as EGF was able to stay bound in the presence of atrazine.

While some of the compounds tested were not potent EGFR inhibitors including lindane, DDE, DDT, alachlor, and dieldrin this does not rule out the possibility that these compounds could disrupt the signaling of other related receptor tyrosine kinases (RTKs). This has already been demonstrated for phenobarbital and the insulin receptor (128). Since many RTKs have highly homologous tyrosine kinase domains, the downstream effects of receptor inaction could overlap (129, 130).

While the EGF endocytosis assay was previously published as a tool for high throughput EGFR inhibitor screening for EGFR-directed chemotherapy discovery, it may also serve as a chemical adverse effect screen (114). Fifty-two percent of exogenously administered EGF traffics

to the liver in animals, and recently EGFR signaling has been shown to regulate 25% of the liver phosphoproteome during the inactive phase in mice (28, 98). EGFR signaling is essential not only in liver homeostasis, but in the pancreas as well. EGFR signaling promotes insulin secretion in  $\beta$ -cells and insulin levels have been observed to be decreased in patients administered EGFR inhibitors (53, 131-133). EGFR inhibition or loss of function is linked to the development of skin rashes and skin inflammation (105, 106, 109, 110, 134). In fact, some of the compounds tested in this study cause a skin rash and related toxic responses upon exposure which is commonly referred to as chloracne (7, 81-86). This chloracne may be mechanistically distinct from the chloracne observed in people exposed to high levels of TCDD. EGFR signaling is also crucial in development and is highly expressed in the placenta. Diminished placental EGFR phosphorylation was observed in Yu-cheng women exposed to PCBs which correlated to lower birth weights (33, 121). Since EGFR signaling is physiologically relevant in liver, pancreas, skin, and *in utero* development this receptor-internalization assay should be considered for screening new chemical compounds for adverse health effects. Many EPA high-throughput screens focus on chemical-induced modulation of nuclear receptor activity, but new assays for RTKs should be considered as well. Since RTK activity regulates almost every facet within the cell including nuclear receptor activity, they should also be considered in adverse outcome chemical testing. The data demonstrate that although the structures of these compounds are diverse, they act through EGFR inhibition. This may allow for an additive risk assessment between these different classes of compounds for a variety of maladies including liver disease, pancreatic dysfunction, skin irritation, and developmental defects. Future *in vivo* studies will evaluate whether the compounds tested promote endocrine and metabolic disruption in a EGFR-dependent manner.

The mean serum levels of *trans*-nonachlor, PCB-126, and PCB-153 in NHANES demonstrate that many people in the general population may be at risk for EGFR inhibition by environmental chemicals. The IC<sub>50</sub> Values shown for the various EGFR inhibitors appear low and similar too or less than the human serum concentrations of these compounds. As these compounds are hydrophobic, with very high hexane:water partition coefficients, these compounds will accumulate on the cell surfaces of the monolayer rather than being evenly distributed in the

culture media. Likewise, the *in vivo* distribution of these compounds is very dependent on the pharmacokinetics of body distribution, being much higher in adipose, and potentially fatty liver. Thus, the observed IC<sub>50</sub> may be considerably lower than the serum concentration that is likely to manifest itself as EGFR inhibition *in vivo*. Future work is needed to establish what serum concentrations of these chemicals elicits EGFR inhibition in varied tissues *in vivo* leading to adverse effects.

Current risk assessment measures for adverse effects due to environmental exposures are limited. For dioxins acting through the aryl hydrocarbon receptor, toxic equivalency factors (TEFs) and toxic equivalencies (TEQs) have been determined, in part, through REP data (135). TEQ allows for analysis of the health effects of mixtures of dioxins with varying potencies. REPs for some environmental chemicals inhibiting EGFR were generated in this dissertation. Since the fluorescent EGF assay is a high throughput it may serve as a preliminary toxicity evaluation tool for other chemicals, generating additional REPs. If EGFR inhibition by environmental chemicals is additive, TEFs and TEQs for EGFR inhibiting chemicals could be generated in the future to aid in the evaluation of complex mixtures of these chemicals. I propose that this could be done in a fashion similar to what was developed for dioxins.

This study demonstrates that EGFR inhibition is a conserved mechanism for diverse EDCs/MDCs that were previously characterized as CAR activators. The high throughput methods used in this investigation may provide a model system for adverse outcome evaluation of new chemicals being manufactured. PCB-126, PCB-153, and *trans*-nonachlor are likely competitive antagonists of EGF binding to EGFR. In contrast, atrazine appears to act as a tyrosine kinase inhibitor that was predicted to bind to the ATP pocket of the EGFR TK domain. The predicted binding sites are indicative of hydrophobic interactions with nonpolar amino acids of the EGFR. Furthermore, this study establishes human specific REPs for EGFR signaling disrupting chemicals (SDCs) and documents two mechanisms for this inhibition. Future studies should determine if atrazine, *trans*-nonachlor, and chlordane diminish EGFR signaling *in vivo* similar to PCBs (96). Epidemiological studies should test whether exposure to these SDCs have additive risk for developmental, dermatological, and metabolic diseases.

CHAPTER 4  
PROTEOMIC ANALYSIS REVEALS MECHANISMS BY WHICH POLYCHLORINATED  
BIPHENYLS SENSITIZE THE LIVER TO DIETARY STEATOHEPATITIS

**INTRODUCTION**

Proteomics is a well-established discovery tool in both hepatology and environmental health research. In this study I aimed to characterize the proteomic alteration do to PCBs and a HFD. Based On the proteomic data I conducted pathway analysis and transcription factor analysis to elucidate mechanism for PCB-mediated steatohepatitis. Previously some PCBs have been shown to activate human and murine aryl hydrocarbon receptor (AhR) and some nuclear receptors [e.g., the pregnane x receptor (PXR) and the constitutive androstane receptor (CAR)]; while inhibiting epidermal growth factor receptor (EGFR) signaling (3, 36, 96, 139, 140). Knocking out PXR or CAR modulated but did not prevent the steatohepatitis associated with Aroclor 1260 and high fat diet co-exposures, implicating additional mechanisms (18). Nuclear receptor modulation by PCBs in the context of NAFLD is clinically relevant as activation of many hepatic nuclear receptors such as farnesoid X receptor (FXR), liver X receptor alpha (LXR $\alpha$ ), and peroxisome proliferator-activated receptors (PPARs) is considered therapeutic and many agonists for these receptors are in clinical trials currently (141, 142). I hypothesize that liver proteomics would discover new mechanisms for PCBs in liver disease progression using our established mouse model (3). Selected mechanisms were validated, and the potential influence of epidermal growth factor signaling was investigated in some cases.

## MATERIALS AND METHODS

### Animal Exposures

The mouse liver samples used in this study were obtained from archived (-80°C) tissues from a prior study (3). The workflow of this study is illustrated in figure 18A. Further description of these mice and samples can be found in chapter 2.

### Peptide Extraction, LC/MS/MS Analysis, MetaCore Analysis, and Data Sharing

Three samples per group were randomly selected for proteomic analysis. Mouse livers were homogenized in 1% SDS RIPA buffer. Proteins were reduced with DTT followed by denaturation with 8M Urea, alkylation with iodacetamide, these reagents were purchased from Sigma-Aldrich (St. Louis, MO). Peptides were digested with Trypsin purchased from Promega (Madison, WI) followed by enrichment and clean up with C18 filters purchased from The Nest Group (Southborough, MA). Protein lysates (100 µg per sample) were trypsinized using filter aided sample preparation (144). Peptide concentrations were measured by a bicinchoninic acid assay, and equal amounts of peptides were injected into the high-performance liquid chromatography machine in a 0.1% formic acid and 80% acetonitrile gradient. A Finnigan LTQ mass spectrometer (ThermoFisher) was used to collect mass spectral data from the LC eluate. The generated msf file from Proteome Discoverer were loaded into Scaffold Q+S v4.4.5. Scaffold was used to calculate the false discovery rate (FDR) using the Peptide and Protein Prophet algorithms.

### MetaCore Analysis

Cellular Localization Analysis, Pathways and Processes Analysis, and Transcription Factor Analysis (TFA) were performed using Metacore Software (Clarivate Analytics, Philadelphia, PA). Hepatic proteins that had significantly differential abundance (p-value < 0.05, by two-way ANOVA examining the diet and exposure factors) were analyzed by MetaCore software (Clarivate Analytics, Philadelphia, PA). Results that met the FDR threshold (< 0.05) were accepted. Transcription factors are listed by highest activity (largest z-score/target gene differential) to the lowest activity.

The data was analyzed with Proteome Discoverer v1.4.1.14. The database used in the Mascot v2.5.1 and SequestHT algorithms was the 3/7/2016 version of the UniprotKB Mus musculus reference proteome canonical and isoform sequences with the nonmurine sequences from the 1/1/2012 version of the gpm.org cRAP database appended to it. For the MetaCore TFA, when making direct comparisons between proteins of the HFD mice and the HFD plus Aroclor co-exposed mice, a criterion of at least a 3-fold increase or 2-fold decrease was used to select the proteins analyzed (Fig S3). Data files for acquired LCMS data (.RAW), search engine files (.mgf), peak list files (.mzML) files, and search results aggregated into a Scaffold3 (.sf3, ProteomeSoftware.com) will be deposited with MassIVE (<http://massive.ucsd.edu/>) data repository with the Center for Computational Mass Spectrometry at the University of California, San Diego and shared with the ProteomeXchange ([www.proteomexchange.org](http://www.proteomexchange.org))

## **Cell Culture**

### **Hepatocyte nuclear factor 4 alpha (HNF4 $\alpha$ ) phosphorylation assay**

AML-12 (CRL-2254) cells obtained from ATCC (Manassas, VA) were exposed to DMEM/F-12 media containing either EGF (1.2 nM) (EMD Millipore, Burlington, MA), Aroclor 1260 (10  $\mu$ g/mL) and EGF (1.2 nM), or 0.5% DMSO for 30 minutes then protein was extracted to measure phosphorylated Hnf4 $\alpha$ , total Hnf4 $\alpha$ , phosphorylated Egfr and total Egfr.

### **Nuclear factor (erythroid-derived 2)-like 2 (NRF2) protein stability assay**

A-431 (CRL-1555) cells obtained from ATCC (Manassas, VA) were exposed to media containing either EGF (1.2 nM), Aroclor 1260 (10  $\mu$ g/mL) and EGF (1.2 nM), or 0.5% DMSO for 2 hours then protein was extracted to measure total Nrf2 and  $\beta$ -actin.

### **Hepatic Stellate Cell (HSC) activation assay**

LX-2 cells were obtained from Sigma-Aldrich (St. Louis, MO) while HepG2 cells (HB-8065) were obtained from ATCC (Manassas, VA). Initially LX-2 and HepG2 cells were cultured in DMEM media containing either 10  $\mu$ g/mL of Aroclor 1260, or 0.5% DMSO. RNA was extracted at 24 hours, and

48 hours. Subsequently, some LX-2 cells were treated with conditioned media from the HepG2 cells and RNA was again prepared.

HepG2 cells are a male human hepatoblastoma cell line. AML-12 cells are mouse hepatocytes derived from a male transgenic mouse that expresses human TGF $\alpha$ . A-431 is a human epidermoid carcinoma cell line derived from a female patient. LX-2 cells are a human stellate cell derived cell line.

Cells were seeded at  $1 \times 10^4$  per well in 12-well plates and grown to confluence for 24 hours. HepG2, A-431 and LX-2 cells were grown in Dulbecco's modified Eagle's medium (DMEM) (VWR, Radnor, PA) supplemented with fetal bovine serum and 1% antimycotic/antibiotic solution (Mediatech, Manassas, VA). AML-12 cells were grown in 1:1 DMEM/F12 media (VWR Radnor, PA) supplemented with ITS Universal Culture Supplement Premix (VWR Radnor, PA), dexamethasone (40 ng/ml), 1% antimycotic/antibiotic solution (Mediatech, Manassas, VA) and 10% fetal bovine serum (VWR Radnor, PA). The cells were incubated in a 5% carbon dioxide atmosphere and 95% humidity at 37° and sub-cultured every 2 days.

### **Western Blot Analysis**

Liver tissue and cells were lysed in RIPA Buffer (100 mg tissue/0.5 mL RIPA supplemented with protease, and phosphatase inhibitors (10  $\mu$ L/mL, Sigma-Aldrich, St. Louis, MO). The following antibodies were used and purchased from Abcam (Cambridge, MA): Hnf4 $\alpha$ , Nrf2, Y1173 EGFR; Thermo-scientific (Waltham, MA): S313 Hnf4 $\alpha$ ; Cell Signaling Technology (Danvers, MA):  $\beta$ -actin; and Santa Cruz (Dallas, TX) EGFR. Full description of western blot analysis methods can be found in chapter 2.

### **Real-time PCR Analysis**

Mouse livers or cells were homogenized, and total RNA was extracted using the RNA-STAT 60 protocol (Tel-Test, Austin, Texas). RNA integrity and quantity were determined with the Nanodrop

(ND-1000, Thermo Scientific, Wilmington Delaware) using the ND-1000 V3.8.1 software package. cDNA was synthesized from total RNA using the QuantiTect Reverse Transcription Kit (Qiagen, Valenci, California). PCR was performed on the BioRad CFX384 Real-Time System using the BioRad iTaq Universal Probes Supermix. Taqman Gene Expression Assays (Thermo-Fisher). Gene expression levels were calculated according to the  $2^{-\Delta\Delta Ct}$  method, and Gapdh was used as the endogenous control.

The following primers were used obtained from Applied Biosystems (): Actin alpha 2, smooth muscle, aorta (*Acta2*); (Hs00426835\_g1) Alpha tocopherol transfer protein (*Ttpa*), (Mm00803828\_m1); Aryl hydrocarbon receptor (*Ahr*); (Mm00478932\_m1), Cytochrome P450, family 2, subfamily c, polypeptide 29, (*Cyp2c29*), (Mm00725580\_s1), Eukaryotic translation initiation factor 4b (*Eif4b*); (Mm00778003\_s1), Glyceraldehyde-3-phosphate dehydrogenase (*Gapdh*); (Mm99999915\_g1) (Hs02786624\_g1); Glutamate-cysteine ligase catalytic subunit (*Gclc*); (Mm00802655\_m1), Glutathione S-Transferase Mu 1 (*Gstm1*); (Mm00833915\_g1), Malic enzyme 1 (*Me1*); (Mm00782380\_s1), Myocyte enhancer factor 2c (*Mef2c*); (Mm01340842\_m1), NAD(P)H quinone oxidoreductase (*Nqo1*); (Mm01253561\_m1), Platelet derived growth factor alpha (*Pdgfa*); (Hs00234994\_m1), Perilipin-2 (*Plin2*); (Hs00605340\_m1), Pyruvate kinase liver and RBC (*Pklr*); (Mm00443090\_m1), and Transforming growth factor-beta (*Tgf-β*); (Hs00998133\_m1). Gapdh was used as a control.

### **Total Glutathione Assay**

Total glutathione concentration was determined by the method of Griffith (145, 146). Liver tissue was homogenized in PBS and centrifuged allowing determination of total thiol (predominately glutathione) through a colorimetric recycling assay at 412 nm. Total glutathione was normalized to liver protein.

### **Statistical Analysis**

Western blot densitometry values, RNA expression values, and glutathione measurements were statistically analyzed using Graphpad Prism Version 7 for Macintosh (San Diego, CA). The data



are expressed as box and whisker plots. Western blot analysis data in figure 21C were compared using one-way ANOVA. qPCR data in figure 23A-C were statistically compared using an unpaired t-test. All other *in vitro* and *in vivo* datasets were compared using two-way ANOVA.  $P < 0.05$  was considered statistically significant. Quantified peptides from MS analysis were statistically compared by two-way ANOVA with a looping two-way ANOVA script in R software package.

## RESULTS

### **Liver proteomic analysis identifies protein alterations due to HFD, Aroclor 1260, and their interaction in a steatohepatitis mouse model**

Mice fed a HFD developed dietary steatosis, but mice fed a HFD and exposed to Aroclor 1260 developed steatohepatitis (57). Control diet fed mice exposed to Aroclor 1260 did not develop steatosis or steatohepatitis (Fig 18A). Significant alterations with protein expression occurred with Aroclor 1260 exposure (154 increased, 93 decreased), HFD (239 increased, 137 decreased), and their interaction (60 increased, 179 decreased) (Fig 18B). These raw mass spectrometry data have been deposited in the MassIVE data repository. Cellular localization of proteins affected is shown in Figure 18C. The proteins significantly altered by a HFD are localized primarily in the mitochondria ( $p = 3e^{-25}$ ) and ER ( $p = 3.5e^{-19}$ ). Proteins significantly altered by Aroclor 1260 exposure are localized primarily within cytoskeleton, ( $p = 8.4e^{-10}$ ). Proteins localized to cytoskeletal regions ( $p = 8.6e^{-7}$ ), were also significantly affected by the interaction of a HFD and Aroclor exposure.

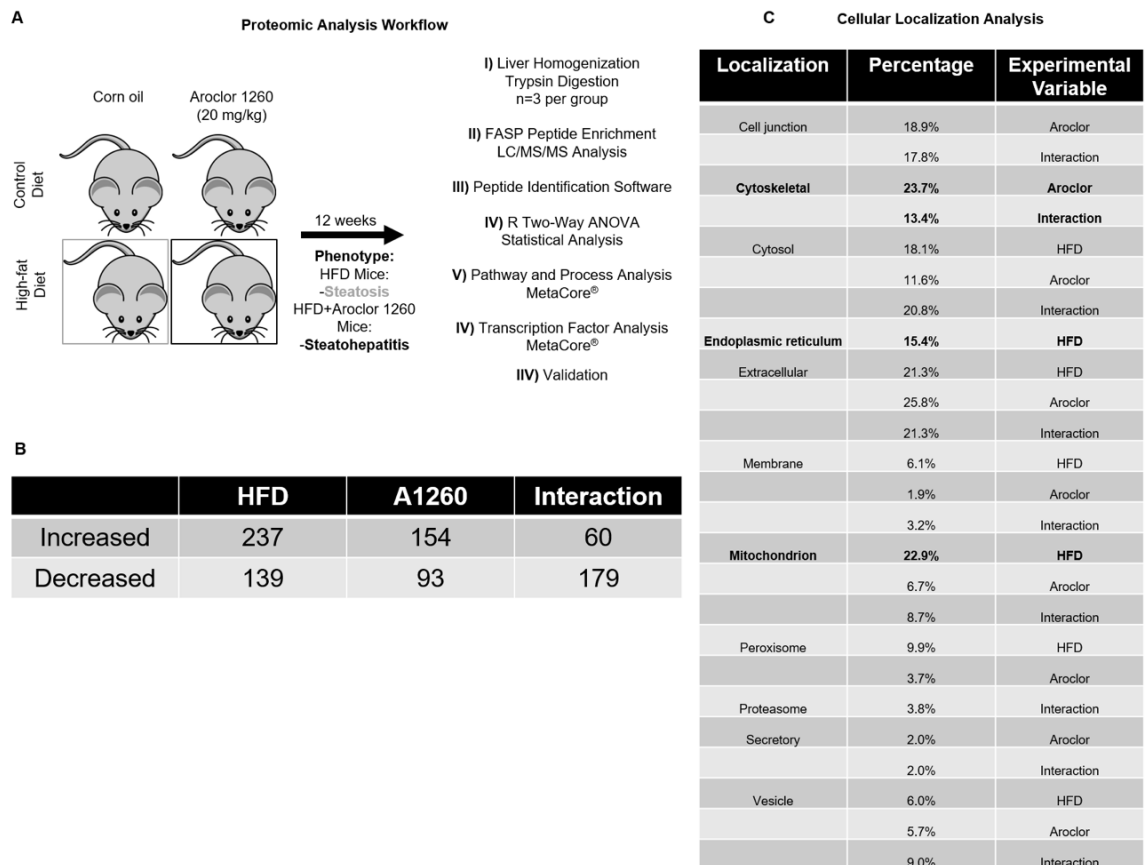


**Figure 18. Liver proteomic analysis identifies proteomic alterations due to HFD, Aroclor 1260, and their interaction in a steatohepatitis mouse model: A.** Proteomic analysis workflow of mouse liver sample to characterize the hepatic events in the progression of dietary steatosis to steatohepatitis. **B.** Significant ( $p=0.05$ ) differential abundances of hepatic proteins due to a HFD, Aroclor 1260 exposure, and their interaction. **C.** Cellular localization of the significant proteins for each variable. Three biological replicates per group was used for the proteomic analysis (12 in total). Peptide abundances were compared by two-way ANOVA and only peptides that were significant ( $p<0.05$ ) were investigated further.

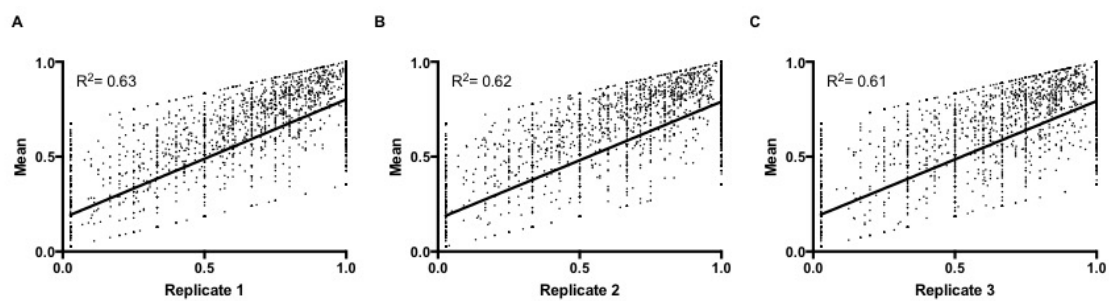


**Figure 19. Linear relationship of peptide expression between biological replicates in LC/MS/MS:** The relative peptide value from each of the biological replicates of each group has a linear relationship with the mean of each quantitative peptide value as is shown in Fig 19**A-C**. Mean vs. replicate 1 ( $R^2 = 0.63$ ), Mean vs. replicate 2 ( $R^2 = 0.62$ ), Mean vs. replicate 3 ( $R^2 = 0.61$ ) demonstrate that the quantitative values for each protein are similar between biological replicates for each of the respective groups.

### **Pathway and processes analysis of proteins altered by either a HFD, Aroclor exposure, or their interaction**

A number of pathways and processes were significantly affected by HFD (n=78), Aroclor 1260 (n=30), or the interaction between the two (n=55). These full results are provided in Tables 2,3,4, and a subset of these are summarized in Fig. 19. Pathways altered by HFD included enhanced endoplasmic reticulum (ER) stress ( $p=3.02e^{-13}$ ) and diminished oxidative phosphorylation ( $p=8e^{-5}$ ). These findings are consistent with previously published studies (147, 148). Pathways and processes altered by Aroclor exposure included cytoskeletal processes and muscle contraction ( $p=5.8e^{-13}$ ), possibly consistent with hepatic stellate cell activation (149); and reduced FXR regulation of glucose and lipid metabolism ( $p=0.002$ ). Aroclor 1260 and HFD interacted to enrich similar cytoskeletal pathways ( $p=0.0001$ ); while diminishing glutathione metabolism ( $p=4e^{-5}$ ); and altering intermediary metabolism.

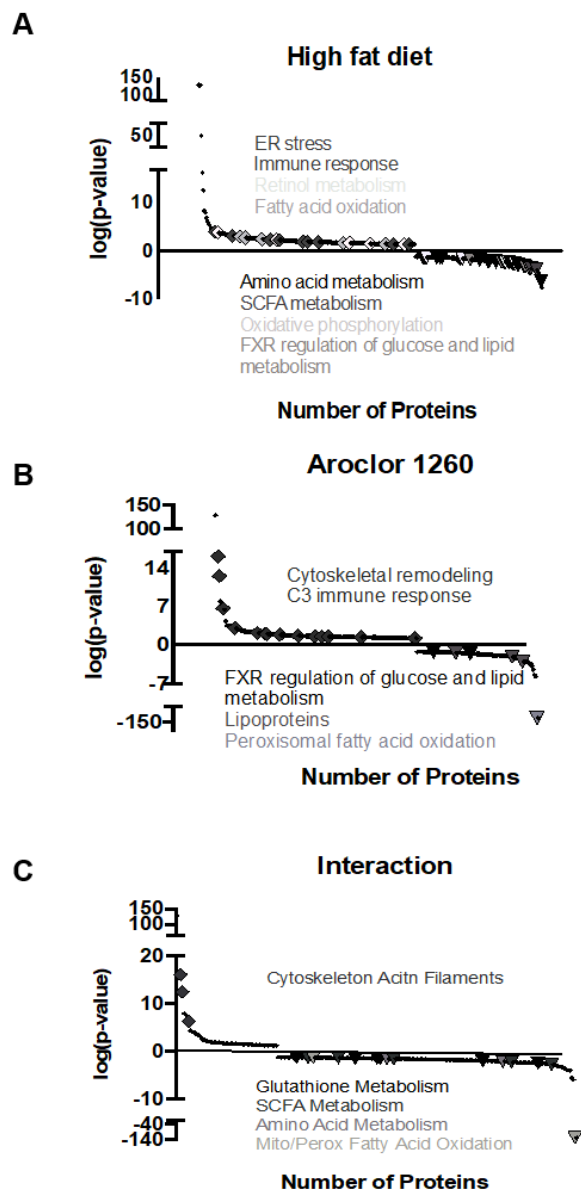


**Figure 20. Pathway analysis of proteins altered by either a HFD, Aroclor exposure or their interaction: A.**  $-\text{Log}(p\text{-value})$  plots and pathway analysis of proteins significantly altered by HFD, **B** Aroclor exposure, or their **C** interaction. Complete list of pathways, processes and statistics are listed in tables 2,3,4 in the supplementary data. All pathways and processes identified through MetaCore analysis had to meet a FDR threshold  $<0.05$ .

Pathways or Processes Enriched by a HFD

Pathway or Process	p-value
Retinol metabolism	9.243E-07
Peroxisomal straight-chain fatty acid beta-oxidation	0.00001685
CFTR folding and maturation (normal and CF)	0.00002797
Vitamin E (alpha-tocopherol) metabolism	0.00003063
Immune response_Antigen presentation by MHC class I_classical pathway	0.00004985
Immune response_Antigen presentation by MHC class I: cross-presentation	0.00009507
n-3 Polyunsaturated fatty acid biosynthesis	0.0001051
Transcription_Negative regulation of HIF1A function	0.0001313
Estradiol metabolism	0.0002659
Peroxisomal branched chain fatty acid oxidation	0.0003864
Triacylglycerol metabolism p.1	0.001046
n-6 Polyunsaturated fatty acid biosynthesis	0.001113
Ascorbate metabolism	0.001169
Fatty Acid Omega Oxidation	0.001434
Oxidative stress_Role of ASK1 under oxidative stress	0.002068
Nitrogen metabolism	0.002441
Regulation of degradation of deltaF508-CFTR in CF	0.003074
Regulation of lipid metabolism_PPAR regulation of lipid metabolism	0.0038
Cholesterol metabolism	0.0041
Mechanisms of deltaF508 CFTR activation by S-nitrosoglutathione	0.005225
Tryptophan metabolism	0.006255
Apoptosis and survival_Endoplasmic reticulum stress response pathway	0.008513
Regulation of degradation of wtCFTR	0.009716
Oxidative stress_Role of Sirtuin 1 and PGC1-alpha in activation of antioxidant defense system	0.01029
Role of ZNF202 in regulation of expression of genes involved in atherosclerosis	0.01069
Immune response_Antigen presentation by MHC class II	0.01188
Signal transduction_mTORC2 upstream signaling	0.01279
Cholesterol and Sphingolipid transport/ Recycling to plasma membrane in lung (normal and CF)	0.01384
Development_Glucocorticoid receptor signaling	0.01497
Leucine, isoleucine and valine metabolism p.2	0.02149
Linoleic acid metabolism	0.02255
Transport_intracellular cholesterol transport	0.02444
Glycolysis and gluconeogenesis	0.0276
Sulfur metabolism	0.0283
Estrone metabolism	0.0283
Propionate metabolism p.1	0.02982
Cholesterol and Sphingolipid transport/ Transport from Golgi and ER to the apical membrane (normal and CF)	0.03138
Bile Acid Biosynthesis	0.03364
Transport_Regulation of ATP-binding transporters by Retinoic acid and orphan nuclear receptor PXR	0.03458
Regulation of metabolism_Bile acids regulation of glucose and lipid metabolism via FXR	0.0379
Apoptosis and survival_TNF-alpha-induced Caspase-8 signaling	0.04134
Pentose phosphate pathway	0.0431
L-Alanine and L-cysteine metabolism	0.0431
Niacin-HDL metabolism	0.0467

Pathways or Processes Diminished by a HFD

Pathway or Process	p-value
Glycine_serine_cysteine and threonine metabolism	3.657E-06
L-Arginine metabolism	0.00003094
Folic acid metabolism	0.0001287
Oxidative phosphorylation	0.0001375
Urea cycle	0.0001606
Aspartate and asparagine metabolism	0.0002403
Glycolysis and gluconeogenesis	0.0005435
Transcription_Effect of Folic acid on genome stability	0.001156
Ubiquinone metabolism	0.002515
Glycogen metabolism	0.00285
Aldosterone biosynthesis and metabolism	0.003078
Lysine metabolism	0.00319
L-Alanine and L-cysteine metabolism	0.004674
Tryptophan metabolism	0.00687
Cortisone biosynthesis and metabolism	0.007072
Selenoamino acid metabolism	0.008286
Tricarboxylic acid cycle	0.009159
Mitochondrial dysfunction in neurodegenerative diseases	0.01057
Phenylalanine metabolism	0.01431
Tyrosine metabolism p.1 (dopamine)	0.01739
Catecholamine metabolism	0.02082
Histamine metabolism	0.0209
Cysteine-glutamate metabolism	0.0209
Development_Transcription factors in segregation of hepatocytic lineage	0.02228
Leucine, isoleucine and valine metabolism p.2	0.02304
Androstenedione and testosterone biosynthesis and metabolism p.2	0.02515
Peroxisomal branched chain fatty acid oxidation	0.02619
Sulfur metabolism	0.02973
Propionate metabolism p.1	0.03132
Nitrogen metabolism	0.03132
dATP/dITP metabolism	0.03697
Regulation of metabolism_Bile acids regulation of glucose and lipid metabolism via FXR	0.03978
Estradiol metabolism	0.04156
Androstenedione and testosterone biosynthesis and metabolism p.3	0.04156
Cell adhesion_Histamine H1 receptor signaling in the interruption of cell barrier integrity	0.04709

**Table 2. Full list of pathways and processes significantly increased or decreased by a HFD:**

All of the significant pathways and processes that are representative of the significant peptides ( $p < 0.05$ ) due to a HFD.

Pathways or Processes Enriched by Aroclor 1260 Exposure

Pathway or Process	p-value
Immune response_Lectin induced complement pathway	1.59E-09
Immune response_Classical complement pathway	2.28E-09
Immune response_Alternative complement pathway	2.28E-09
Alternative complement cascade disruption in age-related macular degeneration	8.2E-07
Complement pathway disruption in thrombotic microangiopathy	0.00011
Immune response_CCR3 signaling in eosinophils	0.000829
Cytoskeleton remodeling_Regulation of actin cytoskeleton by Rho GTPases	0.001399
Apoptosis and survival_Granzyme A signaling	0.00238
Linoleic acid metabolism	0.00254
Retinal ganglion cell damage in glaucoma	0.005297
Immune response_IC3b-induced phagocytosis via alpha-M/beta-2 integrin	0.009561
Transport_Macropinocytosis regulation by growth factors	0.01017
Lysine metabolism	0.01567
Oxidative phosphorylation	0.02579
Immune response_Regulatory role of C1q in platelet activation	0.036
Cytoskeleton remodeling_Substance P mediated membrane blebbing	0.03835
Cytoskeleton remodeling_Alpha-1Aadrenergic receptor-dependent inhibition of PI3K	0.04539
Cell cycle_Chromosome condensation in prometaphase	0.05005

Pathways or Processes Diminished by Aroclor 1260 Exposure

Pathway or Process	p-value
Regulation of lipid metabolism_Regulation of lipid metabolism via LXR, NF-Y and SREBP	0.001905
Regulation of metabolism_Bile acids regulation of glucose and lipid metabolism via FXR	0.002215
Regulation of lipid metabolism_Insulin signaling: generic cascades	0.002902
Transcription_Sirtuin6 regulation and functions	0.00532
Peroxisomal straight-chain fatty acid beta-oxidation	0.006873
Glycolysis and gluconeogenesis	0.009645
Regulation of lipid metabolism_Insulin regulation of fatty acid metabolism	0.01008
NAD metabolism	0.01753
Regulation of lipid metabolism_Regulation of acetyl-CoA carboxylase 2 activity in muscle	0.03236
Regulation of lipid metabolism_Regulation of fatty acid synthase activity in hepatocytes	0.03236
Transcription_ChREBP regulation pathway	0.03904
Adiponectin in pathogenesis of type 2 diabetes	0.04889

**Table 3. Full list of pathways and processes significantly increased or decreased by Aroclor 1260 exposure:** All of the significant pathways and processes that are representative of the significant peptides (p<0.05) due to a Aroclor 1260 exposure.

Pathways or Processes Enriched by Interaction

Pathway or Process	p-value
Cytoskeleton_Actin filaments	9.196E-05
Development_Skeletal muscle development	3.5E-04
Muscle contraction	8.11e-04
Oxidative phosphorylation	0.005614
Development_Delta- and kappa-type opioid receptors signaling via beta-arrestin	0.02543
CFTR folding and maturation (normal and CF)	0.02652
Development_NOTCH1-mediated pathway for NF-KB activity modulation	0.0287
Platelet activation during ADAM-TS13-deficient thrombotic microangiopathy development	0.03088
Cysteine-glutamate metabolism	0.03197
NETosis in SLE	0.03414
Signal transduction_Activin A signaling regulation	0.0363
Sulfur metabolism	0.03846
Estrone metabolism	0.03846
DNA damage_Nucleotide excision repair	0.03954
Transcription_Role of heterochromatin protein 1 (HP1) family in transcriptional silencing	0.04385
Transcription_Sin3 and NuRD in transcription regulation	0.04492
Transcription_Role of Akt in hypoxia induced HIF1 activation	0.04492
Estradiol metabolism	0.04599
N-Glycan biosynthesis p2	0.04707
Development_Notch Signaling Pathway	0.04707
L-Alanine and L-cysteine metabolism	0.04814

Pathways or Processes Diminished by Interaction

Pathway or Process	P-value
Immune response_Lectin induced complement pathway	4.97E-08
Immune response_Classical complement pathway	7.11E-08
Immune response_Alternative complement pathway	7.11E-08
Leucine, isoleucine and valine metabolism.p.2	7.95E-07
Tryptophan metabolism	2.84E-06
Alternative complement cascade disruption in age-related macular degeneration	7.53E-06
Propionate metabolism p.1	1.39E-05
Complement pathway disruption in thrombotic microangiopathy	1.92E-05
Butanoate metabolism	0.00013
Glutathione metabolism	0.000195
Lysine metabolism	0.000311
Mitochondrial unsaturated fatty acid beta-oxidation	0.000844
Development_Angiotensin activation of Akt	0.000901
Triacylglycerol metabolism p.1	0.00195
Propionate metabolism p.2	0.002243
Role of ZNF202 in regulation of expression of genes involved in atherosclerosis	0.003385
L-Arginine metabolism	0.004266
Mitochondrial long chain fatty acid beta-oxidation	0.0049
Mitochondrial ketone bodies biosynthesis and metabolism	0.005568
Histamine metabolism	0.006407
Glycogen metabolism	0.01029
Pentose phosphate pathway	0.01435
Retinal ganglion cell damage in glaucoma	0.01498
Cell adhesion_Histamine H1 receptor signaling in the interruption of cell barrier integrity	0.01498
Gamma-aminobutyrate (GABA) biosynthesis and metabolism	0.02042
Oxidative stress_Role of Sirtuin1 and PGC1-alpha in activation of antioxidant defense system	0.02576
Immune response_CD16 signaling in NK cells	0.03335
Tyrosine metabolism p.1 (dopamine)	0.03514
Inhibition of neutrophil migration by proresolving lipid mediators in COPD	0.03514
Retinol metabolism	0.03514
Catecholamine metabolism	0.03978
Blood coagulation_GPIb-IX-V-dependent platelet activation	0.04074
HETE and HPETE biosynthesis and metabolism	0.04564
Peroxisomal branched chain fatty acid oxidation	0.04664

**Table 4. Full list of pathways and processes significantly increased or decreased by interaction of a HFD and Aroclor exposure:** All of the significant pathways and processes that are representative of the significant peptides (p<0.05) due to an interaction.



## Transcription factor analysis (TFA) results

TFA predicted significant alterations in transcription factor activity with HFD (n=51), Aroclor 1260 (n=42), or their interaction (n=19) (Table 5A-C). HFD increased activity of transcription factors associated with cellular stress [e.g., transcription factor AP-1 (cJun) ( $p=5.5e^{-5}$ ), and nuclear factor NF-kappa-B p65 subunit (NFkB) ( $p=0.004$ )]; and ER stress [e.g., activating transcription factor-6 (ATF-6) ( $p=1.3e^{-7}$ ), activating transcription factor-4(ATF-4) ( $p=0.0006$ ), and X-box binding protein-1 (XBP1) ( $p=0.0008$ )]. Aroclor exposure increased transcriptional activity of the myofibroblast specific transcription factors, myogenic differentiation factor 1 (MYOD) ( $p=0.0007$ ) and BarH-like homeobox gene 2 (BARX2) ( $p=3.3e^{-5}$ ). The interaction between HFD and Aroclor decreased the transcriptional activities of NRF2 (the central regulator of the antioxidant response,  $p=0.0002$ ) and five nuclear receptors [e.g., HNF4 $\alpha$  ( $p=0.0004$ ), hepatocyte nuclear factor gamma (HNF4 $\gamma$ ) ( $p=0.002$ ), estrogen receptor 1 (ESR1) ( $p=0.0002$ ), thyroid receptor beta (TR $\beta$ ) ( $p=0.0004$ ), and LXR $\alpha$  ( $p=0.0004$ )]. The observed reduction in HNF4 $\alpha$  could be pathologically meaningful because HNF4 $\alpha$  is a key regulator of hepatocyte differentiation and function. The preceding results were determined by two-way ANOVA. TFA was also performed through comparison of the HFD plus Aroclor 1260 (HFD+) vs. HFD treated groups of mice by fold-change thresholds (Table 6). Although some differences exist in the TFA results generated by the different methods, NRF2 and HNF4 $\alpha$  remained negatively regulated in both. Myocyte enhancer factor 2c (MEF2C), a positive regulator of HSC activation was increased ( $p=1.6e^{-06}$ ) in HFD+ vs. HFD. By and large, the TFA results support the pathway and process results. Based on consistency, intermediary metabolism (HNF4 $\alpha$ ), glutathione metabolism (NRF2), and cytoskeletal remodeling/fibrosis (MEF2C) were validated.

**A** HFD Transcription Factor Analysis

Transcription Factor	Target Gene Differential	Z-Score Differential	p-value
ATF-6 alpha (50kDa)	6	11.69	8.5e-08
TAFI170	3	7.937	0.0003
Androgen receptor	3	7.937	0.0008
TAF12	2	7.567	0.0007
C/EBPalpha	2	7.567	0.0003
PPAR-alpha	12	7.241	3.12e-06
TFIID 30 kDa subunit	2	6.609	0.0009
TFIID 31 kDa subunit	2	6.609	0.003
HNF3-beta	2	6.609	0.001
ATF-6 alpha (90kDa)	3	6.51	0.001
TR-beta	8	5.803	1.8e-09
GATA-4	9	5.775	2.9e-05
TAF4 (TAFII130)	2	5.64	0.005
TAF5	2	5.64	0.006
ESR1 (nuclear)	30	5.502	2.7e-06
c-Jun	21	4.817	2.4e-05
ATF-4	7	4.691	0.0005
XBP1	7	4.645	0.0006
PPAR-gamma	13	4.449	6.2e-05
FXR	7	4.447	0.0008
RelA (p65 NF-kB subunit)	21	4.318	0.0008
p53	25	4.046	0.0003
HSF1	9	3.898	0.001
RelB (NF-kB subunit)	7	3.861	0.0004
NRF2	-3	3.78	0.0008
LHX2	11	3.512	0.002
HNF3-alpha	7	3.427	0.004
FOXO3A	7	3.357	0.0003
NF-kB1 (p50)	11	3.276	0.003
FKHR	8	3.212	0.007
c-Fos	9	3.133	0.006
HNF4-alpha	10	3.073	9.6e-12
GCR	2	-0.025	6.5e-06
SP1	-4	-1.84	6.6e-06
C/EBPbeta	8	-2.245	5.8e-06
c-Myc	0	-3.767	1.56e-16
YY1	-18	-3.85	0.0003
ERR1	-6	-3.865	0.002
LXR-alpha	-4	-3.71	6.9e-05
NURR1	-3	-5.265	0.002
SP4	-4	-5.305	0.0009
ROR-gamma	-3	-5.521	0.002
BACH1	-3	-5.709	0.001
SREBP1 precursor	-4	-5.753	0.0009
NRF1	-7	-6.094	0.0002
CREB-H	-3	-6.659	0.0007
ERR3	-7	-7.256	0.002
MLX	-2	-7.35	0.002
SREBP1 (nuclear)	-9	-8.192	6.6e-05
HNF1-alpha	-14	-9.272	3.82e-10
SREBP2 (nuclear)	-7	-9.464	3.1e-07

**B** Aroclor 1260 Transcription Factor Analysis

Transcription Factor	Target Gene Differential	Z-Score Differential	p-value
BARX2	4	8.939	2.4e-06
TR-beta	9	8.623	1.9e-07
TAF3	2	7.383	0.002
C/EBPbeta	6	5.317	0.0002
GATA-4	6	5.021	0.0004
C/EBPbeta	13	4.922	1.1e-05
Androgen receptor	17	4.892	8.1e-06
TBP	5	4.855	0.0008
MYOD	6	4.847	0.0006
p53	19	4.616	3.8e-05
XBP1	5	4.408	0.002
C/EBPalpha	8	3.873	0.002
LHX2	8	3.576	0.002
CREB-H	1	0.788	0.0004
ESR1 (nuclear)	7	0.718	0.0001
c-Myc	12	0.688	4e-06
LXR-beta	1	0.557	0.001
SP1	8	0.454	0.0002
HNF4-alpha	0	-2.204	2.5e-05
HNF1-alpha	-4	-3.536	0.007
SREBP1 (nuclear)	-3	-3.816	0.008
PPAR-gamma	-5	-3.866	0.004
HNF3-alpha	-4	-3.913	0.005
USF1	-4	-3.99	0.004
NRF2	-4	-4.003	0.004
PPAR-alpha	-4	-4.097	0.004
PPAR-beta(delta)	-3	-4.136	0.006
NFYA	-4	-4.52	0.002
FBX1	-3	-4.769	0.004
Oct-3/4	-14	-5.119	1.6e-05
HIF1A	-10	-5.268	0.0003
BACH1	-2	-5.729	0.005
TR-alpha	-4	-5.782	0.0005
HFOX13	-2	-5.525	0.004
RXRA	-6	-6.718	3.4e-05
Securin	-2	-6.933	0.002
FXR	-6	-7.6	1.1e-5
ZNF202	-2	-7.856	0.001
SREBP1 precursor	-4	-8.937	3.8e-05
MLX	-2	-10.99	0.0004
ZNF395	-1	-12.4	0.006
LXR-alpha	-8	-13.17	9.6e-10

**C** Interaction Transcription Factor Analysis

Transcription Factor	Target Gene Differential	Z-Score Differential	p-value
hnRNP D-like	1	20.68	0.002
ZBPAT	1	20.68	0.002
GABP beta1	2	9.571	0.0009
ATF-6 alpha (50kDa)	2	7.899	0.001
HNF3-alpha	5	6.269	0.0001
TR-beta	4	6.057	0.0004
p53	9	3.713	0.001
ESR1 (nuclear)	-19	-3.557	0.0002
NFYA	-8	-4.235	0.002
<b>HNF4-alpha</b>	<b>-12</b>	<b>-4.418</b>	<b>0.0002</b>
C/EBPbeta	-14	-4.521	9.7e-05
<b>NRF2</b>	<b>-8</b>	<b>-5.316</b>	<b>0.0001</b>
KLF15	-3	-5.765	0.001
NFYC	-3	-6.092	0.001
CHREBP	-5	-6.342	0.0001
LXR-alpha	-7	-7.281	6.1e-06
HNF4-gamma	-2	-7.298	0.002
MLX	-2	-7.298	0.002
c-Myc	-20	-7.298	1.6e-05

**Table 5. Transcription factor analysis results:** TFA of proteins significantly diminished or enriched by experimental variables. **Table 5A.** HFD, **Table 5B.** Aroclor exposure, or **Table 5C.** interaction. All the transcription factors identified by MetaCore analysis had to meet a FDR threshold <0.05.

### HFD+ (Steatohepatitis) vs. HFD (Dietary Steatosis) Transcription Factor Analysis

Transcription Factor	Target Gene Differential	Z-Score Differential	p-value
PLAG1	2	9.092	0.0006
SIX4	4	8.493	2.8e-05
MYOD	16	7.835	4.3e-09
SP7	4	5.969	0.0005
MEF2C	8	5.799	1.64e-06
ERR3	9	5.687	5.54e-06
SRF	19	5.163	9.02e-06
YB-1	9	4.797	0.0002
PROX1	5	4.751	0.0009
SREBP1 (nuclear)	9	4.657	0.0002
SIX1	4	4.623	0.002
MEF2D	7	4.573	7.9e-05
TR-beta	9	4.252	0.0001
RXRA	10	3.938	0.001
C/EBPbeta	21	3.52	0.0003
NANOG	22	3.189	0.001
E2F1	24	3.155	0.002
YY1	2	1.214	4.04e-7
c-Myc	1	1.186	3e-09
SP1	-2	0.372	0.0001
p53	-2	0.258	8.2e-06
SREBP1 precursor	-1	-0.686	8e-05
<b>HNF4-alpha</b>	<b>-19</b>	<b>-3.37</b>	<b>0.0005</b>
ESR1 (nuclear)	-39	-3.851	6e-05
CREB1	-120	-3.895	1.8e-06
Oct-3/4	-41	-4.269	2.1e-05
FXR	-11	-4.909	0.0001
<b>NRF2</b>	<b>-14</b>	<b>-5.378</b>	<b>4.1e-06</b>
CAR	-4	-5.596	0.0008
PTF1-p48	-4	-5.744	0.0008

**Table 6. Transcription factor analysis of HFD vs HFD+ (steatosis vs. steatohepatitis) peptide data:** Transcription factors determined to have increased or decreased activity based on the peptide fold-changes in steatosis as compared to steatohepatitis samples are listed in Table 6.

### **Aroclor 1260 reduced HNF4 $\alpha$ protein expression and activity, and HNF4 $\alpha$ is a downstream phosphorylation target of the EGFR**

Aroclor 1260 exposure significantly reduced HNF4 $\alpha$  protein levels ( $p=0.02$ ) in mice fed either control diet (56% decrease) or HFD (47% decrease); and HFD significantly reduced HNF4 $\alpha$  mRNA levels ( $p=0.006$ , Fig. 20Ai-ii). Proteomics demonstrated that several HNF4 $\alpha$  target genes were reduced by Aroclor 1260 at the protein level, so mRNA expression for some of these was determined. Albumin mRNA was reduced by Aroclor 1260 exposure ( $p=0.0001$ ), and was markedly suppressed (78%, HFD+ vs. HFD) by a pollutant-diet interaction ( $p=0.0003$ , Fig. 20Bi). Likewise, cytochrome P450 family 2 subfamily c (Cyp2c29) mRNA was decreased 7.6% in HFD+ vs. HFD by a pollutant-diet interaction ( $p=0.03$ , Fig. 20Bii). Ttpa (tocopherol transfer protein) was diminished 12.2% in HFD+ vs. HFD due to interaction ( $p=0.01$ , Fig. 20Biii).

Since PCBs disrupt EGFR signaling, interactions between EGF and PCBs on HNF4 $\alpha$  were evaluated *in vitro* (Fig. 20C). Compared to vehicle control, EGF treatment significantly increased the relative phosphorylation of both EGFR ( $p=0.02$ ) and HNF4 $\alpha$  ( $p=0.02$ ) in AML-12 cells (Fig. 20Ci-ii). These changes were attenuated by Aroclor 1260 exposure as seen by a 46% decreased in EGF vs. EGF+A1260 for phosphorylated EGFR; and a 63% decrease for phosphorylated HNF4 $\alpha$  (Fig. 20Ci-ii). Expression of the HNF4 $\alpha$  target gene, pyruvate kinase, liver and RBC (Pklr) was increased by EGF ( $p=0.0005$ ) at the mRNA level, and this was attenuated 26% by Aroclor 1260 ( $p=0.002$ , Fig. 20D). In total, these data demonstrate that HNF4 $\alpha$  protein, but not mRNA expression, is downregulated by Aroclor 1260 exposure. HNF4 $\alpha$  function was reduced by Aroclor 1260 and/or the interaction between Aroclor 1260 and HFD. The latter interaction may potentially contribute to the observed transition from steatosis to steatohepatitis. Reduction in EGF-dependent HNF4 $\alpha$  phosphorylation by PCBs partially explains the diminished HNF4 $\alpha$  activity. These data validate the observed alterations in some of the intermediary metabolism pathways/processes and TFA.

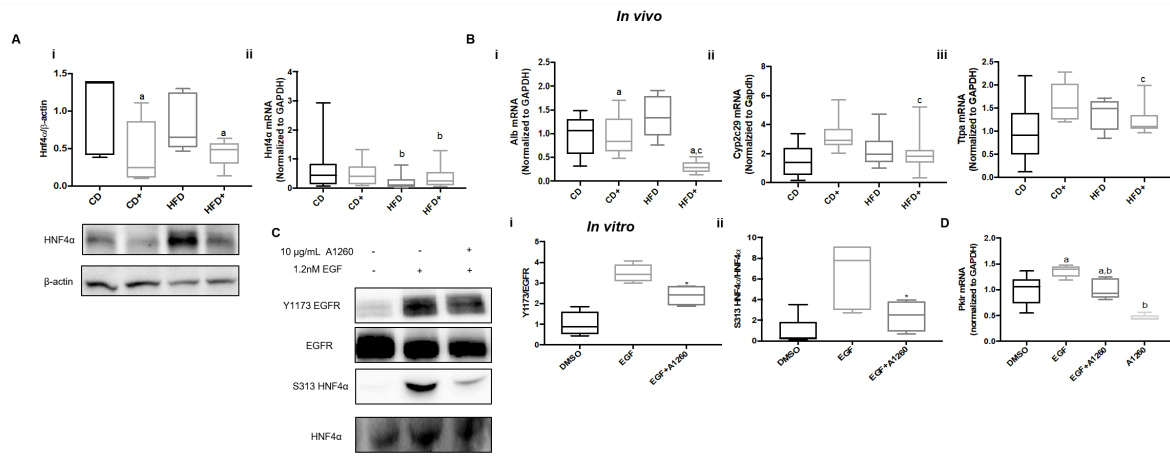


**Figure 21. Aroclor 1260 reduced HNF4 $\alpha$  protein expression and activity, and HNF4 $\alpha$  is a downstream phosphorylation target of the EGFR: A. (i) Immunoblot analysis, and (ii) RT qPCR analysis of hepatic HNF4 $\alpha$  protein and mRNA from mice fed a control diet (CD), control diet and exposed to Aroclor 1260 (20 mg/kg) (CD+), fed a HFD (HFD), and fed a HFD and exposed to Aroclor 1260 (20 mg/kg) (HFD+). B. RT qPCR Analysis of HNF4 $\alpha$  target genes (i) Albumin, (ii) Cyp2c29, and (iii) Ttpa from murine liver. C. Western blot analysis of (i) Y1173 EGFR and (ii) HNF4 $\alpha$  S313 phosphorylation in AML-12 cell lysates exposed to DMSO (0.5%), EGF (1.2 nM), and EGF+A1260 (1.2 nM EGF, 10  $\mu$ g/mL). D. RT qPCR analysis of HNF4 $\alpha$  target gene Pklr in AML-12s after 6-hour incubation with either DMSO (0.5%), EGF (1.2 nM), EGF+A1260 (1.2nM EGF, 10  $\mu$ g/mL), or A1260 (10  $\mu$ g/mL). All data are represented as box and whisker plots. An n=5 was used for the HNF4 $\alpha$  protein levels analysis *in vivo*, an n=10 for Hnf4 $\alpha$  mRNA and HNF4 $\alpha$  target gene mRNA *in vivo*, an n=4 for HNF4 $\alpha$  S313 phosphorylation, and an n=4 for Pklr mRNA. A P<0.05 is denoted with \*. In the *in vivo* datasets an a denotes significance due to Aroclor, b HFD, and c interaction. Two-way ANOVA was used to statistically compare the *in vivo* data. One-way ANOVA was used for the statistical analysis for Fig 20Ci-ii. A two-way ANOVA was used for the statistical analysis in Fig 20D; an a denotes significance due to EGF, b due to Aroclor.**

### **Aroclor 1260 reduced NRF2 protein/mRNA expression and glutathione levels, and NRF2 is an EGF-sensitive target**

Hepatic NRF2 protein and mRNA, and total glutathione were diminished by Aroclor exposure *in vivo* ( $p=0.04$ ,  $p=0.02$ , and  $p=0.03$  respectively, Fig. 21Ai-iii). In control diet fed mice, Aroclor 1260 reduced NRF2 protein by 73%, NRF2 mRNA by 28%, and glutathione by 67%. In HFD-fed mice, Aroclor 1260 reduced NRF2 mRNA by 16%, glutathione by 51%, and NRF2 target gene mRNA [NAD(P)H quinone dehydrogenase 1 (Nqo1), glutathione s-transferase mu 1 (Gstm1), and malic enzyme 1 (Me1)] in liver *in vivo* ( $p=0.014$ ,  $p=0.015$ , and  $p=0.004$ , respectively, Fig. 21Bi-iii). Aroclor 1260 decreased Nqo1 27% in CD-fed mice and 96% in HFD-fed mice; Me1 37% in CD-fed mice and 60% in HFD-fed mice; and Gstm1 64% in HFD-fed mice. Glutamate-cysteine ligase catalytic subunit (Gclc) was decreased 41% by HFD/Aroclor 1260 interaction (vs. HFD,  $p=0.045$ , Fig. 21Biv).

Next, the potential interactive effects of EGF and PCBs were determined on NRF2 protein expression *in vitro* (Figure 22C). EGF-treated A-431 cells had significantly higher NRF2 expression after two hours, suggesting that NRF2 is stabilized by EGF treatment alone as seen by a 72% increase. Aroclor 1260 greatly attenuated this effect ( $p=0.01$ ) as demonstrated by a 49% decrease with EGF and A1260. These data by and large confirm the results regarding glutathione metabolism and NRF2 activity from the pathway/processes analyses and the TFA with some caveats. The protein and gene expression studies demonstrate that the reduction in glutathione metabolism and NRF2 expression/activity are predominantly Aroclor 1260 effects, rather than pollutant-diet interaction effects. While the TFA demonstrated that both Aroclor 1260 and the pollutant-diet interaction impacted NRF2 activity, the glutathione metabolism pathway/process was only affected by the interaction. PCBs may inhibit EGF-dependent NRF2 stabilization by disrupting EGFR signaling.

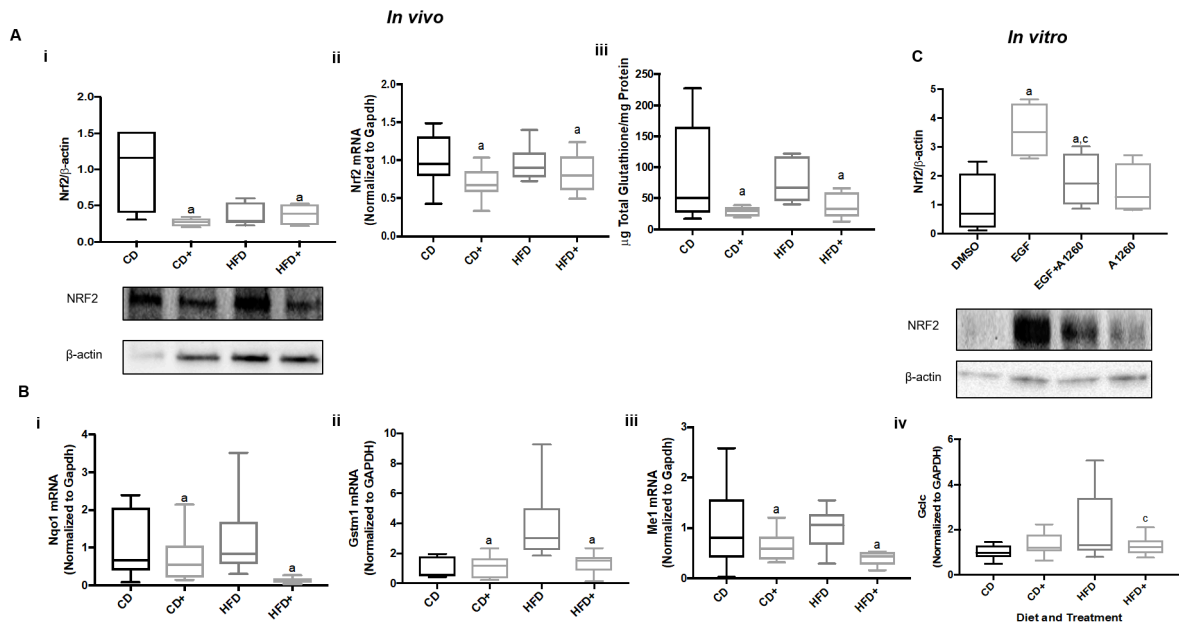


**Figure 22. Aroclor 1260 reduced NRF2 protein/mRNA expression and glutathione levels, and NRF2 is an EGF-sensitive target: A. (i)** Immunoblot analysis, **(ii)** RT qPCR of hepatic NRF2 protein and mRNA, respectively, and **(iii)** total glutathione measurements from mice fed a control diet (CD), control diet and exposed to Aroclor 1260 (20 mg/kg) (CD+), a HFD (HFD), and HFD and exposed to Aroclor 1260 (20 mg/kg). **B.** RT qPCR analysis of hepatic NRF2 target genes **(i)** Nqo1, **(ii)**, Gstm1, **(iii)** Me1, and **(iv)** Gclc in murine liver. **C. (i)** Immunoblot analysis of NRF2 protein expression in A-431 cells exposed to either DMSO (0.5%), EGF (1.2 nM), EGF+A1260 (1.2nM EGF, 10  $\mu$ g/mL), or A1260 (10  $\mu$ g/mL) for 2 hours. A  $p < 0.05$  is denoted by a for Aroclor, b for HFD/EGF or c for interaction in the *in vivo* datasets. All data are represented as box and whisker plots. A sample size of 5 was used for the analysis of the NRF2 protein levels *in vivo*, an  $n = 10$  for NRF2 mRNA and NRF2 target gene mRNA *in vivo*. An  $n = 4$  was used for the NRF2 *in vitro* assay and an a denotes significance due to EGF, and c for interaction. Two-way ANOVA was used to statistically compare all of these datasets for Fig 22.

### **Aroclor exposure activates HSCs through hepatocyte-derived TGF- $\beta$**

Hepatic stellate cells (HSCs) normally store Vitamin A and can transdifferentiate into proliferative myofibroblasts or “activated” HSCs. Since pathway/process analysis and TFA demonstrate that cytoskeletal processes were increased by both Aroclor exposure and the pollutant-HFD interaction, I hypothesized that Aroclor 1260 could activate HSCs. Additionally I aimed to determine if activation of HSCs is hepatocyte mediated or a direct effect on HSCs. This was tested *in vitro*. In cultured LX-2 cells (immortalized human HSCs), Aroclor 1260 did not directly increase actin, alpha 2, smooth muscle, aorta (ACTA2) (active HSC marker) or decrease perilipin 2 (PLIN2) (quiescent HSC marker) mRNA expression (Fig. 22Ai-ii). In contrast, conditioned media from Aroclor 1260-exposed HepG2 cells increased ACTA2 gene expression in LX-2 at 48 hours by 93% (P=0.006, Fig. 22Bi-ii). PLIN2 was unaffected. Aroclor 1260 exposure increased expression of the key fibrogenic cytokine, transforming growth factor-beta (TGF- $\beta$ ), in HepG2 cells by 45% (p=0.03, Fig. 22Cii, but did not change platelet derived growth factor alpha (PDGF $\alpha$ ) expression (Fig 22Ci). Hepatic mRNA expression of MEF2C was significantly increased by 28% (HFD+ vs. HFD) by Aroclor 1260 exposure *in vivo*, confirming TFA results. These data confirm the proteomics results and suggest that PCBs may be pro-fibrotic. PCB-induced stellate cell activation may be indirectly mediated by hepatocyte-derived TGF- $\beta$ .



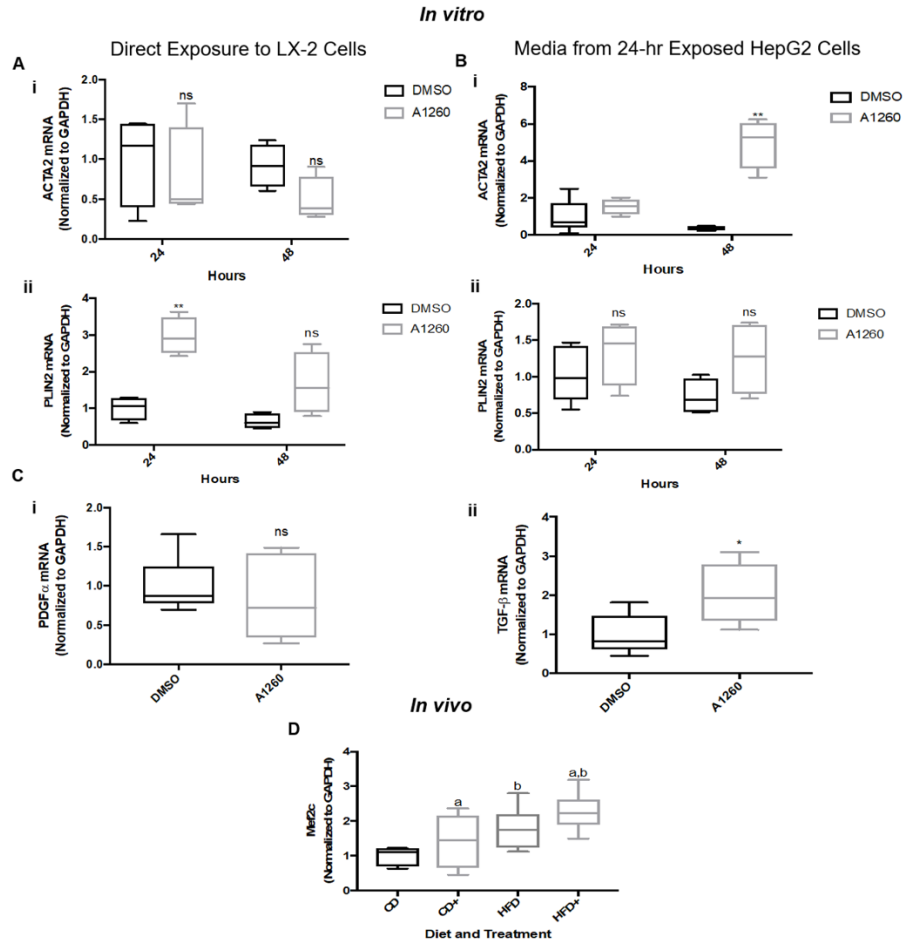


**Figure 23. Aroclor exposure activates HSCs through hepatocyte-derived TGF- $\beta$ :** **A.** RT qPCR analysis of **(i)** ACTA2 and **(ii)** PLIN2 in LX-2 cells directly exposed to either DMSO (0.5%) or A1260 (10  $\mu$ g/mL) for 24 or 48 hours. **B.** RT qPCR analysis of **(i)** ACTA2 and **(ii)** PLIN2 in LX-2 cells exposed to HepG2 media from HepG2 cells exposed to either DMSO (0.5%) or A1260 (10  $\mu$ g/mL) for 24 hours. **C.** Gene expression analysis of **(i)** PDGF $\alpha$  and **(ii)** TGF- $\beta$  in HepG2 cells directly exposed to either DMSO (0.5%) or A1260 (10  $\mu$ g/mL) for 24 hours. **D.** RT qPCR analysis of MEF2C in murine liver of mice fed a control or HFD with either exposure to Aroclor 1260 (20 mg/kg) or vehicle control. A  $p < 0.05$  is denoted with \*,  $p < 0.01$  \*\*. A  $p < 0.05$  is denoted by a for Aroclor, b for HFD or c for interaction. A  $n = 4$  was used for figure 23A-C,  $n = 10$  for figure 23D and the data are presented as box and whisker plots. A two-tailed t-test was used to statistically compare datasets Fig 22A-C and a two-way ANOVA for 18D.

## DISCUSSION

While PCBs have long been associated with liver disease in animal models and more recently, cohort studies, their mode of action remains elusive. This liver proteomics study demonstrates that the mechanisms of PCBs in fatty liver disease progression are multifactorial and complex. While PCB research has primarily focused on the positive PCB responses (e.g., activation of AhR, PXR, CAR, etc.), this study demonstrates that the negative responses to Aroclor 1260 and/or the PCB-HFD interaction generally outnumber the positive ones. Some of the down-regulated pathways and processes were related to hepatocyte function (e.g., metabolism of fatty acids, amino acids, and carbohydrates as well as albumin production) and protection (e.g. the antioxidant response). Key results from the TFA include the negative regulation of NRF2 and myriad nuclear receptors previously implicated in NAFLD (e.g., HNF4 $\alpha$ , FXR, PPAR $\alpha/\delta/\gamma$ , TR $\alpha$ , ER $\alpha$ , RXR $\alpha$ , etc.). Vitamin E is an established treatment for non-alcoholic steatohepatitis (NASH), and many nuclear receptor agonists (e.g., FXR, PPAR $\alpha/\delta$ , TR $\beta$ , etc.) are currently being investigated in NASH clinical trials (150). If antioxidants and nuclear receptor agonists have therapeutic roles in NASH, it is plausible that their reduction by PCBs may be pathogenic.

While the mechanisms of negative regulation of transcription factors by PCBs is largely unknown, this dissertation demonstrates that their regulation may be indirect and related reduced transcription factor expression and EGF-dependent phosphorylation. Perhaps a phosphoproteomics study is required in the future. While mice fed control diet and treated with Aroclor 1260 did not develop NAFLD pathology, the antioxidant and nuclear receptor down-regulation should theoretically sensitize these mice to hypercaloric diets (3). This was indeed the case, as HFD+ mice developed steatohepatitis, while HFD mice developed only steatosis. Human confirmation of these results is required. However, if confirmed, the results could have meaningful clinical implications with regards to NASH pathogenesis and treatment. Moreover, it would solve an important paradox facing endocrine disrupter research. In the US, metabolic diseases like NAFLD have increased in prevalence while overall environmental pollution has declined. However,

if low-level pollution sensitizes to the obesity-related diseases mediated by hypercaloric diets, as suggested by our animal data, then the paradox would be explained.

I propose that progression of dietary steatosis to steatohepatitis is due to a two-hit paradigm. High fat diet is one hit and PCB exposure being the other (3). Before this study, there was limited characterization of the mechanisms/processes in the hit of PCB exposure. In contrast, characterization of the processes in the liver impacted by a HFD are well known, and our results are consistent with previous studies (147, 148). From the pathway and TFA analysis, ER stress response and inflammatory pathways and transcription factors are upregulated due to a HFD. This has been demonstrated in the livers of HFD fed animals previously and ER stress is heavily implicated in dietary steatosis (147, 148). Mitochondrial dysfunction due HFD downregulation of oxidative phosphorylation enzymes was observed from the pathway analysis. This is a common feature in the livers of diet-induced obese mice (151). The first step in the development of dietary steatosis from a HFD seems to be lipid accumulation promoting ER stress and mitochondrial dysfunction. PPAR $\alpha$ , a key transcriptional regulator of lipid metabolism, was predicted to be downregulated with Aroclor 1260 exposure but elevated with a HFD which is consistent with previous studies (3).

It has been demonstrated that PCBs act, in part, through hepatic EGFR inhibition (96, 140). EGFR signaling is critical for liver function and thus, can affect the expression and activity of many proteins. EGFR signaling has been shown to regulate nuclear receptors and transcription factors, but very few studies have characterized its effects on liver identity factors, such as HNF4 $\alpha$ . HNF4 $\alpha$  is a critical nuclear receptor for liver function that has been shown to transcriptionally regulate 60% of liver specific genes; HNF4 $\alpha$ -null mice spontaneously develop NAFLD (152). Previously, loss of HNF4 $\alpha$  has been demonstrated in chemical induced liver injury, but has not been shown for PCB exposure (153) or steatohepatitis (154)

The data demonstrate that HNF4 $\alpha$  and its target genes were downregulated in steatohepatitis similar to other EGF-sensitive transcription factors (96). Albumin, a gene regulated by HNF4 $\alpha$ , has

been shown in human studies to be downregulated with elevated PCBs levels which corroborates this data (13). HNF4 $\alpha$  was then shown to be regulated by EGF signaling by phosphorylation of HNF4 $\alpha$  at S313. The transcription of the HNF4 $\alpha$  target gene, Pklr, was also increased with EGF versus Aroclor 1260 exposure. This EGFR-HNF4 $\alpha$  signaling pathway may be very critical for maintaining liver homeostasis and function (155). Thus, any disruption due to environmental chemicals may act, in part, to promote steatohepatitis

Pathway analysis and TFA identified both glutathione metabolism and NRF2 as being downregulated in steatohepatitis. This observation is consistent with our previous metabolomic studies showing that hepatic glutathione is diminished in a PCB-153 treated HFD fed mouse model (156). Since NRF2 transcriptionally regulates enzymes involved in glutathione synthesis, it was important to validate this finding. NRF2 expression and target genes were diminished with Aroclor exposure *in vivo* as was total glutathione. NRF2 is the main transcriptional regulator of glutathione biosynthesis in the liver and loss of NRF2 greatly limits the liver's endogenous antioxidant capacity. This loss then creates a more pro-oxidative environment that is implicated in the loss of oxidative phosphorylation (151). While loss of total hepatic GSH was not exacerbated in HFD+ as compared to CD+ the GSH:GSSG ratios were not measured. Moreover, the pro-oxidants were not measured. I postulate that HFD+ would have increased pro-oxidants and a decreased GSH:GSSG ratio. This means that the transition from steatosis to steatohepatitis could be mediated by increased oxidative stress in the absence of an upregulate antioxidant response to this stress. Since the HFD increases lipid peroxides, mitochondrial dysfunction and ER stress, the loss of the antioxidant defense system would leave the hepatocyte compromised and susceptible to necrosis (3, 157). This effect would not require the generation of active PCB intermediates *via* cytochrome P450 metabolism, that would need to be detoxified by glutathione conjugation and may explain how the effect occurs in either PCB 153 and now Aroclor 1260 exposed mice when neither this congener nor the PCB mixture is metabolized at an appreciable extent (15). Finally, this EGFR-NRF2 signaling pathway has been well characterized in *C. elegans*, but not in mammalian livers (158) and our observations indicate that this pathway is very likely conserved.

Our data suggest that Aroclor exposure alone *in vivo* can activate HSCs, but it was more pronounced in the livers of mice fed a HFD and exposed to PCBs. In cell culture models, PCBs did not directly activate HSCs. PCBs however did stimulate HepG2 cells to increase expression of the potent HSC activating factor, TGF- $\beta$ . MEF2C, which was predicted to be upregulated in the livers of mice that develop steatohepatitis was elevated at the RNA level and maximum in mice that developed steatohepatitis. MEF2C is an HSC transcription factor that regulates fibrotic gene expression upon HSC activation (159). These data suggest that PCB exposures can promote a fibrotic response through a mechanism involving TGF- $\beta$  production from hepatocytes and MEF2C upregulation. While histologically liver fibrosis was not increased in this model it has been reported in other PCB exposure models that have either longer periods of PCB exposures and/or certain dietary conditions (3, 139). These data suggest that fibrosis in response to PCBs should be re-evaluated in other model systems and human subjects as the data suggest PCBs promote the early stages of fibrosis (e.g. HSC activation).

In conclusion, this study demonstrates that NRF2 and HNF4 $\alpha$  are two EGF-sensitive transcription factors whose activity is downregulated due to PCB exposure in steatohepatitis. Our work demonstrates HSC activation through PCB-mediated effects on hepatocytes. This study also demonstrated that many nuclear receptors that are clinical drug targets for NASH (e.g. FXR, LXR $\alpha$ , PPARs) are downregulated with PCBs. This is the first proteomic study to characterize the effects of PCBs in the progression from dietary steatosis to steatohepatitis and has identified three novel findings: downregulation of NRF2 (antioxidant defense); HNF4 $\alpha$  (liver homeostasis) effects, and activation of HSCs (fibrotic response). Collectively, the data suggests that PCB exposure downregulates the hepatoprotective responses making the liver susceptible to damage caused by a HFD leading to steatohepatitis.

## CHAPTER 5

### PCBs ARE SIGNALING DISRUPTING CHEMICALS THAT PROMOTE SECONDARY NECROSIS IN TASH

#### INTRODUCTION

Elevated PCB body burden in residents of the Anniston, AL cohort is positively associated with liver necrosis marker cytokeratin 18 (KRT18) (13). In animal models that mimic these human exposures, the development of PCB-mediated toxicant associated steatohepatitis (TASH) is contingent upon both the exposure and feeding of a high fat diet (HFD). PCB exposure has been shown to elicit a transcriptional response of xenobiotic metabolizing genes mediated through the constitutive androstane receptor (CAR) (22, 90-92). PCBs were considered direct CAR agonists, but my recent work has demonstrated that they may also act through epidermal growth factor receptor (EGFR) inhibition leading to CAR activation (96, 140). EGFR is a receptor tyrosine kinase that is highly expressed in the liver but little is known about its physiological role in liver homeostasis and metabolism (24). EGFR can regulate the phosphorylation state of many downstream targets including, but not limited to CAR, hepatocyte nuclear factor 4 alpha (HNF4 $\alpha$ ), and nuclear factor (erythroid-derived 2)-like 2 (NRF2) (19). Deficits in cell signaling has a continued relevance in metabolic disease with loss of insulin signaling and diabetes being the strongest example (160). Loss of other signaling pathways in the context of metabolic disease are understudied and may be just as critical as insulin signaling. Kinase inhibition is tightly associated with cell death and is possibly a key event in the development of steatohepatitis. To characterize the complexity of PCB-mediated signaling disruption in the liver, a phosphoproteomic approach was used. In this study, I aimed to characterize the dietary and PCB-mediated effects on the hepatic phosphoproteome in an animal model of TASH and determine how PCBs promote cell death in TASH.

## MATERIALS AND METHODS

### **Animal Studies.**

The C57Bl/6 (male) mouse liver samples used in this study were obtained from archived (-80°C) tissues from a previous study (3). This study used a protocol approved by the University of Louisville Institutional Animal Care and Use Committee. Guidelines provided by the NIH guide for the care and use of laboratory animals were abided by for this research. In this study, three samples per group were randomly selected and used for the proteomic study. The mice fed a HFD and treated with Aroclor 1260 developed steatohepatitis as demonstrated by CAE and H&E staining, elevated pro-inflammatory cytokine and liver enzymes profiles (3).

### **Protein Sample Preparation**

Mouse liver tissue were homogenized in 1% SDS RIPA buffer. Protein lysate (100 µg) per sample was prepared and trypsinized using the filter aided sample prep (FASP) protocol (144). Phosphopeptides were then further enriched with TiO<sub>2</sub> and purified using C18 columns (161). Peptide concentrations were measured by a bicinchoninic acid assay to determine the recovery amount to use for subsequent liquid chromatography and mass spectrometry analysis.

### **Liquid Chromatography**

The columns used were an Acclaim PepMap 100 75µm x 2cm, nanoViper (C18, 3µm, 100Å) trap, and an Acclaim PepMap RSLC 50µm x 15cm, nanoViper (C18, 2µm, 100Å) separating column (ThermoFisher Scientific, Waltham, MA, USA). An EASY-nLC 1000 UHPLC system (ThermoFisher, Waltham, MA) was used with solvents A = 2% v/v acetonitrile / 0.1% v/v formic acid and B = 80% v/v acetonitrile / 0.1% v/v formic acid as mobile phases. Following injection of 500ng of sample onto the trap, separation was accomplished at 300 nL/min with a 110-minute linear gradient from 0% B to 50% B, followed by a 5min linear gradient from 50% B to 95% B, and lastly a 5min wash with 95% B. A 40mm stainless steel emitter (ThermoFisher, Waltham, MA) was coupled to the outlet of the separating column. A Nanospray Flex source (ThermoFisher, Waltham, MA) was used to position the end of the emitter near the ion transfer capillary of the mass spectrometer. The ion transfer capillary temperature of the mass spectrometer was set at 225°C,

and the spray voltage was set at 1.6 kV. Other chromatography settings are provided as supplemental material.

### **Mass Spectrometry**

An Orbitrap Elite – ETD mass spectrometer (ThermoFisher) was used to collect data from the LC eluate. An Nth Order Double Play was created in Xcalibur v2.2. Scan event one of the methods obtained an FTMS MS1 scan (normal mass range; 240,000 resolution, full scan type, positive polarity, profile data type) for the range 300-2000m/z. Scan event two obtained ITMS MS2 scans (normal mass range, rapid scan rate, centroid data type) on up to twenty peaks that had a minimum signal threshold of 5,000 counts from scan event one. The lock mass option was enabled (0% lock mass abundance) using the 371.101236m/z polysiloxane peak as an internal calibrant. Other method settings are provided as supplemental information.

### **Data Analysis with Peaks Studio 7.5**

The raw data files were analyzed separately with Peaks Studio 7.5 using the UniprotKB mouse reviewed canonical and isoform protein sequences current as of 3/21/2017 and the Denovo, PeaksDB, and PeaksPTM algorithms. Identifications at the 1% FDR threshold from the PeaksDB and PeaksPTM results were loaded into the Peaks Label Free Quantification algorithm. Other analysis settings are provided as supplemental information. Data files for acquired LCMS data (.RAW), search engine files (.mgf), peak list files (.mzML) files, and search results aggregated into a Scaffold3 (.sf3, ProteomeSoftware.com) will be deposited with MassIVE (<http://massive.ucsd.edu/>) data repository with the Center for Computational Mass Spectrometry at the University of California, San Diego and shared with the ProteomeXchange ([www.proteomexchange.org](http://www.proteomexchange.org)).

### **MetaCore Analysis**

Proteins with significantly different abundances ( $p < 0.05$ ) with a HFD, Aroclor exposure, or interaction were analyzed with MetaCore pathway, processes, and pathology ontologies. Only pathways, processes, pathologies identified with a false discovery rate (FDR) less than or equal to 0.05 were accepted.



### **PhosphoScanSite Analysis**

Phosphosites were searched using the Massachusetts Institute of Technology's free software PhosphoScansite 3. Low, medium, and high stringency thresholds were used to identify potential kinases that regulate these phospho-substrates.

### **Cell Culture.**

Primary human hepatocytes obtained from BioreclamationIVT supplemented with Invitrogro Hepatocyte Media and Torpedo antibiotic solution (BioreclamationIVT, Westbury, NY). The cells were plated on collagen plates and incubated in a 5% carbon dioxide atmosphere and 95% humidity at 37° C.

### **Cellomic Cell Death Assay**

Primary human hepatocytes were exposed to either 0.5% DMSO or Aroclor 1260 (10 µg/mL) for 6 and 24 hours. At each time point cells were stained with Hoechst 33342 (Thermo-Scientific, Waltham, MA) and imaged. Data for DNA fragmentation percent (Cells below 2N DNA content) and nuclear area were taken at each time point. Apoptosis and necrosis demonstrate DNA fragmentation but apoptotic nuclei are smaller, thus enabling these two factors to be used to distinguish between live, apoptotic, and necrotic cells (162).

### **Western Blot Analysis.**

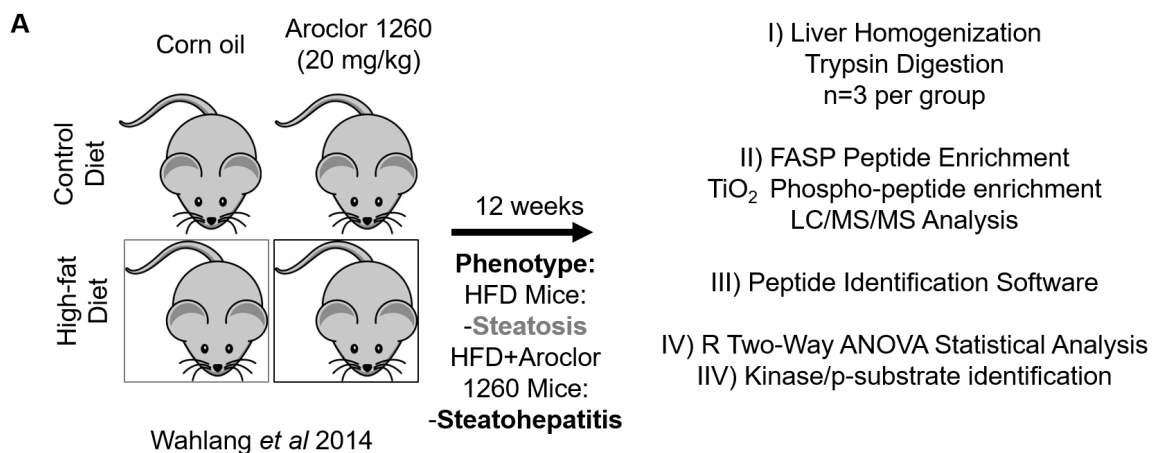
Mouse liver lysates were homogenized in RIPA Buffer (100 mg tissue/0.5 mL RIPA supplemented with protease, and phosphatase inhibitors 10 µl/mL, (Sigma-Aldrich, St. Louis, MO)). The following primary antibodies were used: CK2 $\alpha$ , CK2 phosphosubstrate, PP2 $\alpha$ , and CASP3 (Cell Signaling Technology, Danvers, MA); CK2 $\beta$ , PTP1B, S150 CASP3 (abcam Cambridge, UK). Full description of western blot analysis can be found in chapter 2.

**Statistical Analysis.** Western blot densitometry values, quantified RNA values were statistically analyzed using GraphPad Prism Version 7 for Macintosh (San Diego, CA). The data are expressed as box and whisker plots. Data was compared using two-way ANOVA. P<0.05 was considered statistically significant. Quantified peptides were statistically compared by two-way ANOVA with a looping two-way ANOVA script in R software package.

## RESULTS

### **Phosphoproteomic analysis identifies phosphorylated substrates altered by a HFD, Aroclor**

**exposure, and their interaction.** Due to PCBs being demonstrated to be hepatic EGFR antagonists and EGFR regulates many downstream targets in the liver, an unbiased phosphoproteomic approach was implemented to identify the effects of diet and PCBs on the hepatic phosphoproteome. Fig 24A illustrates the phosphoproteomic workflow and analysis of murine liver from control diet (CD) fed mice or HFD fed mice with or without exposure to Aroclor 1260 (20 mg/kg). Fig 23B demonstrates that 113 phospho-peptides were significantly increased, while 104 were decreased due to a high fat diet. Aroclor 1260 exposure decreased levels of 131 phospho peptides and increased 46. The interaction between a HFD and Aroclor exposure decreased 185 phospho peptides and increased only 9. A majority of the phospho-peptides are significantly diminished with Aroclor 1260 exposure and/or interaction suggesting that PCBs are signaling disrupting chemicals.



**B**

	HFD	A1260	Interaction
Increased	113	46	9
Decreased	104	131	185

**Figure 24. Phosphoproteomic analysis identifies phosphorylated substrates altered by Aroclor 1260 exposure, a HFD, and their interaction: A.** Phosphoproteomic workflow is illustrated. **B.** A HFD enriched 113 p-peptides and diminished 104 p-peptides. Aroclor 1260 exposure enriched 46 p-peptides and diminished 131. The interaction of the two variables enriched 9 p-peptides and diminished 185. Phospho-peptide abundances were compared by two-way ANOVA and only peptides that were significantly changed ( $P < 0.05$ ) were investigated further.

### **MetaCore pathway, processes, and pathology analysis of significant peptides**

Proteins with significant different abundances of phosphosites due to a HFD, Aroclor exposure, or their interaction were analyzed with MetaCore ontologies. **Table 7A** demonstrates that a HFD affected ontologies involved in lipid accumulation, adiponectin signaling, and lipoprotein assembly. **Table 7B** illustrates that Aroclor exposure affects pathways involved in PI3K, insulin, and LXR signaling. **Table 7C** demonstrates that HFD and Aroclor interaction affected liver necrosis and protein chaperones.

**A****HFD affected Pathways, Processes, and Pathologies**

Pathway, Process, or Pathology	p-value	FDR
Liver-lipid accumulation, microvesicular SCAP/SREBP Transcriptional Control of Cholesterol and FA Biosynthesis	2.98E-05	6.86E-03
Signal transduction_Amino acid-dependent mTORC1 activation	1.12E-04	2.67E-02
HSP70 and HSP40-dependent folding in Huntington's disease	1.75E-04	2.67E-02
Butanoate metabolism	3.31E-04	2.74E-02
Adiponectin in pathogenesis of type 2 diabetes	3.60E-04	2.74E-02
Transport_Low density lipoproteins assembly and remodeling	5.17E-04	3.16E-02
	8.31E-04	4.22E-02

**B****Aroclor affected Pathways, Processes, and Pathologies**

Pathway, Process, or Pathology	p-value	FDR
SCAP/SREBP Transcriptional Control of Cholesterol and FA Biosynthesis	4.88E-05	5.24E-03
Development_Leptin signaling via PI3K-dependent pathway	5.32E-05	5.24E-03
Butanoate metabolism	1.58E-04	1.04E-02
Insulin-dependent stimulation of SREBP-1 in type 2 diabetes in liver	2.49E-04	1.23E-02
DNA damage_DBS repair	4.38E-04	2.63E-02
Regulation of lipid metabolism_Regulation of lipid metabolism via LXR, NF-Y and SREBP	6.22E-04	2.45E-02
Regulation of metabolism_Bile acids regulation of glucose and lipid metabolism via FXR	7.78E-04	2.56E-02
Transcription_Epigenetic regulation of gene expression	2.03E-03	5.0E-02
Propionate metabolism p.2	2.71E-03	5.0E-02
Regulation of lipid metabolism_Regulation of acetyl-CoA carboxylase 1 activity	2.82E-03	5.0E-02
Transport_RAN regulation pathway	2.82E-03	5.0E-02
Transcription_Sirtuin6 regulation and functions	2.83E-03	5.0E-02

**C****Interaction affected Pathways, Processes, and Pathologies**

Pathway, Process, or Pathology	p-value	FDR
Liver-necrosis	2.85E-07	1.42E-04
Liver pathology	1.32E-05	3.30E-03
Possible regulation of HSF-1/ chaperone pathway in Huntington's disease	1.52E-04	2.57E-02
Huntingtin-dependend transcription deregulation in Huntington's Disease	2.29E-04	2.57E-02
Liver-necrosis	2.85E-07	1.42E-04

**Table 7: MetaCore pathway, processes, and pathology analysis of peptides affected by a HFD, Aroclor, and their interaction** **A.** Ontologies affected by a HFD, **B.** Aroclor exposure, and **C.** interaction. Phospho-peptides that were significant by two-way ANOVA were used for this analysis and only pathways that met the FDR of 0.05 were used.

**PhosphoScanSite 3 analysis of the significant phosphopeptide demonstrates that many kinases are downregulated with Aroclor exposure and the Aroclor and HFD interaction.**

Using the significant p-substrates and the direction of their abundance was altered due to experimental variables, a kinome analysis was conducted. Fig 25A demonstrates that some kinases were predicted to have higher activity, while others were lower with a HFD. Fig 25B shows that a majority of the kinases are predicted to have lower activity with Aroclor exposure. Fig 25C suggests that all of the kinome is downregulated due to the interaction of a HFD and Aroclor exposure. This would suggest that in the development of TASH, loss of phosphoprotein signaling is a key step.

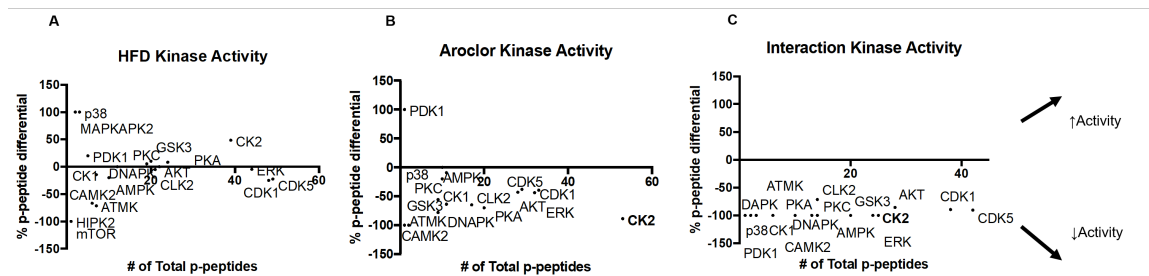


**Figure 25: PhosphoScanSite 3 analysis of the significant phosphopeptides demonstrates that many kinases are downregulated with Aroclor exposure and the Aroclor and HFD interaction**  
**A.** The kinome changes predicted to be altered by a HFD, **B.** Aroclor exposure, **C.** or interaction. P-peptides that were significantly different by two-way ANOVA were used in the PhosphoScanSite 3 analysis to determine what kinase regulates the substrate.

**PP2 $\alpha$  and PTP1b were not significantly upregulated with Aroclor exposure suggesting the cumulative loss of phosphoprotein signaling is due to loss of signaling.** Since the levels of protein phosphorylation are dramatically downregulated with PCB exposure and with dietary interaction, the expression of phosphatases was assessed. Fig 26A-B demonstrate that Ser/Thr phosphatase PP2 $\alpha$  and Tyr phosphatase PTP1B were not significantly changed with PCB exposure or diet. This suggests that the loss of phosphoproteins and kinase activity cannot be explained by increased phosphatase levels, but loss of activation through phosphorylation.



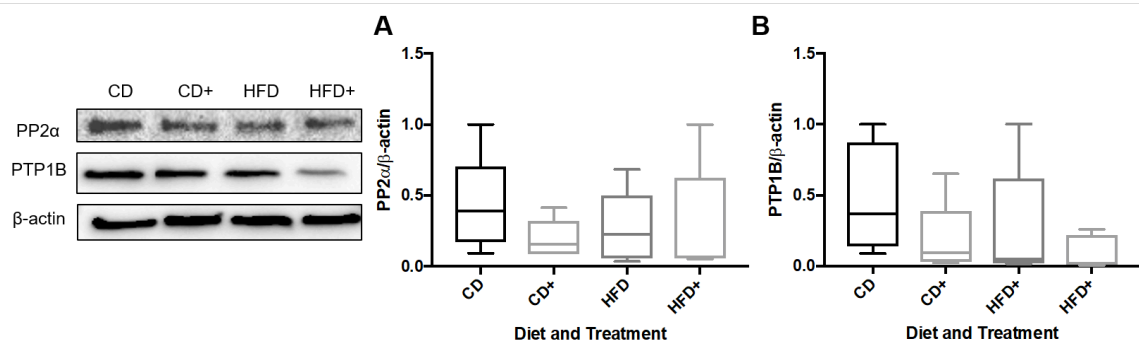


**Figure 26. PP2A and PTP1b were not significantly upregulated with Aroclor exposure suggesting the cumulative loss phosphoprotein signaling is due to loss of phosphorylation.**

**A.** Immunoblot analysis of hepatic PP2α and **B.** PTP1B. A n=5 was used for the immunoblot analysis. A two-way ANOVA was used to statistically compare these datasets.

**Aroclor exposure diminishes CK2 activity and reduces expression of the  $\alpha$  and  $\beta$  subunits but increases the expression of the  $\alpha'$  subunit.** Since CK2 was projected to have decreased kinase activity after Aroclor exposure, CK2 activity and the pattern of expression of its subunits were measured. CK2 can function as a tetramer and is thought to be constitutively active, but little is known in regard to the subunit configuration on kinase activity (163, 164). Fig 3A-D demonstrates that Aroclor exposure diminishes the protein expression of CK2 $\alpha$  97% ( $p < 0.01$ ), and CK2 $\beta$  67% ( $p < 0.01$ ), and CK2 kinase activity 81% ( $p < 0.002$ ) (CD vs CD+) but increases the expression of CK2 $\alpha'$  ( $p < 0.0006$ ). The expression of CK2 $\alpha'$  is most pronounced in the livers of mice that developed TASH. CK2 can function as a tetrameric enzyme with either 2 alpha subunits and 2 beta subunits or 2 alpha' subunits and two beta subunits. Interestingly PCB exposure promotes CK2 alpha' subunit expression which is more pronounced with a HFD and PCB exposure.

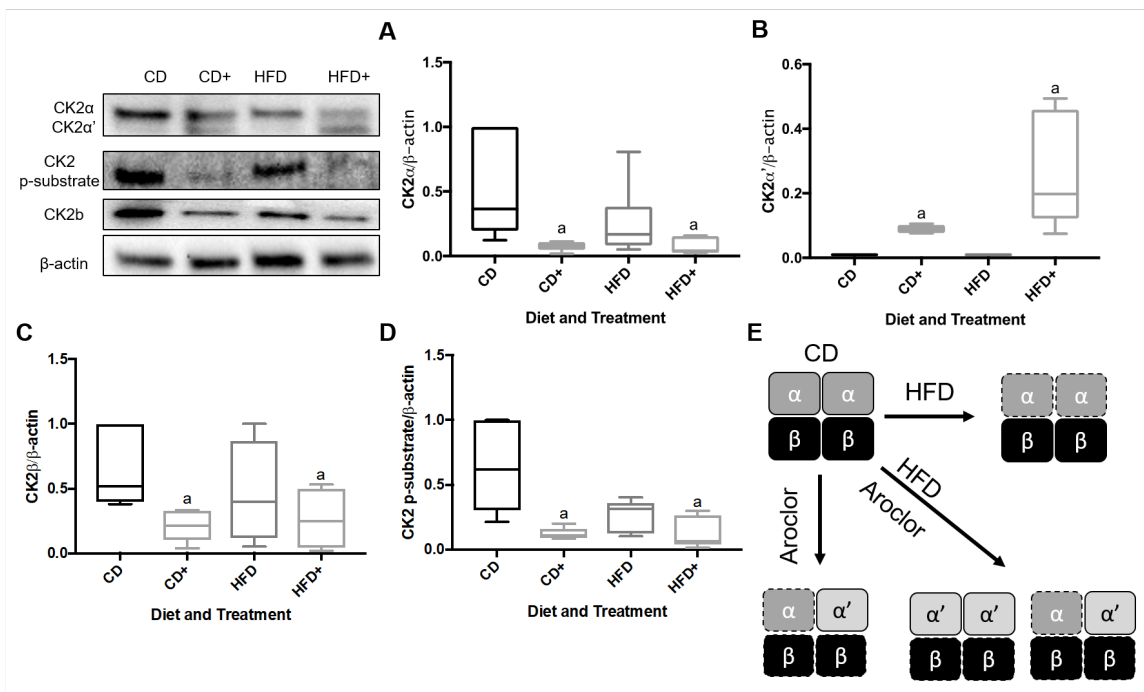


**Figure 27. Aroclor exposure diminishes CK2 activity and reduces expression of the  $\alpha$  and  $\beta$  subunits but increases the expression of the  $\alpha'$  subunit** **A**, Immunoblot analysis of CK2 $\alpha$ , **B**, CK2 $\alpha'$ , **C**, CK2 $\beta$  expression, and **D**, CK2 phospho-substrate. **E**, Illustration of alterations in CK2 subunit expression relative to CD expression. A n=5 was used for the immunoblot analysis. A two-way ANOVA was used to statistically compare these datasets.

**Aroclor exposure prevents CASP3 phosphorylation and promotes secondary necrosis *in vitro*.** CK2 negatively regulates cell death through phosphorylation of caspases at residues surrounding their cleavage sites, thereby, preventing caspase-mediated cell death. Since TASH is distinguished by elevated hepatic cell death and there is a loss of CK2 activity with PCB exposure, caspase-3 (CASP3) phosphorylation and cell death were measured. In Fig 4A CASP3 expression is actually reduced 59% ( $p < 0.0003$ ) with PCB exposure or a HFD 63% ( $p < 0.0001$ ) and its decline is more pronounced with the co-exposure (31%) ( $p < 0.0016$ ) relative to CD expression. Fig 4B demonstrates that phosphorylation of CASP3 at S150 is downregulated with Aroclor exposure (52%) ( $p < 0.006$ ), HFD (49%) ( $p < 0.02$ ), and their interaction (40%) ( $p < 0.0005$ ). (Fig 4C). Primary human hepatocytes exposed to PCBs first undergo a level of apoptosis, 33.3% of cells at 6 hours and 41.7% at 24 hours are apoptotic, followed by 4.2% of cells undergoing secondary necrosis at 6 hours, and 41.7% at 24 hours (Fig 4D). Apoptosis is the preferential method of cell death which concludes with phagocytic clearance. Under circumstances of elevated hepatocyte cell death when cells are not cleared secondary necrosis and inflammation can occur which is considered the full apoptosis program (2). The dramatic loss of CASP3 expression in TASH suggest that this due to post-apoptotic degradation which *in vivo* would present as necrosis due to the fleeting nature of the process.

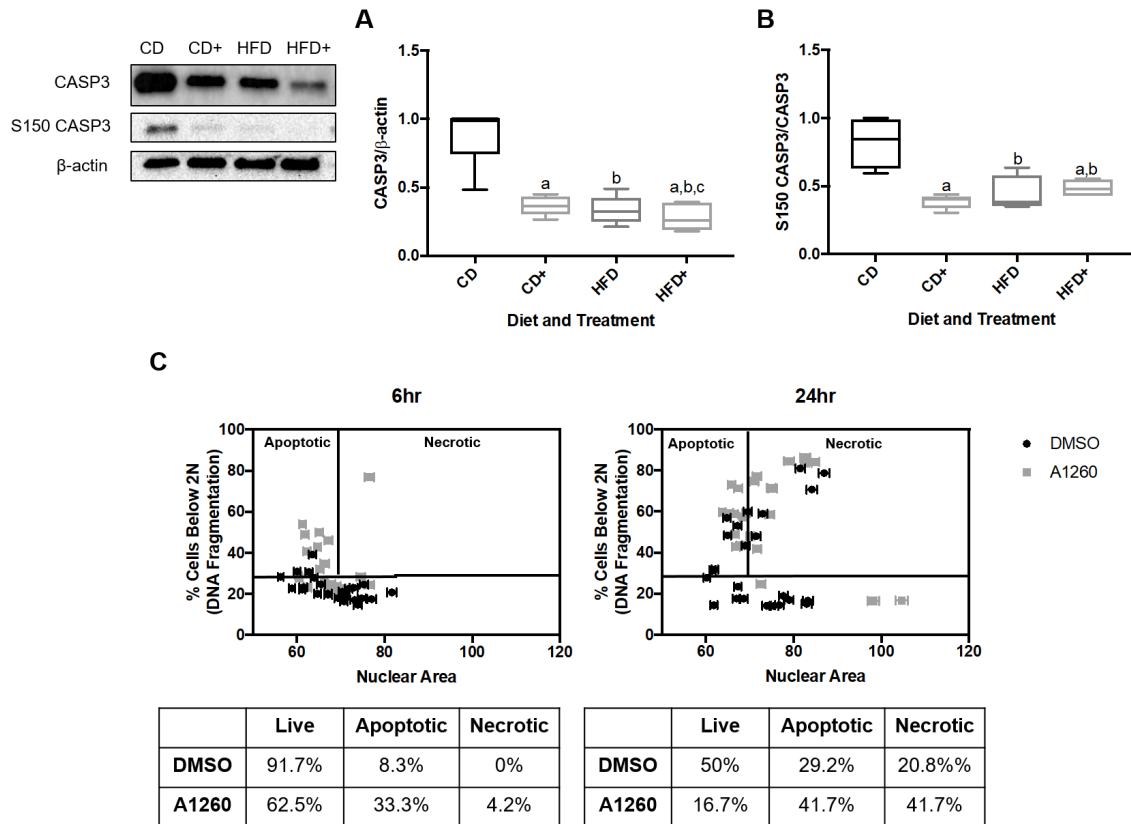


**Figure 28. Aroclor exposure promotes secondary necrosis in TASH** **A.** Immunoblot analysis of hepatic CASP3, **B.** S150 CASP3. **C.** Cellomics cell death measure in primary human hepatocytes at 6 and 24 hours. A n=5 was used for the immunoblot analysis. A n=24 was for the Cellomics assay, each plotted point is a mean for 2500 cells. A two-way ANOVA was used to statistically compare these datasets.

## DISCUSSION

PCBs were previously characterized as EGFR antagonists *in vivo* and *in vitro* and coined “signaling disrupting chemicals” providing a rationale to investigate the hepatic phosphoproteome in an animal model of PCB-mediated TASH (140). Cell signaling through protein phosphorylation *via* kinases is critical for cells to respond to intracellular and extracellular cues rapidly. The most well characterized example of loss of hepatic signaling in metabolic disease is insulin resistance (160). While the insulin receptor is one of the most well studied RTKs in metabolism, EGFR is highly expressed in the liver and is under-studied in the context of NAFLD.

The MetaCore analysis demonstrated that a HFD affects hepatic lipid accumulation which is well-established in many HFD fed animal models (67, 165). Aroclor was found to affect pathways involving PI3K, insulin and LXR which has previously been demonstrated with PCB exposures in the liver (13, 96, 140). The interaction of a HFD and PCB exposure promoted liver necrosis which reproduces previous findings (18, 36, 166).

Interestingly, a majority of the hepatic phosphopeptides were significantly decreased with Aroclor exposure and the PCB-dietary interaction. Roughly, a quarter of the phosphopeptides were diminished in the livers of mice that developed TASH suggesting loss of cell signaling could be a key to the development of TASH. When analyzing the kinome alterations due to the experiment variables, Aroclor exposure suppressed all kinase activity and the Aroclor-HFD interaction exacerbated this effect. Some of these effects have been validated previously, such as, loss of Akt-mTOR and ERK signaling due to PCB exposure (96, 140). Since protein phosphorylation can be regulated by kinases and phosphatases, the abundance of serine/threonine/tyrosine phosphatases were determined.

The initial observation of profound loss of protein phosphorylation in TASH due to Aroclor exposure was followed by measurement of phosphatases to determine whether their expression is higher with exposure or if cell signaling by phosphorylation is lost. Interestingly, serine/threonine phosphatase PP2A and a tyrosine phosphatase, PTP1B, had decreased or were unchanged in expression with PCB exposure in TASH. This would suggest that the loss of protein phosphorylation is due to a loss of regulation by phosphorylation and not an upregulation of

phosphatases activity. One kinase not previously demonstrated to be downregulated by PCBs in the development of TASH was CK2.

CK2 has been shown to negatively regulate cell death through phosphorylation of residues surrounding caspase cleavage sites, thereby, preventing cleavage (167). CK2 is unique, in that it is made up of subunits and is considered constitutively active (163, 164). CK2 is thought to be constitutively active in order to prevent incidental caspase-mediated apoptosis through caspase phosphorylation by CK2 (164, 168). The data suggested that hepatic CK2 activity is decreased during Aroclor exposure. Our validation experiment confirmed this initial observation and demonstrated that the subunit composition is altered with PCB exposure, resulting in an inhibitory effect on kinase activity. Interestingly with PCB exposure, the CK2 $\alpha'$  subunit was more highly expressed, and this was further increased in mice that were exposed and fed a HFD, clearly demonstrating an interaction unique to TASH. CK2 $\alpha'$  is a key effector kinase in interleukin-6 and tumor necrosis factor alpha signaling in inflammation which may explain the elevated expression with PCB exposure (169). Also CK2 $\beta$  is downregulated with Aroclor exposure, as well, which has been shown to be required for the tetrameric formation (163). CK2 is the main regulator CASP3 phosphorylation that negatively regulates apoptosis through prevention of CASP3 self-cleavage and activation (167, 168, 170).

CASP3 is a measure of apoptotic cell death that can be due to intrinsic or extrinsic activation (167, 170). Apoptosis is a programmed form of cell death that is often considered non-inflammatory, as opposed to necrosis (171). Recent data demonstrates that in liver disease models, apoptosis is the initial cell death mechanism observed, but once immune cell-mediated apoptotic cell clearance is saturated (or no immune cells are present as seen in *in vitro* models), secondary necrosis occurs (2). Our data supports this model as CASP3 expression is decreased relative to control with either PCB exposure or a HFD suggesting it is undergoing post-apoptotic degradation. This is further exacerbated in the livers of mice fed a HFD and exposed to PCBs. In primary human hepatocytes exposed to Aroclor 1260, cell apoptosis is first observed at 6 hours, followed by a rise in necrotic death at 24 hours. Since this a rapid PCB effect it would present as necrosis *in vivo*. These findings suggest that PCB exposure promotes apoptosis followed by secondary necrosis.

This adds support to human studies where elevated whole CK-18 (necrosis marker) in serum is associated with PCB load in exposed populations (13).

This is the first phosphoproteomic analysis of an animal model of TASH. Collectively, the data suggest that loss of protein phosphorylation and down-regulation of the hepatic kinome is a major factor in the development of PCB-mediated TASH. This study confirms past studies in PCBs downregulated hepatic AKT, ERK, and mTOR activity. CK2 is one is downregulated in TASH, due to PCB exposure promoting loss of CK2 $\alpha$  and CK2 $\beta$  subunit expression. PCB-mediated loss of CK2 activity prevents negative phospho-regulation of CASP3. Secondary necrosis appears to be the final mechanism of cell death in PCB-mediated TASH *in vivo* and *in vitro*.



## CHAPTER 6

### THERAPEUTIC EFFICACY OF EGF ADMINISTRATION IN PCB-MEDIATED STEATOHEPATITIS AND FIBROSIS

#### INTRODUCTION

PCBs have been demonstrated to act in part through EGFR inhibition *in vitro* and *in vivo* in the development of steatohepatitis. PCB exposures act in part to disrupt the EGFR regulation of the proteome and phosphoproteome but many of the mechanisms of PCBs acting through EGFR inhibition have been correlative and not causative in the NAFLD pathogenesis. It is not currently known whether EGF administration can prevent the development of NAFLD in mice exposed to PCBs. I postulate that EGF administration can rescue hepatic EGFR signaling preventing some of the PCB-mediated pathology previously observed, namely steatohepatitis (3, 18, 166). In this study I aimed to I) determine if EGF administration can rescue hepatic EGFR signaling in PCB-exposed mice, II) determine if EGF administration can prevent either PCB-induced steatohepatitis and or diet induced steatosis as well as fibrotic response.

#### MATERIALS AND METHODS

##### **Animal Studies**

All animal procedures were previously approved by the University of Louisville IACUC and all animals were treated humanely as documented in the “Guide for the Care and Use of Laboratory Animals: Eight Edition” (143). C57Bl/6 male mice (8-10 weeks old) were exposed to either corn oil or Aroclor 1260 (20 mg/kg) by a one-time oral gavage at week 1 (n=17 per group). Mice were fed a 42% HFD (Envigo, Huntingdon, UK) *ad lib*. At week 10 mice were either injected with EGF (0.2µg/g) or saline *via* i.p. once a day for 5 days on week 10 and an additional 5 days of week 11.

Mice were then euthanized *via* intraperitoneal injection of ketamine/xylazine at 120/16 mg/kg.

Mice groups are labeled CS for corn oil gavage with saline injection, CE for corn oil gavage with EGF injection, AS for Aroclor 1260 gavage with saline injection, or AE for Aroclor 1260 gavage with EGF injection.

A separate group of C57Bl/6 mice (8-10 weeks old) were exposed to either corn oil or Aroclor 1260 (20 mg/kg) by a one-time oral gavage at week 1 (n=5 per group). Mice were fed a control diet (Envigo, Huntingdon, UK). At week 2 mice were either injected with EGF (0.002, 0.02, 0.2µg/g) or saline *via* i.p. After 30 minutes mice were then euthanized *via* intraperitoneal (i.p.) injection of ketamine/xylazine 120/16 mg/kg. Serum was extracted, and serum pyruvate and glucose were measured.

#### **Glucose tolerance test (GTT) and Insulin Tolerance Test (ITT)**

)At week 11 mice were fasted for 6 hours and had their fasting blood glucose levels measured with a glucometer (Accu-Check Aviva, Roche, Basel Switzerland). Mice were then injected with insulin (0.5 U/kg) *via* i.p. injection to perform an ITT. Blood glucose levels were then measured at 15, 30, 60, and 120-minute intervals.

At week 12 mice were fasted for 18 hours and had their fasting blood glucose recorded with a glucometer. Mice were then injected with glucose (1 mg/g of body weight in sterile saline) *via* i.p. injection. Blood glucose levels were then measured at 15, 30, 60, and 120-minute intervals.

#### **Liver histological analysis**

Liver sections were fixed with 10% neutral buffered formalin and embedded in paraffin. Sections were stained with hematoxylin-eosin (H&E) or for chloroacetate esterase (CAE) activity (Naphthol AS-D Chloroacetate [Specific Esterase] kit, Sigma Aldrich (St. Louis, MO), or Picro-Sirius Red stain for collagen deposition and fibrosis, Sigma Aldrich (St. Louis, MO). Slides were examined by light microscopy at 20X or 10X and imaged.

### **Serum cytokine, adipokine blood biochemistry measurement**

A Milliplex Serum Adipokine kit was used to measure serum adiponectin, tumor necrosis factor alpha (Tnf $\alpha$ ), resistin, and plasminogen activator inhibitor-1 (PAI-1) on the Luminex IS 100 instrument (Luminex Corp, Austin, TX). Serum low density lipoprotein (LDL), high density lipoprotein (HDL), triglycerides, glucose, and total cholesterol were measured on the Piccolo Xpress Chemical Analyzer using a Lipid Panel Plus reagent disc (Abaxis, Union City, CA)

### **Serum pyruvate and free fatty acid measure**

Serum pyruvate was measured spectrophotometrically by the loss of nicotinamide adenine dinucleotide (NADH) absorbance at 340 nm in the presence of lactate dehydrogenase. A standard curve was used to determine the exact concentration in each sample.

Serum free fatty acids were measured with the Free Fatty Acid Quantification Kit purchased from Sigma-Aldrich (Sigma-Aldrich, St. Louis, MO)

### **Hepatic cholesterol, triglycerides (TGs) and free fatty acid (FFA) measurements**

Liver tissue was homogenized in phosphate buffer saline (PBS) and lipids were extracted with a 3:1 chloroform to methanol separation method (172). The lipid extract was dried and suspended in either Infinity Cholesterol Stable Reagent, Infinity Triglyceride Stable Reagent (Fisher Diagnostics, Middletown, VA), or free fatty acid assay buffer (Sigma-Aldrich, St. Louis, MO) and the absorbance was measured relative to lipid standard curves.

### **Western Blot Analysis**

Mouse liver lysates were homogenized in RIPA Buffer (100 mg tissue/0.5 mL RIPA supplemented with protease, and phosphatase inhibitors 10  $\mu$ l/mL, (Sigma-Aldrich, St. Louis, MO)). Primary antibodies used include EGFR (Santa Cruz, Dallas, TX ), Y1173 EGFR (abcam Cambridge, UK),

CAR (abcam Cambridge, UK),  $\beta$ -actin (CST Danvers, MA), and the secondary HRP antibody (CST Danvers, MA). Full description of western blot analysis methods can be found in chapter 2.

### **Real time quantitative polymerase chain reaction (RT qPCR)**

Mouse livers were homogenized, and total RNA was extracted using the RNA-STAT 60 protocol (Tel-Test, Austin, Texas). Taqman Gene Expression Assays (Thermo-Fisher) Gene expression levels were calculated according to the  $2^{-\Delta\Delta Ct}$  method, and Gapdh was used as the endogenous control. The following Taqman Probes were used Apolipoprotein B (ApoB), *Mm01545159\_m1*; Cluster of differentiation 68 (Cd68), *Mm03047343\_m1*; Cytochrome P450 Family 2 Subfamily B Member 10 (Cyp2b10), *Mm01972453\_m1*; Cytochrome P450 Family 3 Subfamily A Member 11 (Cyp3a11), *Mm00731567\_m1*; Glyceraldehyde-3-phosphate dehydrogenase (Gapdh), *Mm99999915\_g1*; Interleukin-6 (Il-6), *Mm00446190\_m1*; Lymphocyte antigen 6 family member 6D (Ly6g6d), *Mm00459644\_m1*; Myocyte enhancer factor 2c (Mef2c), *Mm01340842\_m1*; Nuclear receptor Subfamily 1 Group I Member 3 (Nr1i3), *Mm01283980*; Toll like receptor 4 (Tlr4), *Mm00445273\_m1*; Transforming growth factor beta (Tgf $\beta$ ), *Mm01227699\_m1*; Tumor necrosis factor alpha (Tnf $\alpha$ ), *Mm00443258\_m1*.

**Statistical Analysis.** Western blot densitometry values, quantified RNA values, macromolecule measures, and other biological measures were statistically analyzed using Graphpad Prism Version 7 for Macintosh (San Diego, CA). The data are expressed as box and whisker plots. Figures 30 Ai, Bi, Ci, Di are represented as mean $\pm$ SEM. Data was compared using two-way ANOVA. A p-value $<$ 0.05 was considered statistically significant.

## RESULTS

### **EGF rescues hepatic EGFR signaling in PCB-exposed mice and downregulates CAR activation**

Since PCBs have been shown to inhibit hepatic EGFR signaling which coincided with the development of steatohepatitis a therapeutic study was implemented to determine if the PCB-mediated effects were through EGFR inhibition *in vivo* and if they could be countered by EGF. First the effects of EGF and Aroclor 1260 exposure were on hepatic EGFR phosphorylation were measured to validate our model system. In Figure 29A western blot analysis of whole liver demonstrates that EGFR phosphorylation at Y1173 is elevated with EGF administration even in mice exposed to PCBs. In un-exposed mice EGF administration elevated EGFR phosphorylation 46% (CS vs. CE) in Aroclor exposed mice EGF administration elevated EGFR phosphorylation 55% (AS vs. AE,  $p < 0.04$ ). Since PCBs are proposed to act through EGFR inhibition indirectly activating CAR, CAR expression and target gene expression were measured. Fig 29B western blot analysis of whole liver demonstrates that CAR protein expression is not altered with any exposure or treatment. Fig 29C shows that qPCR analysis of total liver RNA demonstrates that CAR gene expression is elevated 14% with EGF (CS vs. CE,  $p < 0.04$ ) and 34% with PCB exposure (CS vs. AS,  $p < 0.0001$ ). As reported by Wahlang *et al* 2014 (3) PCB exposure increased Cyp2b10 mRNA by 51%. CAR's target gene Cyp2b10 is downregulated 35% due to interaction of EGF and PCB exposure suggesting PCB-mediated indirect CAR activation likely occurs through inhibition of EGFR phosphorylation ( $p < 0.05$ ) Cyp3a11 mRNA was significantly elevated 32% by Aroclor exposure (CS vs. AS,  $p < 0.04$ ) but is diminished 25% with EGF treatment (AS vs. AE) suggesting CAR activation is negatively regulated by EGFR signaling.

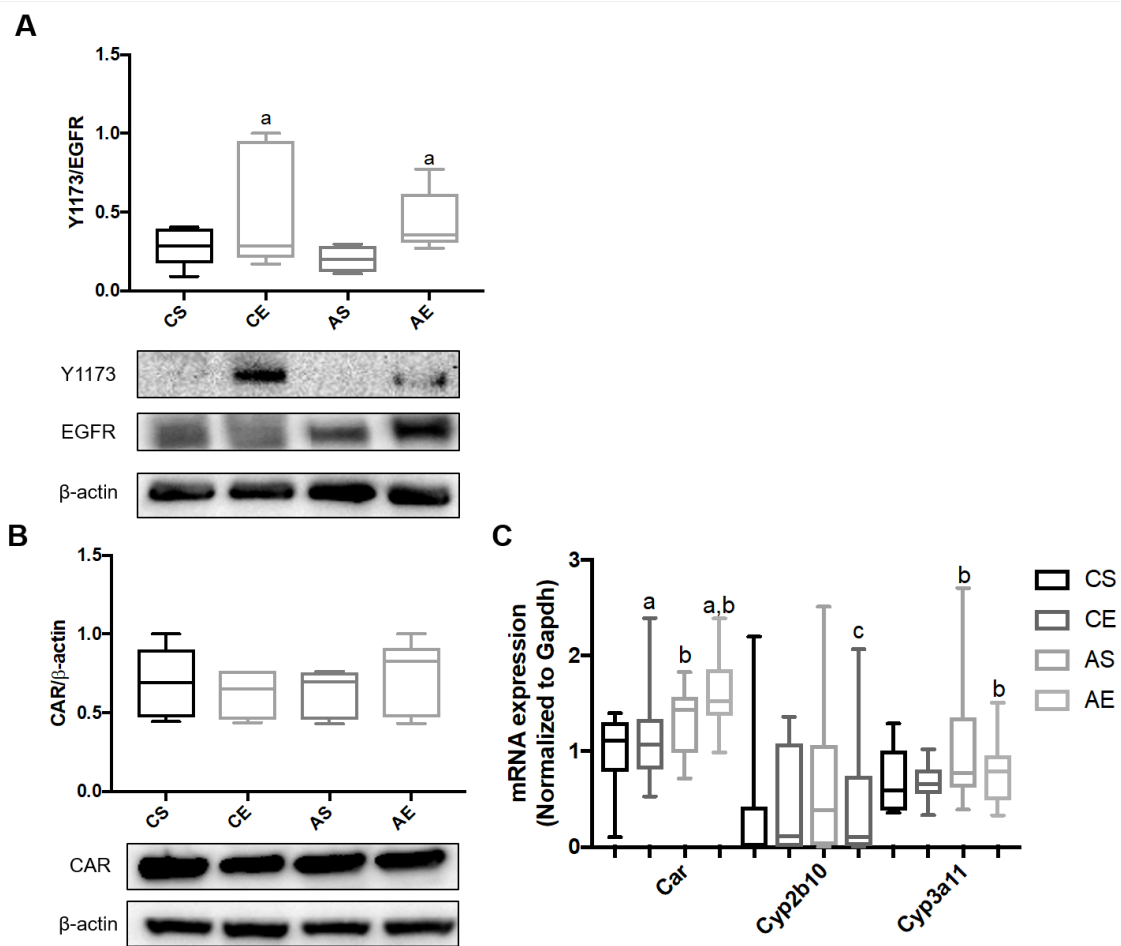


**Figure 29. EGF rescues hepatic EGFR signaling in PCB-exposed mice and downregulates CAR activation:** Immunoblot analysis of **A.** hepatic EGFR protein phosphorylation at Y1173 and **B.** CAR in mice gavaged with corn oil and injected with either saline (CS) or EGF (0.2  $\mu$ g/g) (CE) or gavaged with Aroclor 1260 (20 mg/kg) and injected with saline (AS) or EGF (AE). **C.** qPCR analysis of hepatic *Car*, *Cyp2b10*, and *Cyp3a11* mRNA expression. An n=5 was used for figures 28A-B and an n=17 was used for figure 28C. A two-way ANOVA was used to statistically compare datasets. A  $p < 0.05$  was considered significant. Significance due to EGF is denoted by a, due to Aroclor denoted by b, and due to interaction denoted by c. Data are represented as box and whisker plots.

**EGF promotes hepatic gluconeogenesis and reduces insulin sensitivity but does not affect glucose uptake**

Hepatic EGFR signaling peaks in the inactive phase or fasted state in mice which suggests it may have a regulatory role in glucose metabolism that could be altered due to PCB exposure (28). In Fig 30Ai EGF administration promotes elevation of blood glucose levels at all doses of EGF, while in Fig 30Aii, EGF was shown to elevate fasting blood glucose levels 17% in non-exposed mice (CS vs. CE) and 31% in exposed mice (AS vs. AE) after a 18 hour fast suggestive of increased hepatic gluconeogenesis ( $p < 0.007$ ). Fig 30Bi demonstrates EGF increases pyruvate uptake after 30 minutes in male C57Bl/6 mice. Fig 30Bii shows that Aroclor exposure promotes elevated serum pyruvate 61% (CS vs. AS) in the 12-week study ( $p < 0.0001$ ). Fig 30Ci-ii illustrates that neither EGF nor PCBs affect glucose uptake in a GTT. Fig 30Di-ii demonstrates that EGF administration reduces insulin sensitivity in an ITT. These data support that EGF is glucogenic in the liver and that Aroclor exposure to some extent can potentially prevent EGF-stimulated hepatic uptake of the glucogenic substrate pyruvate.

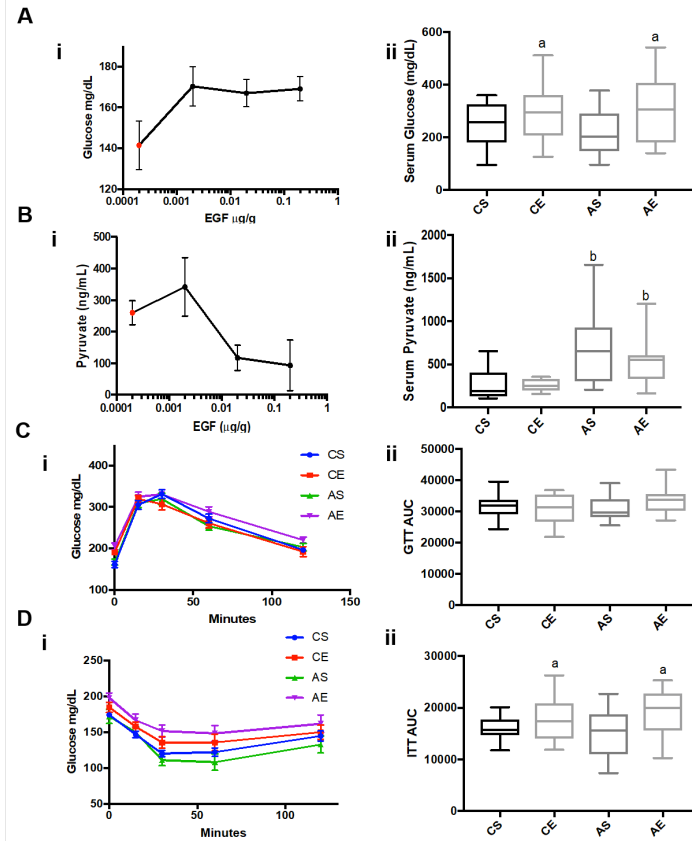


**Figure 30. EGF promotes hepatic gluconeogenesis and reduces insulin sensitivity but does not affect glucose uptake: Ai.** Serum glucose and serum pyruvate **Bi** were measured in mice treated with EGF (0.002, 0.02, 0.2 $\mu$ g/g) or saline control for 30 minutes. **Aii** serum glucose and serum pyruvate **Bii** were measured in mice gavaged with corn oil and injected with either saline (CS) or EGF (0.2  $\mu$ g/g) (CE) or gavaged with Aroclor 1260 (20 mg/kg) and injected with saline (AS) or EGF (AE). **Ci-ii** GTT's were performed in the CS,CE, AS, AE mice as well as **Di-ii** ITT's. A n=5 was used for figures 30Ai and 30Bi. An n=17 was used for figures 30Aii, 230Bii, 30C and 30D. A two-way ANOVA was used to statistically compare datasets. A  $p < 0.05$  was considered significant. Significance due to EGF is denoted by a, due to Aroclor denoted by b, and due to interaction denoted by c. Data are represented as mean $\pm$ SEM for figures 30Ai, Bi, Ci, Di, but are represented as box and whisker plots for figures 30Aii, Bii, Cii, and Dii.



### **EGF promotes lipid redistribution to adipose tissue in Aroclor exposed mice**

Previously PCB exposure was not demonstrated to worsen steatosis in mice fed a HFD but elevated EGFR signaling in mice fed a HFD has been shown to be protective (173). To characterize the effects of PCBs and EGF on steatosis and dyslipidemia, multiple metabolic measures were performed. H&E staining of liver sections (Fig 31A) demonstrates reduced levels of steatosis (47% normal, <5% steatosis) in CE mice in contrast to all steatotic livers in CS mice. In Aroclor exposed mice, EGF administration did not reduce steatosis as in control mice. Fig 31B demonstrates that PCBs and interaction with EGFR elevated hepatic triglycerides (TGs) 42% (CE vs. AE,  $p < 0.03$ , and  $p < 0.006$  respectively), while EGF ( $p < 0.0003$ ), Aroclor ( $p < 0.0003$ ), and interaction ( $p < 0.0005$ ) elevate serum TGs 31% (CS vs. AE). EGF administration diminishes hepatic FFAs 32% (CS vs. CE,  $p < 0.01$ , Fig 30C), while Aroclor exposure increases hepatic FFAs 52% (CS vs. AS,  $p < 0.02$ ), but does not significantly change serum FFAs. As seen in Fig 31C, EGF increases hepatic cholesterol levels 25% (CS vs. CE,  $p < 0.009$ ) but serum cholesterol is only elevated 8.7% due to interaction (CS vs. AE,  $p < 0.0002$ ). Fig 31Di-v demonstrates that serum (31Di) HDL and (31Dii) LDL are increased 4.6% ( $p < 0.0002$ ) and 2.4% ( $p < 0.0034$ ) due to interaction respectively (AS vs. AE). While serum (31Diii) VLDL is elevated 28% (CS vs. AE) due to EGF ( $p < 0.001$ ), Aroclor 1260 ( $p < 0.002$ ), and interaction ( $p < 0.003$ ) between EGF and PCBs, and hepatic ApoB mRNA (31Dv) was elevated 23% (CS vs. AE) due to EGF ( $p < 0.0006$ ), Aroclor ( $p < 0.0001$ ), and interaction ( $p < 0.0001$ ). Since adipokines are diagnostic markers for steatosis the serum levels of adiponectin (negatively associated with steatosis), resistin, and PAI-1 (positively associated with steatosis) were measured (174). Fig 31Ei-v shows that Aroclor ( $p < 0.0009$ ) diminished EGF upregulation of adiponectin (31Ei) 56% (CE vs AE,  $p < 0.007$ ). EGF diminished lipokines (31Eii) PAI-1 ( $p < 0.03$ ) 35%, and (31Eiii) resistin ( $p < 0.03$ ) 17% (AS vs. AE). The weight of the epididymal fat pad normalized to body weight was measured to determine the effects of EGF and PCBs on lipid storage in the adipose. (Figure 31Ev). Fat to body weight ratios were elevated 21% due to interaction (AS vs. AE,  $p < 0.02$ ) suggesting that lipids are not adequately stored in the adipose tissue in mice exposed to Aroclor alone.

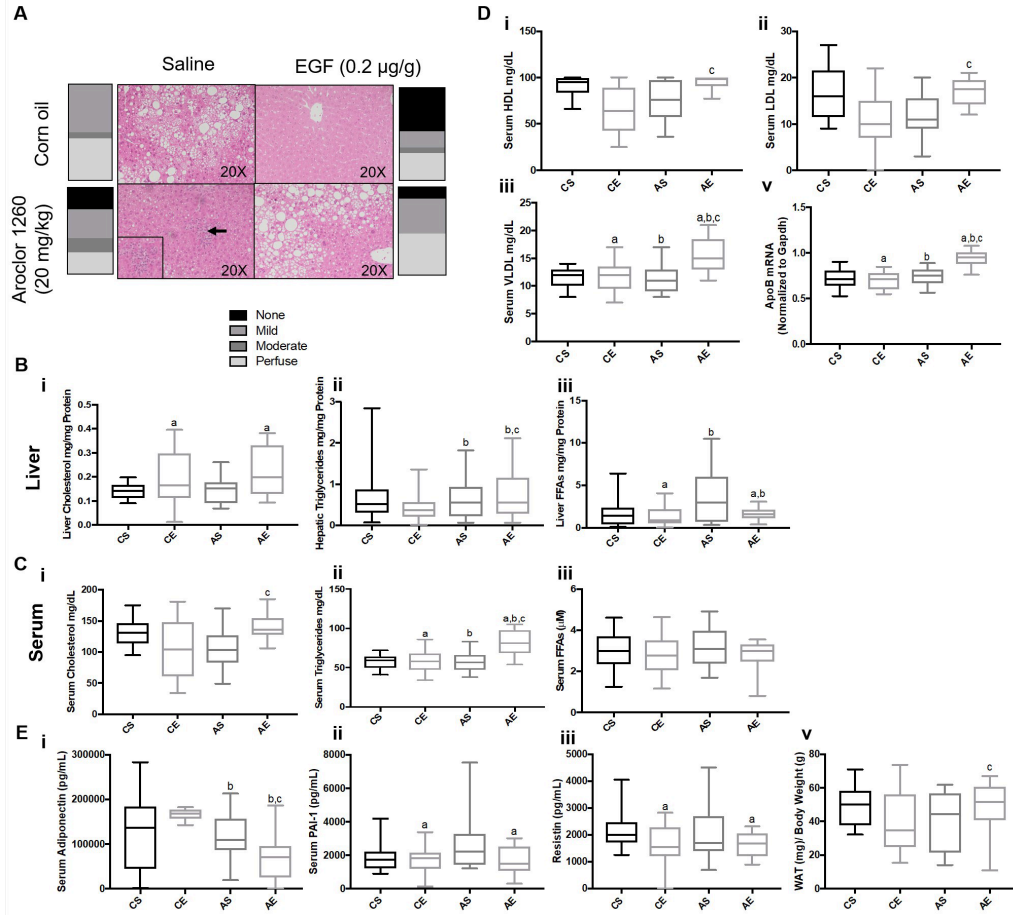


**Figure 31. EGF promotes lipid redistribution to adipose tissue in Aroclor exposed mice: A.** H&E staining of liver section in mice orally gavaged with corn oil and injected with either saline (CS) or EGF (0.2 μg/g) (CE) or gavaged with Aroclor 1260 (20 mg/kg) and injected with saline (AS) or EGF (AE). **B.** Hepatic measures of (i)cholesterol, (ii)triglycerides, and (iii) FFAs in CS, CE, AS, and AE mice. **C.** Serum measures of (i)cholesterol, (ii)triglycerides, and (iii) FFAs in CS, CE, AS, and AE mice. **D.** Serum measures of (i) HDL, (ii) LDL, and (iii) VLDL in CS, CE, AS, and AE mice. **(v)** qPCR analysis of hepatic ApoB mRNA expression in CS, CE, AS, and AE mice. **E.** Serum measures of (i) adiponectin, (ii) PAI-1, and (iii) resistin in CS, CE, AS, and AE mice. **(v)** Weight of epididymal white adipose tissue normalized to total body weight in CS, CE, AS, and AE mice. An n=17 was used for figures 31A-E. A two-way ANOVA was used to statistically compare datasets. A p<0.05 was considered significant. Significance due to EGF is denoted by a, due to Aroclor denoted by b, and due to interaction denoted by c. Data are represented as box and whisker plots for figures 31A-E.

### **EGF reduces PCB-induced steatohepatitis and bridging fibrosis**

PCBs have previously been shown to cause steatohepatitis in mice fed a HFD and to cause bridging fibrosis in mice fed a methionine choline deficient diet (MCD)(3, 18, 139). In others models of liver disease, EGF has been shown to be anti-inflammatory but it has never been tested in an animal model of TASH (32). To assess the effects of EGF and Aroclor exposure on steatohepatitis and fibrosis histological measures, cytokine measures, and qPCR analysis were used. In Fig 32A, CAE staining of liver section demonstrates that EGF reduced neutrophil infiltration in Aroclor-exposed mice treated with EGF. Serum  $Tnf\alpha$  is diminished 32% with EGF (AS vs. AE,  $p<0.02$ ) (Fig 2B). In Fig 32C, hepatic  $Tnf\alpha$  mRNA is shown to be decreased 51% with EGF and PCB interaction (AS vs. AE,  $p<0.03$ ). Hepatic inflammatory gene markers Il-6 (71%,  $p<0.0001$ ), Ly6gd (41%,  $p<0.001$ ), Cd68 (35%,  $p<0.001$ ), and Tlr4 (42%,  $p<0.05$ ) were all diminished with EGF (AS vs. AE). Fig 32D shows the Picro-sirius red staining of liver sections demonstrating that EGF downregulates PCB-mediated bridging fibrosis. Fig 32E demonstrates that EGF diminishes hepatic Tgf- $\beta$  gene expression 17% (AS vs. AE,  $p<0.01$ ) while EGF diminishes Aroclor elevation of Mef2c expression by 23% (AS vs. AE,  $p<0.003$ ).

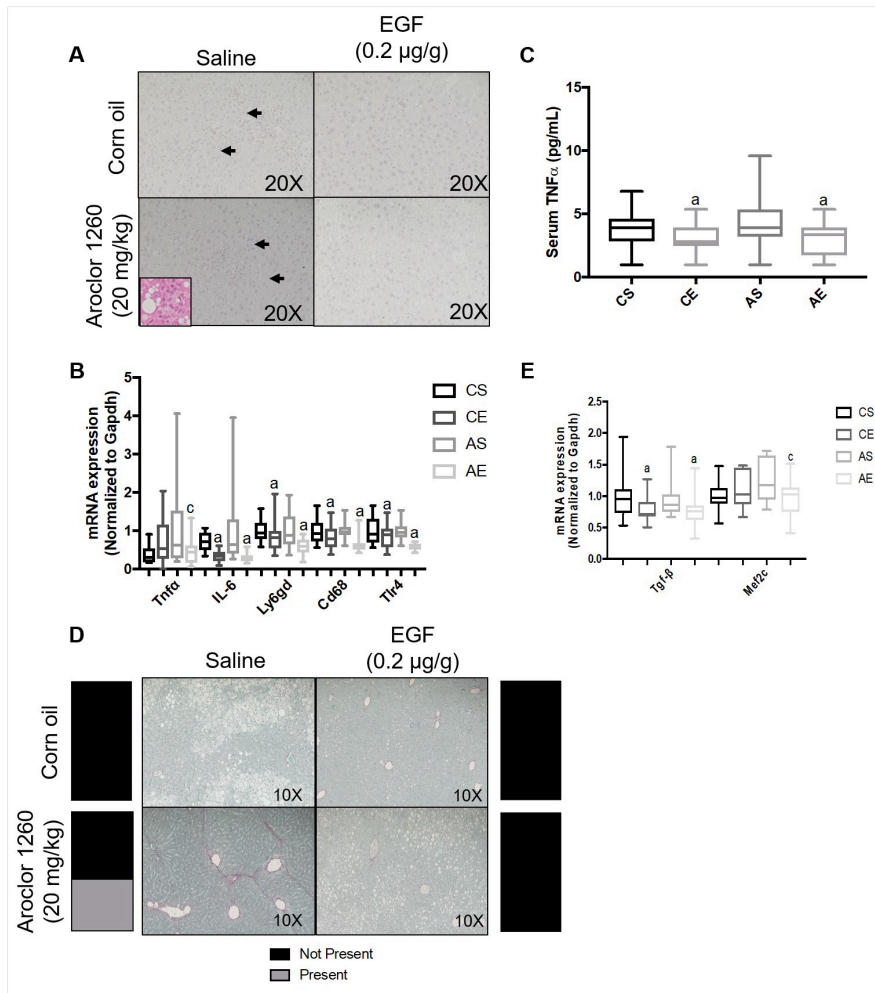


**Figure 32. EGF reduces PCB-induced steatohepatitis and bridging fibrosis:** **A.** Chloroacetate esterase activity staining in liver sections of mice orally gavaged with corn oil and injected with either saline (CS) or EGF (0.2 μg/g) (CE) or gavaged with Aroclor 1260 (20 mg/kg) and injected with saline (AS) or EGF (AE). **B.** Hepatic qPCR analysis of inflammatory gene markers mRNA expression (Tnfa, Il-6, Ly6gd, Cd68, Tlr4) in CS, CE, AS, and AE mice. **C.** Serum measures of TNFα in CS, CE, AS, and AE mice. **D.** Picro-sirius red staining of liver sections of CS, CE, AS, and AE mice to detect collagen deposition. **E.** Hepatic qPCR analysis in CS, CE, AS, and AE mice to measure fibrotic gene marker expression (Tgfβ, Mef2c). An n=17 was used for figures 32A-E. A two-way ANOVA was used to statistically compare datasets. A p<0.05 was considered significant. Significance due to EGF is denoted by a, due to Aroclor denoted by b, and due to interaction denoted by c. Data are represented as box and whisker plots for figures 32B, C, E.

## EGF Promotes Hepatic Lipid Packaging and Export while Preventing PCB-mediated Steatohepatitis and Fibrosis

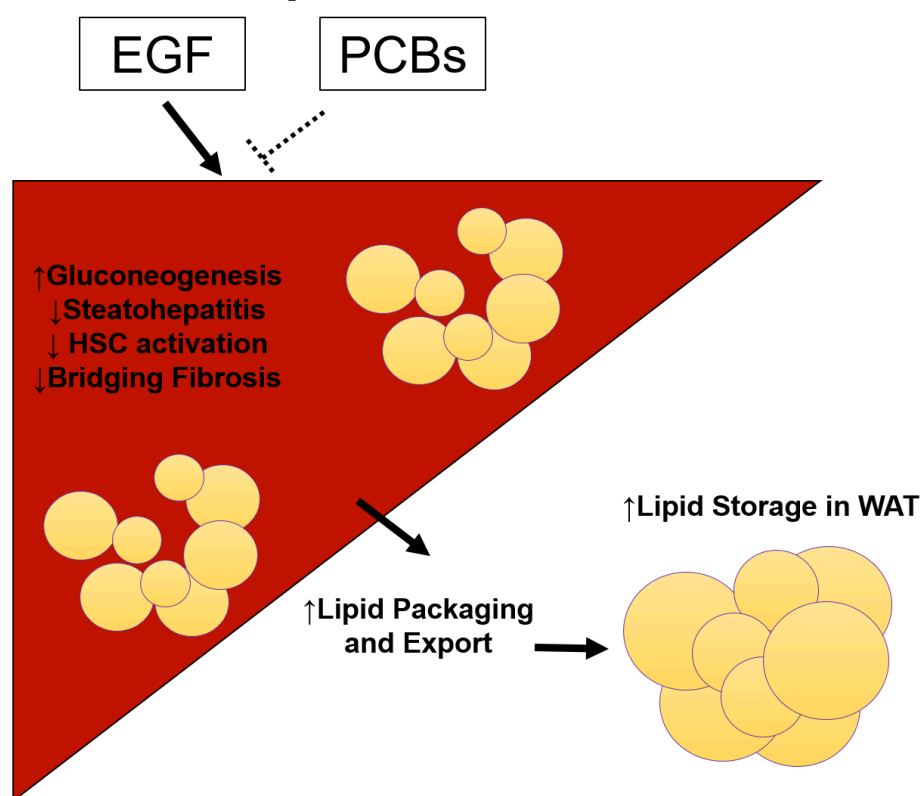


**Figure 33. EGF promotes hepatic lipid packaging and export while preventing PCB-mediated steatohepatitis and fibrosis:** Model demonstrating the hepatoprotective effects of EGF administration in Aroclor exposed mice. EGF is glucogenic and promoted lipid redistribution from the liver to the adipose tissue in Aroclor exposed mice. EGF prevented PCB-mediated steatohepatitis and fibrosis.

## DISCUSSION

PCBs have been shown to cause steatohepatitis in animal models and it is suggested to occur in human populations as well (3, 13, 18). In this study previous mechanistic knowledge that PCBs act through EGFR inhibition was applied to determine if an EGFR ligand can prevent the pathology associated with PCB exposures, namely steatohepatitis (96, 140), in an animal model.

In our animal model, EGF administration did elevate hepatic EGFR phosphorylation even in the Aroclor-exposed mice, while Aroclor-exposed mice had the lowest amount of EGFR phosphorylation. Furthermore, indirect CAR activation was hindered with EGF administration, even in the presence of PCBs suggesting that the mechanism of indirect CAR activation through PCB-mediated EGFR inhibition must occur *in vivo*, validating our previous *in vitro* model systems (96, 140). While these mechanistic data support PCB-mediated EGFR inhibition, further evaluation of EGF's therapeutic efficacy on PCB-mediated disease endpoints were the critical findings of this study.

Previously, EGFR signaling was found to peak in the liver in the fasted state or inactive phase suggesting it may play a role in maintaining metabolic homeostasis for the organism when nutrients are not being consumed (28). When mice were injected with EGF at increasing dosage their serum glucose levels were elevated while their serum pyruvate levels were diminished relative to saline controls. This would suggest that EGF promoted gluconeogenesis from uptake of glucogenic substrates, such as, pyruvate. Serum pyruvate levels were elevated with Aroclor exposure suggesting that PCBs may prevent EGFR-mediated pyruvate uptake pathway. EGFR glucogenic effects were demonstrated before in primary hepatocytes but not *in vivo* (175). These data suggest that EGFR signaling in the liver may act in part to maintain blood glucose levels in the inactive phase. Interestingly EGF administration lowered insulin sensitivity regardless of PCB exposure suggesting that EGFR and insulin receptor (IR) may be opposing growth factor receptors in their effects on glucose metabolism in the liver. While insulin sensitivity was slightly lowered with EGF administration, glucose uptake was not affected suggesting that these mice were able to adequately handle glucose. Next, the effects of PCBs and EGF administration were analyzed in the context of steatosis and lipid metabolism.

PCBs were not previously shown to affect steatosis in HFD fed-mice, but EGFR has previously been shown to be downregulated in steatosis and could reduce fatty liver when restored genetically (173). In non-exposed mice EGF diminished lipid accumulation and prevented steatosis in 47% of the mice relative to saline non-exposed mice. EGF administration also reduced hepatic free fatty acids (FFAs), but elevated hepatic cholesterol regardless of PCB exposure. PCB exposure in contrast elevated hepatic free fatty acids and triglycerides. EGF in Aroclor-exposed mice still develop steatosis but most of that fat appears to be packaged and redistributed to the adipose tissue for storage. Lipid metabolism in the liver is also affected by multiple adipokines such as adiponectin, resistin, and PAI-1 (174). PCB exposure decreased EGF's upregulation of adiponectin levels, the hepatoprotective adipokine that promotes hepatic beta-oxidation (176). EGF administration reduced resistin and PAI-1 which are adipokines that worsen metabolic syndrome (174). EGF in non-PCB treated mice seemed to reduce steatosis but in Aroclor-exposed mice it may also be protective in reducing hepatic FFAs and promoting storage in the adipose. Since PCBs most insidious effect previously described in the liver is the development of steatohepatitis, the protective effects of EGF in PCB exposed mice will be discussed next (3, 18).

Steatohepatitis due to PCB-exposure has been shown to be contingent upon a HFD and in this study mice fed a HFD and exposed to Aroclor alone do develop steatohepatitis characterized by neutrophil infiltration, and elevated cytokine levels and expression. EGF administration ameliorated steatohepatitis in mice exposed to PCBs. EGF's anti-inflammatory effects in the liver has been demonstrated previously in alcoholic liver disease models (32) but this is the first time in an animal model of toxicant associated steatohepatitis. It is not currently known if EGF is anti-inflammatory through eliciting protective effects in hepatocytes by priming them or through boosting immune cell clearance of dying hepatocytes, thereby, reducing chronic inflammation or possibly both. These findings suggest that EGF administration can partly prevent PCB-mediated steatohepatitis demonstrating it's potential therapeutic efficacy. PCB exposures in mice has been shown to promote hepatic fibrosis in mice fed a methionine-choline deficient diet, but not previously in HFD fed mice (139).

In this study, only a subset of Aroclor alone exposed mice develop bridging fibrosis from multiple portal areas characterized by collagen deposition. In mice exposed to Aroclor but treated with EGF there was no bridging fibrosis present suggesting that EGF can be anti-fibrotic in mice exposed to PCBs. While the bridging fibrosis due to PCB exposure alone is minor it may be exacerbated with longer periods of exposure. Gene markers for fibrosis and hepatic stellate cells activation were diminished with EGF treatment as well supporting its anti-fibrotic effects.

In conclusion EGF is a glucogenic growth factor that can reduce diet-induced steatosis in HFD fed mice, unless they are exposed to PCBs. EGF treatment in Aroclor exposed mice promotes packaging and redistribution of lipids to the adipose tissue, thereby diminishing the FFA abundance in the liver. EGF treatment reduced PCB-mediated steatohepatitis and bridging fibrosis supporting its potential therapeutic efficacy in this model. This work has clinical implications as there are currently no approved therapeutics for NAFLD and EGF administration did limit multiple disease endpoints in the liver initiated by PCB exposures or a HFD. Future study is needed to determine if there are any adverse effects due to EGF treatment and if this therapy is beneficial in human models of NAFLD.



## CHAPTER 7

### CONCLUSIONS

In conclusion PCBs disrupt EGFR signaling in multiple model systems including murine liver (*in vivo*), and murine and human hepatic cell lines (*in vitro*). The downstream of EGFR, effector kinases, Akt and mTOR are all downregulated along with the expression of STAT3, and cRAF with PCB exposure *in vivo* (Chapter 2).

Both NDL and DL PCBs appear to be capable of disrupting EGF endocytosis largely through prevention of EGF binding, blocking receptor internalization. Ligand receptor modeling suggest that PCBs can bind hydrophobic pockets within the EGF binding domain of the EGFR preventing EGF binding. This theory is also reinforced by the fact that EGF pre-treated cells that did not undergo endocytosis (cells on ice to prevent endocytosis) and then were exposed to PCBs followed by incubation at 37° C still have reduced EGF endocytosis. This suggests that PCBs can displace bound EGF from its binding pocket (Chapter 3).

PCBs can disrupt the EGFR-NRF2 signaling pathway leading to diminished total glutathione, NRF2 target gene expression, and NRF2 protein expression. This is the first demonstration of EGFR regulating NRF2 in mammalian hepatic models but seems to be a conserved pathway between *C. elegans* and humans. PCB exposure and a HFD interaction also downregulate HNF4 $\alpha$  activity and expression disrupting hepatic identity gene expression. PCBs also promote a fibrotic response through hepatic release of fibrotic factors activating HSCs (Chapter 4).

Phosphoproteomic analysis demonstrates that PCBs downregulate almost 25% of the hepatic phosphoproteome in the development of TASH reinforcing the concept that PCBs act through signaling disruption. PCBs do not elevate phosphatase expression suggesting this is purely a loss of phosphoprotein signaling. PCB exposure also downregulate subunit expression of CK2 leading to increased CASP3 activation and initial hepatic apoptosis but ultimately secondary necrosis *in vivo* and *in vitro* (Chapter 5).

While findings from this research do support that PCBs do in part act through inhibition of hepatic EGFR signaling, PCBs may act more broadly in disrupting ligand-receptor interaction of multiple membrane receptors or limiting ligand secretion from other metabolic organs. The latter has been supported from epidemiological studies where exposed humans have PCB dependent decrease in leptin and insulin with increasing PCB load (13). This could in part contribute to the limited phosphoprotein signaling capability of the liver. In essence, loss of protein phosphorylation signaling pathways limits how the hepatocyte can react to metabolic changes leading to sustained cell death or necrosis.

A majority of my dissertation was involved in the characterization of the PCB-mediated effects through EGFR inhibition in the pathogenesis of NAFLD. To conclude my dissertation I wanted to determine if I could counter the effects of PCB-mediated EGFR inhibition and if this would be therapeutically effective in the context of NAFLD. Mice exposed to Aroclor 1260 and then treated with EGF have improved liver function and demonstrate reduced pathology. EGF prevented PCB-mediated steatohepatitis and fibrosis and promoted redistribution of lipids to the adipose tissue. This was the first study evaluating a therapeutic regimen for TASH can has clinical impacts or the future of NAFLD therapeutics.

In essence, my dissertation impacts two branches of science one (basic hepatology/cell signaling) being characterization of the function of hepatic EGFR and two (mechanisms of toxicology) elucidating an amenable mechanism of action for PCB-mediated NAFLD through EGFR inhibition (Figure 34).

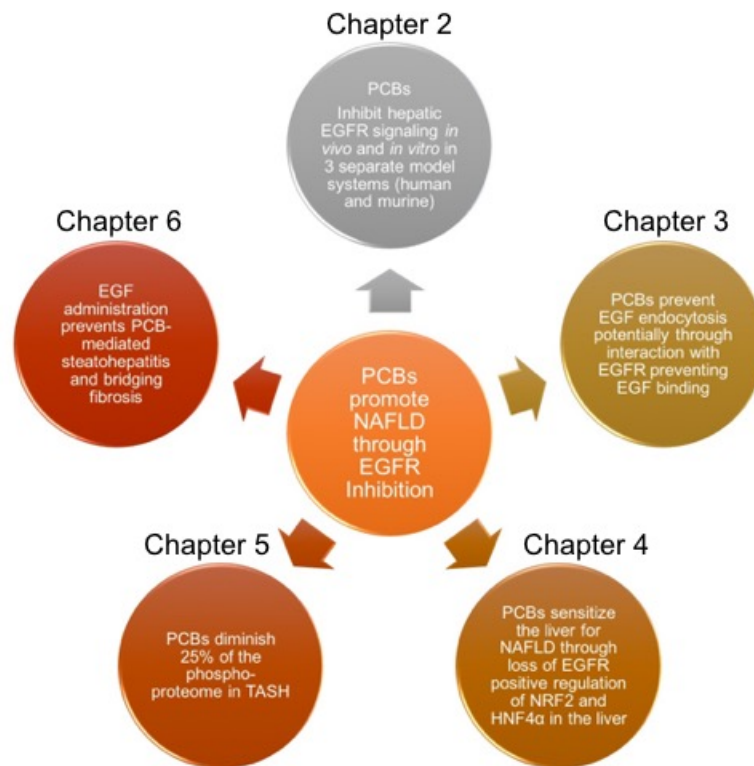


**Figure 34. PCBs act through EGFR inhibition in the pathogenesis of NAFLD:** Chapter 2 demonstrates that PCBs prevent hepatic EGFR signaling in multiple model systems. Chapter 3 illustrates that PCBs can prevent EGF endocytosis potentially through prevention of EGF ligand binding. Chapter 4 shows that PCB-mediated loss of EGFR-NRF@ and EGFR-HNF4 $\alpha$  signaling sensitizes the liver to NAFLD. Chapter 5 demonstrates that loss of protein phosphorylation is a key event in the development of PCB-mediated NAFLD. Chapter 6 provides evidence that EGF administration can prevent PCB-mediated steatohepatitis and bridging fibrosis

## REFERENCES

1. Younossi ZM, Koenig AB, Abdelatif D, Fazel Y, Henry L, Wymer M. Global epidemiology of nonalcoholic fatty liver disease-Meta-analytic assessment of prevalence, incidence, and outcomes. *Hepatology* (Baltimore, Md). 2016;64(1):73-84. Epub 2015/12/29. doi: 10.1002/hep.28431. PubMed PMID: 26707365.
2. Silva MT. Secondary necrosis: the natural outcome of the complete apoptotic program. *FEBS letters*. 2010;584(22):4491-9. Epub 2010/10/27. doi: 10.1016/j.febslet.2010.10.046. PubMed PMID: 20974143.
3. Wahlang B, Song M, Beier JI, Cameron Falkner K, Al-Eryani L, Clair HB, Prough RA, Osborne TS, Malarkey DE, Christopher States J, Cave MC. Evaluation of Aroclor 1260 exposure in a mouse model of diet-induced obesity and non-alcoholic fatty liver disease. *Toxicol Appl Pharmacol*. 2014;279(3):380-90. Epub 2014/07/08. doi: 10.1016/j.taap.2014.06.019. PubMed PMID: 24998970; PMCID: PMC4225625.
4. Al-Eryani L, Wahlang B, Falkner KC, Guardiola JJ, Clair HB, Prough RA, Cave M. Identification of Environmental Chemicals Associated with the Development of Toxicant-associated Fatty Liver Disease in Rodents. *Toxicologic pathology*. 2015;43(4):482-97. Epub 2014/10/19. doi: 10.1177/0192623314549960. PubMed PMID: 25326588; PMCID: PMC4501484.
5. Cave M, Falkner KC, Ray M, Joshi-Barve S, Brock G, Khan R, Bon Homme M, McClain CJ. Toxicant-associated steatohepatitis in vinyl chloride workers. *Hepatology*. 2010;51(2):474-81. doi: 10.1002/hep.23321. PubMed PMID: 19902480.
6. Cohen JC, Horton JD, Hobbs HH. Human fatty liver disease: old questions and new insights. *Science* (New York, NY). 2011;332(6037):1519-23. Epub 2011/06/28. doi: 10.1126/science.1204265. PubMed PMID: 21700865; PMCID: PMC3229276.
7. Registry AFTSaD. Toxicological profile for selected PCBs (Aroclor -1260, -1254, -1248, -1242, -1232, -1221, and -1016). Registry. 1989 June 1989. Report No.
8. Schechter A, Colacino J, Haffner D, Patel K, Opel M, Papke O, Birnbaum L. Perfluorinated compounds, polychlorinated biphenyls, and organochlorine pesticide contamination in composite food samples from Dallas, Texas, USA. *Environ Health Perspect*. 2010;118(6):796-802. Epub 2010/02/12. doi: 10.1289/ehp.0901347. PubMed PMID: 20146964; PMCID: Pmc2898856.
9. Safe S, Bandiera S, Sawyer T, Robertson L, Safe L, Parkinson A, Thomas PE, Ryan DE, Reik LM, Levin W, et al. PCBs: structure-function relationships and mechanism of action. *Environ Health Perspect*. 1985;60:47-56. PubMed PMID: 2992927; PMCID: 1568577.
10. Cave M, Appana S, Patel M, Falkner KC, McClain CJ, Brock G. Polychlorinated biphenyls, lead, and mercury are associated with liver disease in American adults: NHANES 2003-2004. *Environ Health Perspect*. 2010;118(12):1735-42. Epub 2010/12/04. doi: 10.1289/ehp.1002720. PubMed PMID: 21126940; PMCID: Pmc3002193.
11. Wang SL, Tsai PC, Yang CY, Leon Guo Y. Increased risk of diabetes and polychlorinated biphenyls and dioxins: a 24-year follow-up study of the Yucheng cohort. *Diabetes Care*. 2008;31(8):1574-9. Epub 2008/05/20. doi: dc07-2449 [pii] 10.2337/dc07-2449. PubMed PMID: 18487481; PMCID: 2494618.
12. Yu ML, Guo YL, Hsu CC, Rogan WJ. Increased mortality from chronic liver disease and cirrhosis 13 years after the Taiwan "yucheng" ("oil disease") incident. *American journal of industrial medicine*. 1997;31(2):172-5. Epub 1997/02/01. PubMed PMID: 9028433.

13. Clair HB, Pinkston CM, Rai SN, Pavuk M, Dutton ND, Brock G, Prough RA, Falkner KC, McClain CJ, Cave MC. Liver Disease in a Residential Cohort with Elevated Polychlorinated Biphenyl Exposures. *Toxicological sciences : an official journal of the Society of Toxicology*. 2018. Epub 2018/04/24. doi: 10.1093/toxsci/kfy076. PubMed PMID: 29684222.
14. Li MC, Tsai PC, Chen PC, Hsieh CJ, Leon Guo YL, Rogan WJ. Mortality after exposure to polychlorinated biphenyls and dibenzofurans: 30 years after the "Yucheng accident". *Environmental research*. 2013;120:71-5. Epub 2012/10/03. doi: 10.1016/j.envres.2012.09.003. PubMed PMID: 23026800; PMCID: PMC3598583.
15. Ritter R, Scherlinger M, MacLeod M, Moeckel C, Jones KC, Hungerbuehler K. Intrinsic human elimination half-lives of polychlorinated biphenyls derived from the temporal evolution of cross-sectional biomonitoring data from the United Kingdom. *Environ Health Perspect*. 2011;119(2):225-31. Epub 2010/10/12. doi: 10.1289/ehp.1002211. PubMed PMID: 20934951; PMCID: PMC3040610.
16. Baskin-Bey ES, Anan A, Isomoto H, Bronk SF, Gores GJ. Constitutive androstane receptor agonist, TCPOBOP, attenuates steatohepatitis in the methionine choline-deficient diet-fed mouse. *World journal of gastroenterology*. 2007;13(42):5635-41. Epub 2007/10/24. PubMed PMID: 17948939; PMCID: Pmc4172744.
17. Dong B, Saha PK, Huang W, Chen W, Abu-Elheiga LA, Wakil SJ, Stevens RD, Ilkayeva O, Newgard CB, Chan L, Moore DD. Activation of nuclear receptor CAR ameliorates diabetes and fatty liver disease. *Proceedings of the National Academy of Sciences of the United States of America*. 2009;106(44):18831-6. Epub 2009/10/24. doi: 10.1073/pnas.0909731106. PubMed PMID: 19850873; PMCID: Pmc2773998.
18. Wahlang B, Prough RA, Falkner KC, Hardesty JE, Song M, Clair HB, Clark BJ, States JC, Arteel GE, Cave MC. Polychlorinated Biphenyl-Xenobiotic Nuclear Receptor Interactions Regulate Energy Metabolism, Behavior, and Inflammation in Non-alcoholic-Steatohepatitis. *Toxicological sciences : an official journal of the Society of Toxicology*. 2016;149(2):396-410. Epub 2015/11/28. doi: 10.1093/toxsci/kfv250. PubMed PMID: 26612838.
19. Mutoh S, Sobhany M, Moore R, Perera L, Pedersen L, Sueyoshi T, Negishi M. Phenobarbital indirectly activates the constitutive active androstane receptor (CAR) by inhibition of epidermal growth factor receptor signaling. *Science signaling*. 2013;6(274):ra31. Epub 2013/05/09. doi: 10.1126/scisignal.2003705. PubMed PMID: 23652203.
20. Connor K, Safe S, Jefcoate CR, Larsen M. Structure-dependent induction of CYP2B by polychlorinated biphenyl congeners in female Sprague-Dawley rats. *Biochemical pharmacology*. 1995;50(11):1913-20. Epub 1995/11/27. PubMed PMID: 8615872.
21. Kocarek TA, Schuetz EG, Guzelian PS. Differentiated induction of cytochrome P450b/e and P450p mRNAs by dose of phenobarbital in primary cultures of adult rat hepatocytes. *Mol Pharmacol*. 1990;38(4):440-4. Epub 1990/10/01. PubMed PMID: 2233686.
22. Oshida K, Vasani N, Jones C, Moore T, Hester S, Nesnow S, Auerbach S, Geter DR, Aleksunes LM, Thomas RS, Applegate D, Klaassen CD, Corton JC. Identification of chemical modulators of the constitutive activated receptor (CAR) in a gene expression compendium. *Nuclear receptor signaling*. 2015;13:e002. Epub 2015/05/08. doi: 10.1621/nrs.13002. PubMed PMID: 25949234; PMCID: PMC4422105.
23. Negishi M. Phenobarbital Meets Phosphorylation of Nuclear Receptors. *Drug metabolism and disposition: the biological fate of chemicals*. 2017;45(5):532-9. Epub 2017/03/31. doi: 10.1124/dmd.116.074872. PubMed PMID: 28356313; PMCID: PMC5399647.
24. Avraham R, Yarden Y. Feedback regulation of EGFR signalling: decision making by early and delayed loops. *Nature reviews Molecular cell biology*. 2011;12(2):104-17. Epub 2011/01/22. doi: 10.1038/nrm3048. PubMed PMID: 21252999.
25. Komposch K, Sibilica M. EGFR Signaling in Liver Diseases. *International journal of molecular sciences*. 2016;17(1). Epub 2016/01/06. doi: 10.3390/ijms17010030. PubMed PMID: 26729094; PMCID: PMC4730276.
26. Herbst RS. Review of epidermal growth factor receptor biology. *International journal of radiation oncology, biology, physics*. 2004;59(2 Suppl):21-6. Epub 2004/05/15. doi: 10.1016/j.ijrobp.2003.11.041. PubMed PMID: 15142631.

27. Yewale C, Baradia D, Vhora I, Patil S, Misra A. Epidermal growth factor receptor targeting in cancer: a review of trends and strategies. *Biomaterials*. 2013;34(34):8690-707. Epub 2013/08/21. doi: 10.1016/j.biomaterials.2013.07.100. PubMed PMID: 23953842.
28. Robles MS, Humphrey SJ, Mann M. Phosphorylation Is a Central Mechanism for Circadian Control of Metabolism and Physiology. *Cell metabolism*. 2017;25(1):118-27. Epub 2016/11/08. doi: 10.1016/j.cmet.2016.10.004. PubMed PMID: 27818261.
29. Lee JB, Shin B, Lee SH, Lee BY, Kim TH, Kim MG, Yoo SD. Exposure assessment of epidermal growth factor to various tissues in mice after intravenous and subcutaneous administration. *The Journal of pharmacy and pharmacology*. 2015;67(11):1519-27. Epub 2015/08/11. doi: 10.1111/jphp.12464. PubMed PMID: 26255780.
30. Collin de l'Hortet A, Zerrad-Saadi A, Prip-Buus C, Fauveau V, Helmy N, Ziol M, Vons C, Billot K, Baud V, Gilgenkrantz H, Guidotti JE. GH administration rescues fatty liver regeneration impairment by restoring GH/EGFR pathway deficiency. *Endocrinology*. 2014;155(7):2545-54. Epub 2014/04/09. doi: 10.1210/en.2014-1010. PubMed PMID: 24708244.
31. Scheving LA, Zhang X, Stevenson MC, Threadgill DW, Russell WE. Loss of hepatocyte EGFR has no effect alone but exacerbates carbon tetrachloride-induced liver injury and impairs regeneration in hepatocyte Met-deficient mice. *American journal of physiology Gastrointestinal and liver physiology*. 2015;308(5):G364-77. Epub 2014/11/22. doi: 10.1152/ajpgi.00364.2014. PubMed PMID: 25414100; PMCID: PMC4346751.
32. Deaciuc IV, D'Souza NB, Burikhanov R, Lee EY, Tarba CN, McClain CJ, de Villiers WJ. Epidermal growth factor protects the liver against alcohol-induced injury and sensitization to bacterial lipopolysaccharide. *Alcoholism, clinical and experimental research*. 2002;26(6):864-74. Epub 2002/06/18. PubMed PMID: 12068256.
33. Sunahara GI, Nelson KG, Wong TK, Lucier GW. Decreased human birth weights after in utero exposure to PCBs and PCDFs are associated with decreased placental EGF-stimulated receptor autophosphorylation capacity. *Mol Pharmacol*. 1987;32(5):572-8. Epub 1987/11/01. PubMed PMID: 3119985.
34. Kim KS, Lee YM, Kim SG, Lee IK, Lee HJ, Kim JH, Kim J, Moon HB, Jacobs DR, Jr., Lee DH. Associations of organochlorine pesticides and polychlorinated biphenyls in visceral vs. subcutaneous adipose tissue with type 2 diabetes and insulin resistance. *Chemosphere*. 2014;94:151-7. doi: 10.1016/j.chemosphere.2013.09.066. PubMed PMID: 24161582.
35. McFarland VA, Clarke JU. Environmental occurrence, abundance, and potential toxicity of polychlorinated biphenyl congeners: considerations for a congener-specific analysis. *Environ Health Perspect*. 1989;81:225-39. Epub 1989/05/01. PubMed PMID: 2503374; PMCID: Pmc1567542.
36. Wahlang B, Falkner KC, Clair HB, Al-Eryani L, Prough RA, States JC, Coslo DM, Omiecinski CJ, Cave MC. Human receptor activation by aroclor 1260, a polychlorinated biphenyl mixture. *Toxicological sciences : an official journal of the Society of Toxicology*. 2014;140(2):283-97. Epub 2014/05/09. doi: 10.1093/toxsci/kfu083. PubMed PMID: 24812009; PMCID: PMC4176050.
37. Schecter A, Colacino J, Haffner D, Patel K, Opel M, Papke O, Birnbaum L. Perfluorinated Compounds, Polychlorinated Biphenyl, and Organochlorine Pesticide Contamination in Composite Food Samples from Dallas, Texas. *Environ Health Perspect*. 2010. Epub 2010/02/12. doi: 10.1289/ehp.0901347. PubMed PMID: 20146964.
38. Serdar B, LeBlanc WG, Norris JM, Dickinson LM. Potential effects of polychlorinated biphenyls (PCBs) and selected organochlorine pesticides (OCPs) on immune cells and blood biochemistry measures: a cross-sectional assessment of the NHANES 2003-2004 data. *Environmental health : a global access science source*. 2014;13:114. doi: 10.1186/1476-069X-13-114. PubMed PMID: 25515064; PMCID: 4290093.
39. Kumar J, Lind L, Salihovic S, van Bavel B, Ingelsson E, Lind PM. Persistent organic pollutants and liver dysfunction biomarkers in a population-based human sample of men and women. *Environmental research*. 2014;134:251-6. Epub 2014/09/01. doi: 10.1016/j.envres.2014.07.023. PubMed PMID: 25173059.
40. Yorita Christensen KL, Carrico CK, Sanyal AJ, Gennings C. Multiple classes of environmental chemicals are associated with liver disease: NHANES 2003-2004. *International*

- journal of hygiene and environmental health. 2013. doi: 10.1016/j.ijheh.2013.01.005. PubMed PMID: 23491026; PMCID: 3713174.
41. Ghosh S, Murinova L, Trnovec T, Loffredo CA, Washington K, Mitra PS, Dutta SK. Biomarkers linking PCB exposure and obesity. *Current pharmaceutical biotechnology*. 2014;15(11):1058-68. PubMed PMID: 25420728; PMCID: 4292903.
  42. Goncharov A, Bloom M, Pavuk M, Birman I, Carpenter DO. Blood pressure and hypertension in relation to levels of serum polychlorinated biphenyls in residents of Anniston, Alabama. *J Hypertens*. 2010;28(10):2053-60. Epub 2010/07/21. doi: 10.1097/HJH.0b013e32833c5f3e. PubMed PMID: 20644494.
  43. Silverstone AE, Rosenbaum PF, Weinstock RS, Bartell SM, Foushee HR, Shelton C, Pavuk M. Polychlorinated biphenyl (PCB) exposure and diabetes: results from the Anniston Community Health Survey. *Environmental health perspectives*. 2012;120(5):727-32. Epub 2012/02/16. doi: 10.1289/ehp.1104247. PubMed PMID: 22334129; PMCID: 3346783.
  44. Patel CJ, Bhattacharya J, Butte AJ. An Environment-Wide Association Study (EWAS) on type 2 diabetes mellitus. *PLoS One*. 2010;5(5):e10746. Epub 2010/05/28. doi: 10.1371/journal.pone.0010746. PubMed PMID: 20505766; PMCID: 2873978.
  45. Aminov Z, Haase RF, Pavuk M, Carpenter DO, Anniston Environmental Health Research C. Analysis of the effects of exposure to polychlorinated biphenyls and chlorinated pesticides on serum lipid levels in residents of Anniston, Alabama. *Environmental health : a global access science source*. 2013;12:108. doi: 10.1186/1476-069X-12-108. PubMed PMID: 24325314; PMCID: 3893492.
  46. Al-Eryani L, Wahlang B, Falkner KC, Guardiola JJ, Clair HB, Prough RA, Cave M. Identification of Environmental Chemicals Associated with the Development of Toxicant-associated Fatty Liver Disease in Rodents. *Toxicologic pathology*. 2014. doi: 10.1177/0192623314549960. PubMed PMID: 25326588.
  47. Sawyer T, Safe S. PCB isomers and congeners: induction of aryl hydrocarbon hydroxylase and ethoxyresorufin O-deethylase enzyme activities in rat hepatoma cells. *Toxicology letters*. 1982;13(1-2):87-93. PubMed PMID: 6817473.
  48. Al-Salman F, Plant N. Non-coplanar polychlorinated biphenyls (PCBs) are direct agonists for the human pregnane-X receptor and constitutive androstane receptor, and activate target gene expression in a tissue-specific manner. *Toxicol Appl Pharmacol*. 2012;263(1):7-13. Epub 2012/06/06. doi: 10.1016/j.taap.2012.05.016. PubMed PMID: 22664347.
  49. Gschwind A, Zwick E, Prenzel N, Leserer M, Ullrich A. Cell communication networks: epidermal growth factor receptor transactivation as the paradigm for interreceptor signal transmission. *Oncogene*. 2001;20(13):1594-600. Epub 2001/04/21. doi: 10.1038/sj.onc.1204192. PubMed PMID: 11313906.
  50. Caron A, Richard D, Laplante M. The Roles of mTOR Complexes in Lipid Metabolism. *Annual review of nutrition*. 2015;35:321-48. Epub 2015/07/18. doi: 10.1146/annurev-nutr-071714-034355. PubMed PMID: 26185979.
  51. Taniguchi CM, Emanuelli B, Kahn CR. Critical nodes in signalling pathways: insights into insulin action. *Nature reviews Molecular cell biology*. 2006;7(2):85-96. Epub 2006/02/24. doi: 10.1038/nrm1837. PubMed PMID: 16493415.
  52. Bernal-Mizrachi E, Kulkarni RN, Scott DK, Mauvais-Jarvis F, Stewart AF, Garcia-Ocana A. Human beta-cell proliferation and intracellular signaling part 2: still driving in the dark without a road map. *Diabetes*. 2014;63(3):819-31. Epub 2014/02/22. doi: 10.2337/db13-1146. PubMed PMID: 24556859; PMCID: PMC3931400.
  53. Miettinen P, Ormio P, Hakonen E, Banerjee M, Otonkoski T. EGF receptor in pancreatic beta-cell mass regulation. *Biochemical Society transactions*. 2008;36(Pt 3):280-5. Epub 2008/05/17. doi: 10.1042/bst0360280. PubMed PMID: 18481942.
  54. Scheving LA, Zhang X, Garcia OA, Wang RF, Stevenson MC, Threadgill DW, Russell WE. Epidermal growth factor receptor plays a role in the regulation of liver and plasma lipid levels in adult male mice. *American journal of physiology Gastrointestinal and liver physiology*. 2014;306(5):G370-81. Epub 2014/01/11. doi: 10.1152/ajpgi.00116.2013. PubMed PMID: 24407590; PMCID: PMC3949019.
  55. Taylor KW, Novak RF, Anderson HA, Birnbaum LS, Blystone C, Devito M, Jacobs D, Kohrle J, Lee DH, Rylander L, Rignell-Hydbom A, Tornero-Velez R, Turyk ME, Boyles AL, Thayer KA,

- Lind L. Evaluation of the association between persistent organic pollutants (POPs) and diabetes in epidemiological studies: a national toxicology program workshop review. *Environ Health Perspect.* 2013;121(7):774-83. Epub 2013/05/09. doi: 10.1289/ehp.1205502. PubMed PMID: 23651634; PMCID: PMC3701910.
56. Wahlang B, Prough RA, Falkner KC, Hardesty JE, Song M, Clair HB, Clark BJ, States JC, Arteel GE, Cave MC. Polychlorinated Biphenyl-Xenobiotic Nuclear Receptor Interactions Regulate Energy Metabolism, Behavior, and Inflammation in Nonalcoholic-Steatohepatitis. *Toxicological sciences : an official journal of the Society of Toxicology.* 2015. Epub 2015/11/28. doi: 10.1093/toxsci/kfv250. PubMed PMID: 26612838.
57. Wahlang B, Song M, Beier JI, Falkner KC, Al-Eryani L, Clair HB, Prough RA, Osborne TS, Malarkey DE, States JC, Cave MC. Evaluation of Aroclor 1260 exposure in a mouse model of diet-induced obesity and non-alcoholic fatty liver disease. *Toxicology and applied pharmacology.* 2014;279(3):380-90. doi: 10.1016/j.taap.2014.06.019. PubMed PMID: WOS:000342278000014.
58. Falkner KC, Rushmore TH, Linder MW, Prough RA. Negative regulation of the rat glutathione S-transferase A2 gene by glucocorticoids involves a canonical glucocorticoid consensus sequence. *Mol Pharmacol.* 1998;53(6):1016-26. PubMed PMID: 9614203.
59. Lamba JK, Lamba V, Yasuda K, Lin YS, Assem M, Thompson E, Strom S, Schuetz E. Expression of constitutive androstane receptor splice variants in human tissues and their functional consequences. *The Journal of pharmacology and experimental therapeutics.* 2004;311(2):811-21. Epub 2004/06/15. doi: 10.1124/jpet.104.069310. PubMed PMID: 15194709.
60. Gao J, He J, Zhai Y, Wada T, Xie W. The constitutive androstane receptor is an anti-obesity nuclear receptor that improves insulin sensitivity. *The Journal of biological chemistry.* 2009;284(38):25984-92. Epub 2009/07/21. doi: 10.1074/jbc.M109.016808. PubMed PMID: 19617349; PMCID: PMC2757999.
61. NTP. Toxicology and carcinogenesis studies of a binary mixture of 3,3',4,4',5-pentachlorobiphenyl (PCB 126) (Cas No. 57465-28-8) and 2,2',4,4',5,5'-hexachlorobiphenyl (PCB 153) (CAS No. 35065-27-1) in female Harlan Sprague-Dawley rats (gavage studies). National Toxicology Program technical report series. 2006(530):1-258. Epub 2006/12/13. PubMed PMID: 17160104.
62. Lin FH, Clark G, Birnbaum LS, Lucier GW, Goldstein JA. Influence of the Ah locus on the effects of 2,3,7,8-tetrachlorodibenzo-p-dioxin on the hepatic epidermal growth factor receptor. *Mol Pharmacol.* 1991;39(3):307-13. Epub 1991/03/01. PubMed PMID: 1848654.
63. Eum SY, Lee YW, Hennig B, Toborek M. Interplay between epidermal growth factor receptor and Janus kinase 3 regulates polychlorinated biphenyl-induced matrix metalloproteinase-3 expression and transendothelial migration of tumor cells. *Molecular cancer research : MCR.* 2006;4(6):361-70. Epub 2006/06/17. doi: 10.1158/1541-7786.mcr-05-0119. PubMed PMID: 16778083.
64. CDC. National Report on Human Exposures to Environmental Chemicals, Centers for Disease Control. (Methylmercury results have been compared to total mercury in CDC biomonitoring.). 2005.
65. Wang J, Wu Y, Dong M, He X, Wang Z, Li J, Wang Y. Observation of hepatotoxicity during long-term gefitinib administration in patients with non-small-cell lung cancer. *Anti-cancer drugs.* 2016;27(3):245-50. Epub 2015/12/04. doi: 10.1097/cad.0000000000000323. PubMed PMID: 26633888; PMCID: PMC4736296.
66. Karlsson HK, Zierath JR, Kane S, Krook A, Lienhard GE, Wallberg-Henriksson H. Insulin-stimulated phosphorylation of the Akt substrate AS160 is impaired in skeletal muscle of type 2 diabetic subjects. *Diabetes.* 2005;54(6):1692-7. Epub 2005/05/28. PubMed PMID: 15919790.
67. Angrish MM, Kaiser JP, McQueen CA, Chorley BN. Tipping the Balance: Hepatotoxicity and the 4 Apical Key Events of Hepatic Steatosis. *Toxicological sciences : an official journal of the Society of Toxicology.* 2016;150(2):261-8. Epub 2016/03/17. doi: 10.1093/toxsci/kfw018. PubMed PMID: 26980302.
68. Min HK, Mirshahi F, Verdianelli A, Pacana T, Patel V, Park CG, Choi A, Lee JH, Park CB, Ren S, Sanyal AJ. Activation of the GP130-STAT3 axis and its potential implications in nonalcoholic fatty liver disease. *American journal of physiology Gastrointestinal and liver physiology.* 2015;308(9):G794-803. Epub 2015/03/10. doi: 10.1152/ajpgi.00390.2014. PubMed PMID: 25747354; PMCID: PMC4421014.



69. Sookoian S, Castano G, Gianotti TF, Gemma C, Rosselli MS, Pirola CJ. Genetic variants in STAT3 are associated with nonalcoholic fatty liver disease. *Cytokine*. 2008;44(1):201-6. Epub 2008/09/16. doi: 10.1016/j.cyto.2008.08.001. PubMed PMID: 18789715.
70. Miller AM, Wang H, Bertola A, Park O, Horiguchi N, Ki SH, Yin S, Lafdil F, Gao B. Inflammation-associated interleukin-6/signal transducer and activator of transcription 3 activation ameliorates alcoholic and nonalcoholic fatty liver diseases in interleukin-10-deficient mice. *Hepatology (Baltimore, Md)*. 2011;54(3):846-56. Epub 2011/07/05. doi: 10.1002/hep.24517. PubMed PMID: 21725996; PMCID: PMC3197882.
71. Knebel B, Lehr S, Hartwig S, Haas J, Kaber G, Dicken HD, Susanto F, Bohne L, Jacob S, Nitzgen U, Passlack W, Muller-Wieland D, Kotzka J. Phosphorylation of sterol regulatory element-binding protein (SREBP)-1c by p38 kinases, ERK and JNK influences lipid metabolism and the secretome of human liver cell line HepG2. *Archives of physiology and biochemistry*. 2014;120(5):216-27. Epub 2014/10/30. doi: 10.3109/13813455.2014.973418. PubMed PMID: 25353341.
72. Czaja MJ, Liu H, Wang Y. Oxidant-induced hepatocyte injury from menadione is regulated by ERK and AP-1 signaling. *Hepatology (Baltimore, Md)*. 2003;37(6):1405-13. Epub 2003/05/30. doi: 10.1053/jhep.2003.50233. PubMed PMID: 12774020.
73. Hong MY, Lumibao J, Mistry P, Saleh R, Hoh E. Fish Oil Contaminated with Persistent Organic Pollutants Reduces Antioxidant Capacity and Induces Oxidative Stress without Affecting Its Capacity to Lower Lipid Concentrations and Systemic Inflammation in Rats. *The Journal of nutrition*. 2015;145(5):939-44. Epub 2015/03/20. doi: 10.3945/jn.114.206607. PubMed PMID: 25788582; PMCID: PMC4408738.
74. Liu C, Yang J, Fu W, Qi S, Wang C, Quan C, Yang K. Coactivation of the PI3K/Akt and ERK signaling pathways in PCB153-induced NF-kappaB activation and caspase inhibition. *Toxicol Appl Pharmacol*. 2014;277(3):270-8. Epub 2014/04/15. doi: 10.1016/j.taap.2014.03.027. PubMed PMID: 24726520.
75. Birnbaum LS, Dutton ND, Cusack C, Mennemeyer ST, Pavuk M. Anniston community health survey: Follow-up and dioxin analyses (ACHS-II)--methods. *Environmental science and pollution research international*. 2016;23(3):2014-21. Epub 2015/05/20. doi: 10.1007/s11356-015-4684-3. PubMed PMID: 25982988; PMCID: PMC4648703.
76. Park SH, Hong YS, Ha EH, Park H. Serum concentrations of PCBs and OCPs among prepubertal Korean children. *Environmental science and pollution research international*. 2016;23(4):3536-47. Epub 2015/10/23. doi: 10.1007/s11356-015-5578-0. PubMed PMID: 26490932.
77. Elobeid MA, Padilla MA, Brock DW, Ruden DM, Allison DB. Endocrine disruptors and obesity: an examination of selected persistent organic pollutants in the NHANES 1999-2002 data. *International journal of environmental research and public health*. 2010;7(7):2988-3005. Epub 2010/08/19. doi: 10.3390/ijerph7072988. PubMed PMID: 20717554; PMCID: PMC2922741.
78. Rinsky JL, Hopenhayn C, Golla V, Browning S, Bush HM. Atrazine exposure in public drinking water and preterm birth. *Public health reports (Washington, DC : 1974)*. 2012;127(1):72-80. Epub 2012/02/03. doi: 10.1177/003335491212700108. PubMed PMID: 22298924; PMCID: PMC3234399.
79. Heindel JJ, Newbold R, Schug TT. Endocrine disruptors and obesity. *Nature reviews Endocrinology*. 2015;11(11):653-61. Epub 2015/09/24. doi: 10.1038/nrendo.2015.163. PubMed PMID: 26391979.
80. Heindel JJ, Blumberg B, Cave M, Machtinger R, Mantovani A, Mendez MA, Nadal A, Palanza P, Panzica G, Sargis R, Vandenberg LN, Vom Saal F. Metabolism disrupting chemicals and metabolic disorders. *Reproductive toxicology (Elmsford, NY)*. 2017;68:3-33. Epub 2016/10/21. doi: 10.1016/j.reprotox.2016.10.001. PubMed PMID: 27760374; PMCID: PMC5365353.
81. Ju Q, Zouboulis CC, Xia L. Environmental pollution and acne: Chloracne. *Dermato-endocrinology*. 2009;1(3):125-8. Epub 2010/05/04. PubMed PMID: 20436879; PMCID: PMC2835904.
82. Fischbein A, Wolff MS, Lilis R, Thornton J, Selikoff IJ. Clinical findings among PCB-exposed capacitor manufacturing workers. *Annals of the New York Academy of Sciences*. 1979;320:703-15. Epub 1979/05/31. PubMed PMID: 110206.

83. Reggiani G, Bruppacher R. Symptoms, signs and findings in humans exposed to PCBs and their derivatives. *Environ Health Perspect.* 1985;60:225-32. Epub 1985/05/01. PubMed PMID: 2992922; PMCID: PMC1568540.
84. Emmett EA, Maroni M, Schmith JM, Levin BK, Jefferys J. Studies of transformer repair workers exposed to PCBs: I. Study design, PCB concentrations, questionnaire, and clinical examination results. *American journal of industrial medicine.* 1988;13(4):415-27. Epub 1988/01/01. PubMed PMID: 3129934.
85. Fischbein A, Thornton J, Wolff MS, Bernstein J, Selifoff IJ. Dermatological findings in capacitor manufacturing workers exposed to dielectric fluids containing polychlorinated biphenyls (PCBs). *Archives of environmental health.* 1982;37(2):69-74. Epub 1982/03/01. PubMed PMID: 6462115.
86. Fischbein A, Rizzo JN, Solomon SJ, Wolff MS. Oculodermatological findings in workers with occupational exposure to polychlorinated biphenyls (PCBs). *British journal of industrial medicine.* 1985;42(6):426-30. Epub 1985/06/01. PubMed PMID: 3924093; PMCID: PMC1007503.
87. Cave M, Falkner KC, Henry L, Costello B, Gregory B, McClain CJ. Serum cytokeratin 18 and cytokine elevations suggest a high prevalence of occupational liver disease in highly exposed elastomer/polymer workers. *Journal of occupational and environmental medicine.* 2011;53(10):1128-33. Epub 2011/09/15. doi: 10.1097/JOM.0b013e31822cfd68. PubMed PMID: 21915069; PMCID: PMC3190062.
88. Wahlang B, Beier JI, Clair HB, Bellis-Jones HJ, Falkner KC, McClain CJ, Cave MC. Toxicant-associated steatohepatitis. *Toxicologic pathology.* 2013;41(2):343-60. doi: 10.1177/0192623312468517. PubMed PMID: 23262638.
89. Dix DJ, Houck KA, Martin MT, Richard AM, Setzer RW, Kavlock RJ. The ToxCast program for prioritizing toxicity testing of environmental chemicals. *Toxicological sciences : an official journal of the Society of Toxicology.* 2007;95(1):5-12. Epub 2006/09/12. doi: 10.1093/toxsci/kfl103. PubMed PMID: 16963515.
90. Kiyosawa N, Kwekel JC, Burgoon LD, Dere E, Williams KJ, Tashiro C, Chittim B, Zacharewski TR. Species-specific regulation of PXR/CAR/ER-target genes in the mouse and rat liver elicited by o, p'-DDT. *BMC genomics.* 2008;9:487. Epub 2008/10/18. doi: 10.1186/1471-2164-9-487. PubMed PMID: 18925944; PMCID: PMC2577663.
91. Sakai H, Iwata H, Kim EY, Tsydenova O, Miyazaki N, Petrov EA, Batoev VB, Tanabe S. Constitutive androstane receptor (CAR) as a potential sensing biomarker of persistent organic pollutants (POPs) in aquatic mammal: molecular characterization, expression level, and ligand profiling in Baikal seal (*Pusa sibirica*). *Toxicological sciences : an official journal of the Society of Toxicology.* 2006;94(1):57-70. Epub 2006/08/25. doi: 10.1093/toxsci/kfl088. PubMed PMID: 16929008.
92. Wei P, Zhang J, Dowhan DH, Han Y, Moore DD. Specific and overlapping functions of the nuclear hormone receptors CAR and PXR in xenobiotic response. *The pharmacogenomics journal.* 2002;2(2):117-26. Epub 2002/06/07. PubMed PMID: 12049174.
93. Bondy GS, Newsome WH, Armstrong CL, Suzuki CA, Doucet J, Fernie S, Hierlihy SL, Feeley MM, Barker MG. trans-Nonachlor and cis-nonachlor toxicity in Sprague-Dawley rats: comparison with technical chlordane. *Toxicological sciences : an official journal of the Society of Toxicology.* 2000;58(2):386-98. Epub 2000/12/02. PubMed PMID: 11099650.
94. ATSDR. Toxicological profile for chlordane. Agency for Toxic Substances and Disease Registry (ATSDR). Atlanta, GA: U.S. Department of Health and Human Services, 1994.
95. Montgomery MP, Kamel F, Saldana TM, Alavanja MC, Sandler DP. Incident diabetes and pesticide exposure among licensed pesticide applicators: Agricultural Health Study, 1993-2003. *American journal of epidemiology.* 2008;167(10):1235-46. Epub 2008/03/18. doi: 10.1093/aje/kwn028. PubMed PMID: 18343878; PMCID: PMC2832308.
96. Hardesty JE, Wahlang B, Falkner KC, Clair HB, Clark BJ, Ceresa BP, Prough RA, Cave MC. Polychlorinated Biphenyls Disrupt Hepatic Epidermal Growth Factor Receptor Signaling. *Xenobiotica; the fate of foreign compounds in biological systems.* 2016:1-40. Epub 2016/07/28. doi: 10.1080/00498254.2016.1217572. PubMed PMID: 27458090.
97. Natarajan A, Wagner B, Sibilila M. The EGF receptor is required for efficient liver regeneration. *Proceedings of the National Academy of Sciences of the United States of America.*

- 2007;104(43):17081-6. Epub 2007/10/18. doi: 10.1073/pnas.0704126104. PubMed PMID: 17940036; PMCID: Pmc2040457.
98. Jorgensen PE, Poulsen SS, Nexo E. Distribution of i.v. administered epidermal growth factor in the rat. *Regulatory peptides*. 1988;23(2):161-9. Epub 1988/11/01. PubMed PMID: 3266016.
99. Lorient Y, Perlemuter G, Malka D, Penault-Llorca F, Boige V, Deutsch E, Massard C, Armand JP, Soria JC. Drug insight: gastrointestinal and hepatic adverse effects of molecular-targeted agents in cancer therapy. *Nature clinical practice Oncology*. 2008;5(5):268-78. Epub 2008/03/20. doi: 10.1038/ncponc1087. PubMed PMID: 18349858.
100. Fong Y, Bentrem DJ. CASH (Chemotherapy-Associated Steatohepatitis) costs. *Annals of surgery*. 2006;243(1):8-9. Epub 2005/12/24. PubMed PMID: 16371729; PMCID: PMC1449964.
101. Fountas A, Diamantopoulos LN, Tsatsoulis A. Tyrosine Kinase Inhibitors and Diabetes: A Novel Treatment Paradigm? *Trends Endocrinol Metab*. 2015;26(11):643-56. doi: 10.1016/j.tem.2015.09.003. PubMed PMID: 26492832.
102. Prada PO, Ropelle ER, Mourao RH, de Souza CT, Pauli JR, Cintra DE, Schenka A, Rocco SA, Rittner R, Franchini KG, Vassallo J, Velloso LA, Carvalheira JB, Saad MJ. EGFR tyrosine kinase inhibitor (PD153035) improves glucose tolerance and insulin action in high-fat diet-fed mice. *Diabetes*. 2009;58(12):2910-9. Epub 2009/08/22. doi: 10.2337/db08-0506. PubMed PMID: 19696185; PMCID: PMC2780887.
103. Dikshith TSS DP. *Industrial Guide to Chemical and Drug Safety*: Wiley; 2003 April 2003. 629 p.
104. CDC. Occupational Safety and Health Guideline for Atrazine. CDC, 1992 1992. Report No.
105. Holcman M, Sibilina M. Mechanisms underlying skin disorders induced by EGFR inhibitors. *Molecular & cellular oncology*. 2015;2(4):e1004969. Epub 2016/06/17. doi: 10.1080/23723556.2015.1004969. PubMed PMID: 27308503; PMCID: PMC4905346.
106. Mascia F, Lam G, Keith C, Garber C, Steinberg SM, Kohn E, Yuspa SH. Genetic ablation of epidermal EGFR reveals the dynamic origin of adverse effects of anti-EGFR therapy. *Science translational medicine*. 2013;5(199):199ra10. Epub 2013/08/24. doi: 10.1126/scitranslmed.3005773. PubMed PMID: 23966299.
107. ATSDR. Toxicological profile for DDT, DDE, DDD. U.S. Department of Health and Human Services; Atlanta, GA, 2002.
108. ATSDR. Toxicological profile for Aldrin/Dieldrin. U.S. Department of Health and Human Services; Atlanta, GA, 2002.
109. Campbell P, Morton PE, Takeichi T, Salam A, Roberts N, Proudfoot LE, Mellerio JE, Aminu K, Wellington C, Patil SN, Akiyama M, Liu L, McMillan JR, Aristodemou S, Ishida-Yamamoto A, Abdul-Wahab A, Petrof G, Fong K, Harnchoowong S, Stone KL, Harper JI, McLean WH, Simpson MA, Parsons M, McGrath JA. Epithelial inflammation resulting from an inherited loss-of-function mutation in EGFR. *The Journal of investigative dermatology*. 2014;134(10):2570-8. Epub 2014/04/03. doi: 10.1038/jid.2014.164. PubMed PMID: 24691054; PMCID: PMC4090136.
110. Lichtenberger BM, Gerber PA, Holcman M, Buhren BA, Amberg N, Smolle V, Schrupf H, Boelke E, Ansari P, Mackenzie C, Wollenberg A, Kislat A, Fischer JW, Rock K, Harder J, Schroder JM, Homey B, Sibilina M. Epidermal EGFR controls cutaneous host defense and prevents inflammation. *Science translational medicine*. 2013;5(199):199ra11. Epub 2013/08/24. doi: 10.1126/scitranslmed.3005886. PubMed PMID: 23966300.
111. Hansen LA, Alexander N, Hogan ME, Sundberg JP, Dlugosz A, Threadgill DW, Magnuson T, Yuspa SH. Genetically null mice reveal a central role for epidermal growth factor receptor in the differentiation of the hair follicle and normal hair development. *The American journal of pathology*. 1997;150(6):1959-75. Epub 1997/06/01. PubMed PMID: 9176390; PMCID: PMC1858310.
112. Miettinen PJ, Chin JR, Shum L, Slavkin HC, Shuler CF, Derynck R, Werb Z. Epidermal growth factor receptor function is necessary for normal craniofacial development and palate closure. *Nature genetics*. 1999;22(1):69-73. Epub 1999/05/13. doi: 10.1038/8773. PubMed PMID: 10319864.
113. Miettinen PJ, Berger JE, Meneses J, Phung Y, Pedersen RA, Werb Z, Derynck R. Epithelial immaturity and multiorgan failure in mice lacking epidermal growth factor receptor. *Nature*. 1995;376(6538):337-41. Epub 1995/07/27. doi: 10.1038/376337a0. PubMed PMID: 7630400.

114. Wang J, Xie X. Development of a quantitative, cell-based, high-content screening assay for epidermal growth factor receptor modulators. *Acta pharmacologica Sinica*. 2007;28(10):1698-704. Epub 2007/09/22. doi: 10.1111/j.1745-7254.2007.00640.x. PubMed PMID: 17883960.
115. Haigler H, Ash JF, Singer SJ, Cohen S. Visualization by fluorescence of the binding and internalization of epidermal growth factor in human carcinoma cells A-431. *Proceedings of the National Academy of Sciences of the United States of America*. 1978;75(7):3317-21. Epub 1978/07/01. PubMed PMID: 356052; PMCID: PMC392766.
116. Ferguson KM, Berger MB, Mendrola JM, Cho HS, Leahy DJ, Lemmon MA. EGF activates its receptor by removing interactions that autoinhibit ectodomain dimerization. *Molecular cell*. 2003;11(2):507-17. Epub 2003/03/07. PubMed PMID: 12620237.
117. Kim S, Thiessen PA, Bolton EE, Chen J, Fu G, Gindulyte A, Han L, He J, He S, Shoemaker BA, Wang J, Yu B, Zhang J, Bryant SH. PubChem Substance and Compound databases. *Nucleic acids research*. 2016;44(D1):D1202-13. Epub 2015/09/25. doi: 10.1093/nar/gkv951. PubMed PMID: 26400175; PMCID: PMC4702940.
118. Moustakas DT, Lang PT, Pegg S, Pettersen E, Kuntz ID, Brooijmans N, Rizzo RC. Development and validation of a modular, extensible docking program: DOCK 5. *Journal of computer-aided molecular design*. 2006;20(10-11):601-19. Epub 2006/12/07. doi: 10.1007/s10822-006-9060-4. PubMed PMID: 17149653.
119. Park JH, Liu Y, Lemmon MA, Radhakrishnan R. Erlotinib binds both inactive and active conformations of the EGFR tyrosine kinase domain. *The Biochemical journal*. 2012;448(3):417-23. Epub 2012/10/30. doi: 10.1042/bj20121513. PubMed PMID: 23101586; PMCID: PMC3507260.
120. Tzamelis I, Pissios P, Schuetz EG, Moore DD. The xenobiotic compound 1,4-bis[2-(3,5-dichloropyridyloxy)]benzene is an agonist ligand for the nuclear receptor CAR. *Molecular and cellular biology*. 2000;20(9):2951-8. Epub 2000/04/11. PubMed PMID: 10757780; PMCID: PMC85552.
121. Lucier GW, Nelson KG, Everson RB, Wong TK, Philpot RM, Tiernan T, Taylor M, Sunahara GI. Placental markers of human exposure to polychlorinated biphenyls and polychlorinated dibenzofurans. *Environmental Health Perspectives*. 1987;76:79-87. PubMed PMID: PMC1474460.
122. Ozcan F, Klein P, Lemmon MA, Lax I, Schlessinger J. On the nature of low- and high-affinity EGF receptors on living cells. *Proceedings of the National Academy of Sciences of the United States of America*. 2006;103(15):5735-40. Epub 2006/03/31. doi: 10.1073/pnas.0601469103. PubMed PMID: 16571657; PMCID: PMC1458642.
123. Needham SR, Roberts SK, Arkhipov A, Mysore VP, Tynan CJ, Zanetti-Domingues LC, Kim ET, Losasso V, Korovesis D, Hirsch M, Rolfe DJ, Clarke DT, Winn MD, Lajevardipour A, Clayton AH, Pike LJ, Perani M, Parker PJ, Shan Y, Shaw DE, Martin-Fernandez ML. EGFR oligomerization organizes kinase-active dimers into competent signalling platforms. *Nature communications*. 2016;7:13307. Epub 2016/11/01. doi: 10.1038/ncomms13307. PubMed PMID: 27796308; PMCID: PMC5095584.
124. Ward CW, Lawrence MC, Streltsov VA, Adams TE, McKern NM. The insulin and EGF receptor structures: new insights into ligand-induced receptor activation. *Trends in biochemical sciences*. 2007;32(3):129-37. Epub 2007/02/07. doi: 10.1016/j.tibs.2007.01.001. PubMed PMID: 17280834.
125. Citri A, Yarden Y. EGF-ERBB signalling: towards the systems level. *Nature reviews Molecular cell biology*. 2006;7(7):505-16. Epub 2006/07/11. doi: 10.1038/nrm1962. PubMed PMID: 16829981.
126. Krall JA, Beyer EM, MacBeath G. High- and low-affinity epidermal growth factor receptor-ligand interactions activate distinct signaling pathways. *PLoS One*. 2011;6(1):e15945. Epub 2011/01/26. doi: 10.1371/journal.pone.0015945. PubMed PMID: 21264347; PMCID: PMC3018525.
127. Fernandez-Pol JA. Epidermal growth factor receptor of A431 cells. Characterization of a monoclonal anti-receptor antibody noncompetitive agonist of epidermal growth factor action. *The Journal of biological chemistry*. 1985;260(8):5003-11. Epub 1985/04/25. PubMed PMID: 2985573.
128. Yasujima T, Saito K, Moore R, Negishi M. Phenobarbital and Insulin Reciprocate Activation of the Nuclear Receptor Constitutive Androstane Receptor through the Insulin Receptor. *The Journal of pharmacology and experimental therapeutics*. 2016;357(2):367-74. Epub 2016/03/20. doi: 10.1124/jpet.116.232140. PubMed PMID: 26994072; PMCID: PMC4851327.

129. Zwick E, Bange J, Ullrich A. Receptor tyrosine kinase signalling as a target for cancer intervention strategies. *Endocrine-related cancer*. 2001;8(3):161-73. Epub 2001/09/22. PubMed PMID: 11566607.
130. Robinson DR, Wu YM, Lin SF. The protein tyrosine kinase family of the human genome. *Oncogene*. 2000;19(49):5548-57. Epub 2000/12/15. doi: 10.1038/sj.onc.1203957. PubMed PMID: 11114734.
131. Lee HY, Jung H, Jang IH, Suh PG, Ryu SH. Cdk5 phosphorylates PLD2 to mediate EGF-dependent insulin secretion. *Cellular signalling*. 2008;20(10):1787-94. Epub 2008/07/16. doi: 10.1016/j.cellsig.2008.06.009. PubMed PMID: 18625302.
132. Lee HY, Yea K, Kim J, Lee BD, Chae YC, Kim HS, Lee DW, Kim SH, Cho JH, Jin CJ, Koh DS, Park KS, Suh PG, Ryu SH. Epidermal growth factor increases insulin secretion and lowers blood glucose in diabetic mice. *Journal of cellular and molecular medicine*. 2008;12(5a):1593-604. Epub 2007/12/07. doi: 10.1111/j.1582-4934.2007.00169.x. PubMed PMID: 18053093; PMCID: PMC3918075.
133. Prada PO, Ropelle ER, Mourao RH, de Souza CT, Pauli JR, Cintra DE, Schenka A, Rocco SA, Rittner R, Franchini KG, Vassallo J, Velloso LA, Carvalheira JB, Saad MJ. Expression of Concern. EGFR Tyrosine Kinase Inhibitor (PD153035) Improves Glucose Tolerance and Insulin Action in High-Fat Diet-Fed Mice. *Diabetes* 2009;58:2910-2919. DOI: 10.2337/db08-0506. PMID: 19696185. *Diabetes*. 2017;66(4):1098. Epub 2017/02/12. doi: 10.2337/db17-ec04a. PubMed PMID: 28188141.
134. Sibilina M, Wagner B, Hoebertz A, Elliott C, Marino S, Jochum W, Wagner EF. Mice humanised for the EGF receptor display hypomorphic phenotypes in skin, bone and heart. *Development (Cambridge, England)*. 2003;130(19):4515-25. Epub 2003/08/20. doi: 10.1242/dev.00664. PubMed PMID: 12925580.
135. van Ede KI, van Duursen MB, van den Berg M. Evaluation of relative effect potencies (REPs) for dioxin-like compounds to derive systemic or human-specific TEFs to improve human risk assessment. *Archives of toxicology*. 2016;90(6):1293-305. Epub 2016/05/11. doi: 10.1007/s00204-016-1724-9. PubMed PMID: 27161441; PMCID: PMC4873528.
136. Foulds CE, Trevino LS, York B, Walker CL. Endocrine-disrupting chemicals and fatty liver disease. *Nat Rev Endocrinol*. 2017;13(8):445-57. Epub 2017/05/20. doi: 10.1038/nrendo.2017.42. PubMed PMID: 28524171; PMCID: PMC5657429.
137. Lang AL, Beier JI. Interaction of volatile organic compounds and underlying liver disease: a new paradigm for risk. *Biol Chem*. 2018. Epub 2018/06/21. doi: 10.1515/hsz-2017-0324. PubMed PMID: 29924722.
138. Rantakokko P, Mannisto V, Airaksinen R, Koponen J, Viluksela M, Kiviranta H, Pihlajamaki J. Persistent organic pollutants and non-alcoholic fatty liver disease in morbidly obese patients: a cohort study. *Environmental health : a global access science source*. 2015;14:79. doi: 10.1186/s12940-015-0066-z. PubMed PMID: 26420011; PMCID: 4588245.
139. Wahlang B, Perkins JT, Petriello MC, Hoffman JB, Stromberg AJ, Hennig B. A compromised liver alters polychlorinated biphenyl-mediated toxicity. *Toxicology*. 2017;380:11-22. Epub 2017/02/07. doi: 10.1016/j.tox.2017.02.001. PubMed PMID: 28163111; PMCID: PMC5374277.
140. Hardesty JE, Al-Eryani L, Wahlang B, Falkner KC, Shi H, Jin J, Vivace B, Ceresa BP, Prough RA, Cave MC. Epidermal Growth Factor Receptor Signaling Disruption by Endocrine and Metabolic Disrupting Chemicals. *Toxicological sciences : an official journal of the Society of Toxicology*. 2018. Epub 2018/01/13. doi: 10.1093/toxsci/kfy004. PubMed PMID: 29329451.
141. Souza-Mello V. Peroxisome proliferator-activated receptors as targets to treat non-alcoholic fatty liver disease. *World journal of hepatology*. 2015;7(8):1012-9. Epub 2015/06/09. doi: 10.4254/wjh.v7.i8.1012. PubMed PMID: 26052390; PMCID: PMC4450178.
142. Carr RM, Reid AE. FXR agonists as therapeutic agents for non-alcoholic fatty liver disease. *Current atherosclerosis reports*. 2015;17(4):500. Epub 2015/02/19. doi: 10.1007/s11883-015-0500-2. PubMed PMID: 25690590.
143. Council NR. *Guide for the Care and Use of Laboratory Animals: Eighth Edition*. Washington, DC: The National Academies Press; 2011. 246 p.

144. Wisniewski JR, Zougman A, Nagaraj N, Mann M. Universal sample preparation method for proteome analysis. *Nature methods*. 2009;6(5):359-62. Epub 2009/04/21. doi: 10.1038/nmeth.1322. PubMed PMID: 19377485.
145. Tamasi V, Jeffries JM, Arteel GE, Falkner KC. Ebselen augments its peroxidase activity by inducing nrf-2-dependent transcription. *Archives of biochemistry and biophysics*. 2004;431(2):161-8. Epub 2004/10/19. doi: 10.1016/j.abb.2004.07.030. PubMed PMID: 15488464.
146. Griffith OW. Determination of glutathione and glutathione disulfide using glutathione reductase and 2-vinylpyridine. *Analytical biochemistry*. 1980;106(1):207-12. Epub 1980/07/15. PubMed PMID: 7416462.
147. Dara L, Ji C, Kaplowitz N. The contribution of endoplasmic reticulum stress to liver diseases. *Hepatology (Baltimore, Md)*. 2011;53(5):1752-63. Epub 2011/03/09. doi: 10.1002/hep.24279. PubMed PMID: 21384408; PMCID: PMC3082587.
148. Malhi H, Kaufman RJ. Endoplasmic reticulum stress in liver disease. *Journal of hepatology*. 2011;54(4):795-809. Epub 2010/12/15. doi: 10.1016/j.jhep.2010.11.005. PubMed PMID: 21145844; PMCID: PMC3375108.
149. Tsuchida T, Friedman SL. Mechanisms of hepatic stellate cell activation. *Nature reviews Gastroenterology & hepatology*. 2017;14(7):397-411. Epub 2017/05/11. doi: 10.1038/nrgastro.2017.38. PubMed PMID: 28487545.
150. Cave MC, Clair HB, Hardesty JE, Falkner KC, Feng W, Clark BJ, Sidey J, Shi H, Aqel BA, McClain CJ, Prough RA. Nuclear receptors and nonalcoholic fatty liver disease. *Biochimica et biophysica acta*. 2016. Epub 2016/03/11. doi: 10.1016/j.bbagr.2016.03.002. PubMed PMID: 26962021.
151. Garcia-Ruiz I, Solis-Munoz P, Fernandez-Moreira D, Grau M, Colina F, Munoz-Yague T, Solis-Herruzo JA. High-fat diet decreases activity of the oxidative phosphorylation complexes and causes nonalcoholic steatohepatitis in mice. *Dis Model Mech*. 2014;7(11):1287-96. Epub 2014/09/28. doi: 10.1242/dmm.016766. PubMed PMID: 25261569; PMCID: PMC4213732.
152. Gunewardena S, Walesky C, Apte U. Global Gene Expression Changes in Liver Following Hepatocyte Nuclear Factor 4 alpha deletion in Adult Mice. *Genomics data*. 2015;5:126-8. Epub 2015/06/30. doi: 10.1016/j.gdata.2015.05.037. PubMed PMID: 26120557; PMCID: PMC4477707.
153. Nishikawa T, Bell A, Brooks JM, Setoyama K, Melis M, Han B, Fukumitsu K, Handa K, Tian J, Kaestner KH, Vodovotz Y, Locker J, Soto-Gutierrez A, Fox IJ. Resetting the transcription factor network reverses terminal chronic hepatic failure. *The Journal of clinical investigation*. 2015;125(4):1533-44. Epub 2015/03/17. doi: 10.1172/jci73137. PubMed PMID: 25774505; PMCID: PMC4396487.
154. Baciuc C, Pasini E, Angeli M, Schwenger K, Afrin J, Humar A, Fischer S, Patel K, Allard J, Bhat M. Systematic integrative analysis of gene expression identifies HNF4A as the central gene in pathogenesis of non-alcoholic steatohepatitis. *PLoS one*. 2017;12(12):e0189223. Epub 2017/12/08. doi: 10.1371/journal.pone.0189223. PubMed PMID: 29216278; PMCID: PMC5720788.
155. Kitade M, Factor VM, Andersen JB, Tomokuni A, Kaji K, Akita H, Holczbauer A, Seo D, Marquardt JU, Conner EA, Lee SB, Lee YH, Thorgeirsson SS. Specific fate decisions in adult hepatic progenitor cells driven by MET and EGFR signaling. *Genes & development*. 2013;27(15):1706-17. Epub 2013/08/06. doi: 10.1101/gad.214601.113. PubMed PMID: 23913923; PMCID: PMC3744728.
156. Shi X, Wahlang B, Wei XL, Yin XM, Falkner KC, Prough RA, Kim SH, Mueller EG, McClain CJ, Cave M, Zhang X. Metabolomic Analysis of the Effects of Polychlorinated Biphenyls in Nonalcoholic Fatty Liver Disease. *Journal of proteome research*. 2012;11(7):3805-15. doi: 10.1021/pr300297z. PubMed PMID: WOS:000306049800025.
157. Fernandes RS, Cotter TG. Apoptosis or necrosis: intracellular levels of glutathione influence mode of cell death. *Biochemical pharmacology*. 1994;48(4):675-81. Epub 1994/08/17. PubMed PMID: 8080440.
158. Rongo C. Epidermal growth factor and aging: a signaling molecule reveals a new eye opening function. *Aging*. 2011;3(9):896-905. Epub 2011/09/21. doi: 10.18632/aging.100384. PubMed PMID: 21931179; PMCID: PMC3227454.

159. Wang X, Tang X, Gong X, Albanis E, Friedman SL, Mao Z. Regulation of hepatic stellate cell activation and growth by transcription factor myocyte enhancer factor 2. *Gastroenterology*. 2004;127(4):1174-88. Epub 2004/10/14. PubMed PMID: 15480995.
160. Diagnosis and classification of diabetes mellitus. *Diabetes Care*. 2009;32 Suppl 1:S62-7. Epub 2009/01/06. doi: 10.2337/dc09-S062. PubMed PMID: 19118289; PMCID: PMC2613584.
161. Murray RD, Merchant ML, Hardin E, Clark B, Khundmiri SJ, Lederer ED. Identification of an RNA-binding protein that is phosphorylated by PTH and potentially mediates PTH-induced destabilization of Npt2a mRNA. *American journal of physiology Cell physiology*. 2016;310(3):C205-15. Epub 2016/02/03. doi: 10.1152/ajpcell.00192.2015. PubMed PMID: 26834145.
162. Zhivotosky B, Orrenius S. Assessment of apoptosis and necrosis by DNA fragmentation and morphological criteria. *Current protocols in cell biology*. 2001;Chapter 18:Unit 18.3. Epub 2008/01/30. doi: 10.1002/0471143030.cb1803s12. PubMed PMID: 18228342.
163. Graham KC, Litchfield DW. The regulatory beta subunit of protein kinase CK2 mediates formation of tetrameric CK2 complexes. *The Journal of biological chemistry*. 2000;275(7):5003-10. Epub 2000/02/15. PubMed PMID: 10671540.
164. Sarno S, Ghisellini P, Pinna LA. Unique activation mechanism of protein kinase CK2. The N-terminal segment is essential for constitutive activity of the catalytic subunit but not of the holoenzyme. *The Journal of biological chemistry*. 2002;277(25):22509-14. Epub 2002/04/17. doi: 10.1074/jbc.M200486200. PubMed PMID: 11956194.
165. Lockman KA, Htun V, Sinha R, Treskes P, Nelson LJ, Martin SF, Rogers SM, Le Bihan T, Hayes PC, Plevris JN. Proteomic profiling of cellular steatosis with concomitant oxidative stress in vitro. *Lipids in health and disease*. 2016;15:114. Epub 2016/07/03. doi: 10.1186/s12944-016-0283-7. PubMed PMID: 27368608; PMCID: PMC4930558.
166. Wahlang B, Falkner KC, Gregory B, Ansert D, Young D, Conklin DJ, Bhatnagar A, McClain CJ, Cave M. Polychlorinated biphenyl 153 is a diet-dependent obesogen that worsens nonalcoholic fatty liver disease in male C57BL6/J mice. *The Journal of nutritional biochemistry*. 2013;24(9):1587-95. doi: 10.1016/j.jnutbio.2013.01.009. PubMed PMID: 23618531; PMCID: 3743953.
167. Kurokawa M, Kornbluth S. Caspases and kinases in a death grip. *Cell*. 2009;138(5):838-54. Epub 2009/09/10. doi: 10.1016/j.cell.2009.08.021. PubMed PMID: 19737514; PMCID: PMC3390419.
168. Turowec JP, Vilk G, Gabriel M, Litchfield DW. Characterizing the convergence of protein kinase CK2 and caspase-3 reveals isoform-specific phosphorylation of caspase-3 by CK2alpha': implications for pathological roles of CK2 in promoting cancer cell survival. *Oncotarget*. 2013;4(4):560-71. Epub 2013/04/20. doi: 10.18632/oncotarget.948. PubMed PMID: 23599180; PMCID: PMC3720604.
169. Nomoto K, Nishida T, Nakanishi Y, Fujimoto M, Takasaki I, Tabuchi Y, Tsuneyama K. Deficiency in galectin-3 promotes hepatic injury in CDAA diet-induced nonalcoholic fatty liver disease. *TheScientificWorldJournal*. 2012;2012:959824. Epub 2012/05/18. doi: 10.1100/2012/959824. PubMed PMID: 22593713; PMCID: PMC3349166.
170. Wilson CH, Kumar S. Caspases in metabolic disease and their therapeutic potential. *Cell death and differentiation*. 2018;25(6):1010-24. Epub 2018/05/11. doi: 10.1038/s41418-018-0111-x. PubMed PMID: 29743560; PMCID: PMC5988802.
171. Strzyz P. Cell death: Pulling the apoptotic trigger for necrosis. *Nature reviews Molecular cell biology*. 2017;18(2):72. Epub 2017/01/12. doi: 10.1038/nrm.2017.1. PubMed PMID: 28074061.
172. Bligh EG, Dyer WJ. A rapid method of total lipid extraction and purification. *Canadian journal of biochemistry and physiology*. 1959;37(8):911-7. Epub 1959/08/01. doi: 10.1139/o59-099. PubMed PMID: 13671378.
173. Zimmers TA, Jin X, Zhang Z, Jiang Y, Koniaris LG. Epidermal growth factor receptor restoration rescues the fatty liver regeneration in mice. *American journal of physiology Endocrinology and metabolism*. 2017;313(4):E440-e9. Epub 2017/06/29. doi: 10.1152/ajpendo.00032.2017. PubMed PMID: 28655714; PMCID: PMC5668597.
174. Jung UJ, Choi MS. Obesity and its metabolic complications: the role of adipokines and the relationship between obesity, inflammation, insulin resistance, dyslipidemia and nonalcoholic fatty liver disease. *International journal of molecular sciences*. 2014;15(4):6184-223. Epub 2014/04/16. doi: 10.3390/ijms15046184. PubMed PMID: 24733068; PMCID: PMC4013623.

175. Rashed SM, Patel TB. Regulation of hepatic energy metabolism by epidermal growth factor. *European journal of biochemistry*. 1991;197(3):805-13. Epub 1991/05/08. PubMed PMID: 1903108.

176. Combs TP, Marliss EB. Adiponectin signaling in the liver. *Reviews in endocrine & metabolic disorders*. 2014;15(2):137-47. Epub 2013/12/04. doi: 10.1007/s11154-013-9280-6. PubMed PMID: 24297186; PMCID: PMC4152934.



## APPENDIX I

### SUPPLEMENTAL MATERIALS FOR CHAPTER 3

Hardesty JE, Al-Eryani L, Wahlang B, Falkner KC, Shi H, Jin J, Vivace B, Ceresa BP, Prough RA, Cave MC. Epidermal Growth Factor Receptor Signaling Disruption by Endocrine and Metabolic Disrupting Chemicals. *Toxicological sciences : an official journal of the Society of Toxicology*. 2018. Epub 2018/01/13. doi: 10.1093/toxsci/kfy004. PubMed PMID: 29329451.

### MATERIALS AND METHODS

#### **EGF Endocytosis Assay in A-431 Cells:**

This assay was modified from previously described methods (114). A-431 cells were used as they express  $2.6 \times 10^6$  epidermal growth factor receptors per cell (115). Alexa Fluor 555 labeled EGF was purchased from Thermo Scientific, (Philadelphia, PA) and was used at 20 ng/100 $\mu$ L. This concentration was used as it was previously shown to give robust signal in the Cellomics assay (114). After a 3-hour serum starvation A-431 cells were exposed to varying concentrations of the compounds ( $10^{-12}$  -  $10^{-3}$ M) for 10 minutes. Positive control cells were treated with 0.1% DMSO and negative control cells were treated with 20 ng/100  $\mu$ L of unlabeled EGF purchased from Millipore (Norwood, OH). This served as a negative control since the EGF receptors would be saturated and endocytosed preventing fluorescently labeled EGF from binding thus preventing any signal. Cells were then treated with 20 ng/100  $\mu$ L of Alexa Fluor 555 labeled EGF for 30 minutes. This was followed by 3 washes with pre-warmed PBS and incubation with 3.7% formaldehyde for 15 minutes. Cell nuclei were then stained with Hoechst 33342 purchased from Thermo Scientific (Philadelphia, PA) at 1  $\mu$ g/100  $\mu$ L for 15 minutes. Images and data were obtained *via* an ArrayScan HCS 4.0 Reader. Filter sets specific for Hoechst labeled nuclei and the Alexa Fluor 555-EGF were used for detection. A 20X microscope objective was used for imaging and the SpotDetector bioapplication

was used to acquire and analyze images. Approximately 500 cells from randomized fields were analyzed for each well. The equation used to normalize 555-EGF count/nuclei values is listed below.

$$\text{Alexa Fluor 555 EGF Endocytosis} = \left(1 - \frac{\text{Exp-DMSO}}{\text{EGF-DMSO}}\right) * 100$$

This assay was also conducted with 1pM of *trans*-nonachlor, PCB-126, PCB-153 and 0.041 pg/100  $\mu$ L of chlordane, and 100pM of atrazine either in 10% serum containing media as compared to 0% serum media (Fig S2).

#### **MTT Assay:**

A-431 and HepG2 cells were cultured in 96-well plates as previously described. Cells were exposed to either 0.1% DMSO (vehicle control) or the following compounds *trans*-nonachlor, chlordane, atrazine, PCB-126, PCB-153, dieldrin, alachlor, lindane, DDE, or DDT at the following concentrations 100 nM, 1  $\mu$ M, 10  $\mu$ M, 100  $\mu$ M, or 1 mM. for 24 hours. Cells were then incubated with MTT (0.2 mg/mL) for 3-4 hours. The formazan dye was then released by incubation with DMSO and absorbance measured at 540 nm spectrophotometrically by the Bio-Tek Synergy HT Multi-mode micro plate reader (Winooski, VT).

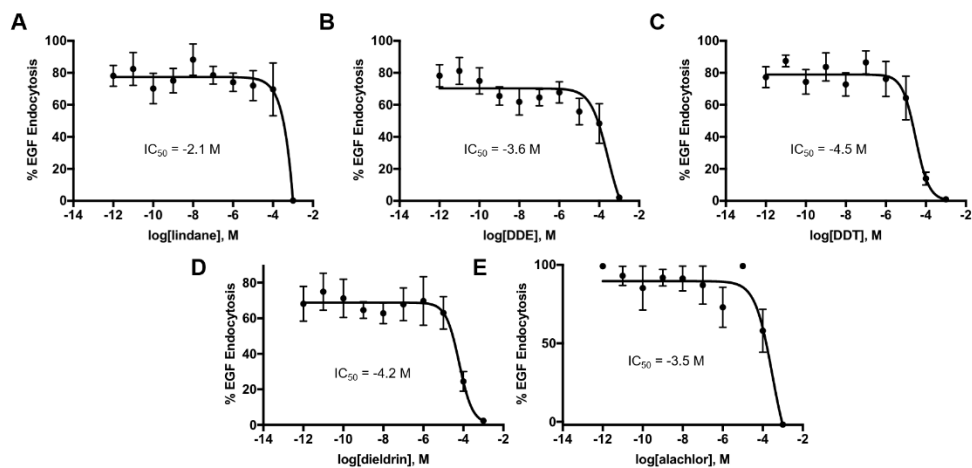


**Figure 35. Lindane, Dieldrin, DDT, DDE, Alachlor are not potent EGFR antagonists: A.** Lindane ( $\log IC_{50} = -2.1 \pm 0.48$ ), **B.** dieldrin ( $\log IC_{50} = -4.2 \pm 0.2$ ), **C.** DDT ( $\log IC_{50} = -4.5 \pm 0.16$ ), **D.** DDE ( $\log IC_{50} = -3.6 \pm 0.26$ ), and **E.** alachlor ( $\log IC_{50} = -3.5 \pm 0.27$ ) could not prevent fluorescent EGF endocytosis until the micromolar range. These were least potent compounds tested and were not potent EGFR antagonists. Curves were fitted with a sigmoidal dose response equation with GraphPad Prism 7 software. An  $n=8$  was used for each concentration and mean  $\pm$  SEM were calculated using the equation described in methods.

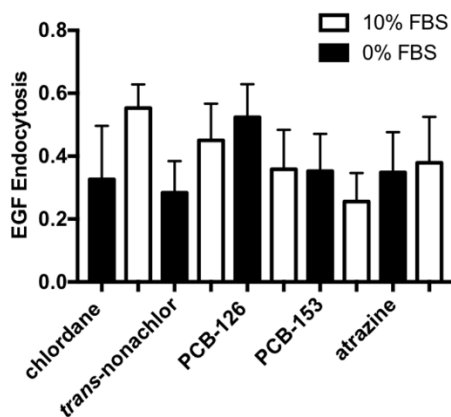


**Figure 36. Pre-clearing compounds in 10% serum media does not alter EGF endocytosis in A-431 cells:** When incubating either chlordane, *trans*-nonachlor, PCB-126, PCB-153, or atrazine at 1 pM with 10% serum containing media or 0% serum there is no effect on 555-EGF endocytosis. An n=8 was used and the data are presented as mean  $\pm$  SEM. A two-tailed unpaired t-test was used to statistically compare the 10% serum vs. the 0% serum values for the select compounds. A  $P^* < .05$  was considered significant.

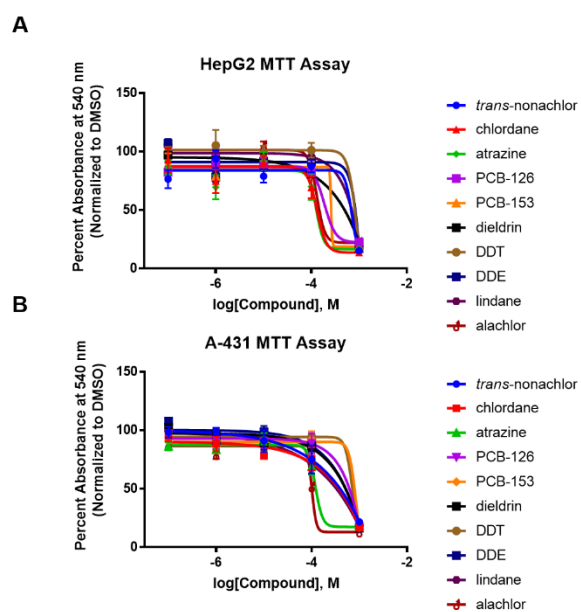


**Figure 37. Cytotoxicity of *trans*-nonachlor, chlordane, atrazine, PCB-126, PCB-153, dieldrin, alachlor, lindane, DDE, and DDT in HepG2 and A-431 cells:** In **A** HepG2 and **B** A-431 cells the screening library compounds do not demonstrate overt cytotoxicity until the 100  $\mu$ M to 1 mM concentration range. An n=4 was used and the data are represented as mean  $\pm$  SEM. Experimental absorbance values were normalized to a 0.1% DMSO control.

## APPENDIX II

### License User Agreement

#### Xenobiotica

All articles published by Taylor & Francis / Routledge under the Creative Commons Attribution-Non-Commercial License <http://creativecommons.org/licenses/by-nc/3.0/> on an open-access basis are licensed by the respective authors of such articles for use and distribution by you, on a non-commercial basis, subject to citation of the original source in accordance with the terms of the license under which the work was published (please check the license statement for the relevant article(s)). No permission is required from the authors or publishers for non-commercial reuse. Requests for commercial reuse should be directed to the rightsholder. Appropriate attribution can be provided by citing the original article, for example, "The Version of Scholarly Record of this Article is published in (JOURNAL TITLE) (year of publication), available online at: <http://www.tandfonline.com/> (Article DOI)." For any reuse or redistribution of an article, users must also make clear the license terms under which the article was published and retain all copyright notices and disclaimers. This permission does not cover any third-party copyrighted material which may appear in the work requested.

#### Reference:

Polychlorinated Biphenyls Disrupt Hepatic Epidermal Growth Factor Receptor Signaling. *Xenobiotica; the fate of foreign compounds in biological systems*. 2016:1-40. Epub 2016/07/28. doi: 10.1080/00498254.2016.1217572. PubMed PMID: 27458090

#### Toxicological Sciences

This is the most permissive of the Creative Commons licenses and allows for maximum dissemination and use of the licensed work. The license permits others to use, reproduce, disseminate or display the article in any way, including for commercial purposes, so long as they credit the author for the original creation.

The majority of our journals offer this license to authors. A small number of our journals charge a higher open access publication charge for use of CC-BY compared to the prices for publication under the other Creative Commons licenses. Please visit the 'Instructions to Authors' page of an individual journal to find out license prices.

The CC-BY license is mandated by the RCUK and Wellcome Trust Policies on Open Access – [click here](#) for more information.

Reference:

Hardesty JE, Al-Eryani L, Wahlang B, Falkner KC, Shi H, Jin J, Vivace B, Ceresa BP, Prough RA, Cave MC. Epidermal Growth Factor Receptor Signaling Disruption by Endocrine and Metabolic Disrupting Chemicals. *Toxicological sciences : an official journal of the Society of Toxicology*. 2018. Epub 2018/01/13. doi: 10.1093/toxsci/kfy004. PubMed PMID: 29329451.

## CURRICULUM VITAE

Josiah Hardesty (Hardesty JE)

(Home) Apt 201 3707 Terrace Hill Dr. Louisville, KY 40245

(Work) 505 S. Hancock St. Rm. 542D, Louisville, KY 40202

josiah.hardesty@louisville.edu

### Education

---

08/2009 - 05/2013	B.S. in Biology (Cum Laude), University of Kentucky, Lexington, KY
08/2014 – 06/2016	M.S. in Biochemistry and Molecular Genetics, University of Louisville, Louisville, KY
08/2014-08/2018	Ph.D. in Biochemistry and Molecular Genetics, University of Louisville, Louisville, KY

### Academic Appointments

---

08/2014 – 08/2018	Graduate Research Assistant Department of Biochemistry and Molecular Genetics University of Louisville Louisville, KY
-------------------	--

### Professional Memberships and Activities

---

2015 – Present	Member of Ohio Valley Society of Toxicology (OVSOT)
2015 – Present	Member of Society of Toxicology (SOT)
2015 – Present	Member of American Association for the Study of Liver Diseases (AASLD)
08/2016- 09/2017	Student President and Ambassador Department of Biochemistry and Molecular Genetics University of Louisville Louisville, KY



10/2014 – Present      Science Policy and Outreach Group (SPOG)  
University of Louisville  
Louisville, KY

### **Honors and Awards**

---

08/2014 – 08/2016      IPIBS Fellowship  
University of Louisville  
Louisville, KY

09/2016                  NIEHS Student Travel Award

05/2017                  DDW Abstract of Distinction

07/2017 – Present      NIH NIEHS 1F31ES028982  
University of Louisville  
Louisville, KY

### **Committee Assignments and Administrative Services**

---

10/2014 – 11/2015      Seminar Event Planning Committee Member  
Department of Biochemistry and Molecular Genetics  
University of Louisville  
Louisville, KY

05/2017                  Organizer of The Bloch Lecture Presented by Dr. Phillip A. Sharp  
Department of Biochemistry and Molecular Genetics  
University of Louisville  
Louisville, KY

08/2016 – 09/2017      Member of the Graduate Executive Council  
Department of Biochemistry and Molecular Genetics  
University of Louisville  
Louisville, KY

## **Educational Activities**

---

08/2015 -12/2015	Teaching Assistant for Biochemistry I Department of Biochemistry and Molecular Genetics University of Louisville Louisville, KY
05/2015 – Present	Trained Rotating Medical Students University of Louisville School of Medicine Louisville, KY
06/2017 – 08/2017	Organizer of Student Journal Club Department of Biochemistry and Molecular Genetics University of Louisville Louisville, KY
01/2018 – 05/2018	Teaching Assistant for Dental Biochemistry Department of Biochemistry and Molecular Genetics University of Louisville Louisville, KY

## **Grants and Contracts**

---

05/2012 – 02/2017	NIH/NIEHS   R01ES021375   \$337,500 PCBs worsen obesity/metabolic syndrome through toxic metabolic endotoxemia PI Dr. Matt Cave
07/2017 – 07/2020	NIH NIEHS   1F31ES028982   \$30,496 PCBs exacerbates NAFLD through inhibition of EGFR PI Josiah Hardesty

## Abstracts and Presentations

---

### Posters

#### Local/Regional Meetings

1. "PCBs Decrease Hepatic Epidermal Growth Factor Signaling in NASH"

**Hardesty JE**, Wahlang B, Clair HB, Falkner KC, Clark BJ, Ceresa BP, Prough RA, Cave MC.

Ohio Valley Society of Toxicology (OVSOT) Summer Meeting

Cincinnati, OH | 06/2015

2. "Aroclor 1260 and Dietary Alterations in the Hepatic Proteome Contribute to Steatohepatitis"

**Hardesty JE**, Wahlang B, Clair HB, Shi H, Jian J, Wilkey D, Falkner KC, Merchant M, Prough RA, Cave MC.

Ohio Valley Society of Toxicology (OVSOT) Summer Meeting

Cincinnati, OH | 06/2016

3. "Aroclor 1260 and Dietary Alterations in the Hepatic Proteome Contribute to Steatohepatitis"

**Hardesty JE**, Wahlang B, Clair HB, Shi H, Jian J, Wilkey D, Falkner KC, Merchant M, Prough RA, Cave MC.

Ohio Valley Society of Toxicology (OVSOT)

Indianapolis, IN | 10/2016

4. "PCBs and a HFD Alter the Hepatic Phosphoproteome in NASH"

**Hardesty JE**, Wahlang B, Shi H, Jian J, Clair HB, Wilkey D, Falkner KC, Watson C, Merchant M, Prough RA, Cave MC

Ohio Valley Society of Toxicology (OVSOT)

West Lafayette, IN | 12/2017

5. "PCBs Decrease Hepatic Epidermal Growth Factor Signaling in NASH"

**Hardesty JE**, Wahlang B, Clair HB, Falkner KC, Clark BJ, Ceresa BP, Prough RA, Cave MC.

Research Louisville!

Louisville, KY | 09/2015

6. "Aroclor 1260 and Dietary Alterations in the Hepatic Proteome Contribute to Steatohepatitis"

**Hardesty JE**, Wahlang B, Clair HB, Shi H, Jian J, Wilkey D, Falkner KC, Merchant M, Prough

RA, Cave MC.

Research Louisville!

Louisville, KY | 09/2016

7. "PCBs and a HFD Alter the Hepatic Phosphoproteome in NASH"

**Hardesty JE**, Wahlang B, Shi H, Jian J, Clair HB, Wilkey D, Falkner KC, Watson C, Merchant M,  
Prough RA, Cave MC

Research Louisville!

Louisville, KY | 09/2017

### **National Meetings**

8. "Organopollutant Exposures Further Decrease Epidermal Growth Factor Signaling in Non  
-Alcoholic Steatohepatitis and Alter Hepatic Energy Metabolism"

**Hardesty JE**, Wahlang B, Clair HB, Falkner KC, Clark BJ, Ceresa BP, Prough RA, Cave MC.

American Association for the Study of Liver Disease (AASLD)

San Francisco, CA | 10/2015

9. "Aroclor 1260 and Dietary Alterations in the Hepatic Proteome Contribute to Steatohepatitis"

**Hardesty JE**, Wahlang B, Clair HB, Shi H, Jian J, Wilkey D, Falkner KC, Merchant M, Prough  
RA, Cave MC.

American Association for the Study of Liver Disease (AASLD)

Boston, MA | 10/2016

10. "PCBs and a HFD Alter the Hepatic Phosphoproteome in NASH"

**Hardesty JE**, Wahlang B, Shi H, Jian J, Clair HB, Wilkey D, Falkner KC, Watson C, Merchant M,  
Prough RA, Cave MC

American Association for the Study of Liver Disease (AASLD)

Washington D.C. | 10/2017

11. "Diverse Chemicals Act Through EGFR Inhibition"

**Hardesty JE**, Al-Eryani L, Wahlang B, Shi H, Jian J, Falkner KC, Ceresa BP, Prough RA, Cave MC

American Association for the Study of Liver Disease (AASLD)

Washington D.C. | 10/2017

12. "PCB Exposures Further Decrease Epidermal Growth Factor Signaling in Non-Alcoholic Steatohepatitis and Alter Hepatic Energy Metabolism"

**Hardesty JE**, Wahlang B, Clair HB, Falkner KC, Clark BJ, Ceresa BP, Prough RA, Cave MC.

Society of Toxicology (SOT)

New Orleans, LA | 03/2016

13. "PCB Exposure and Dietary Alterations in the Hepatic Proteome Contribute to Steatohepatitis"

**Hardesty JE**, Wahlang B, Clair HB, Shi H, Jian J, Wilkey D, Falkner KC, Merchant M, Prough RA, Cave MC.

Society of Toxicology (SOT)

Baltimore, MD | 03/2017

14. "Aroclor 1260 and Dietary Alterations in the Hepatic Proteome Contribute to Steatohepatitis"

**Hardesty JE**, Wahlang B, Clair HB, Shi H, Jian J, Wilkey D, Falkner KC, Merchant M, Prough RA, Cave MC.

NIEHS 25 Years of Endocrine Disruption Research

Bethesda, MD | 09/2016

15. "Aroclor 1260 and Dietary Alterations in the Hepatic Proteome Contribute to Steatohepatitis"

**Hardesty JE**, Wahlang B, Clair HB, Shi H, Jian J, Wilkey D, Falkner KC, Merchant M, Prough RA, Cave MC.

Digestive Disease Week (DDW)

Chicago, IL | 05/2017

## Oral Presentations

### International Meeting

16. "PCB 126 Prevents EGF Endocytosis, Phosphorylation, and Signaling"

**Hardesty JE**, Al-Eryani L, Wahlang B, Shi H, Jian J, Falkner KC, Ceresa BP, Prough RA, Cave MC

Dioxin Meeting

Vancouver, Canada | 08/2017

### Publications

---

1. Wahlang, B, Prough, RA, Falkner, KC, **Hardesty, JE**, Song, M, Clair, HB, Clark, BJ, States, JC, Arteel, GA and Cave, MC (2015) Polychlorinated biphenyl-xenobiotic nuclear receptor interactions regulate energy metabolism, behavior and inflammation in nonalcoholic-steatohepatitis, *Toxicological Sciences*. PMID: 26612838 PMCID: PMC4751229
2. Clair, HB, **Hardesty, JE**, Prough, RA, Falkner, KC Sidey, JM, Feng, W, Clark, BJ, McClain, CJ, Aqelf, BA and Cave, MC (2016) Nuclear Receptors and Nonalcoholic Fatty Liver Disease, *BBAGRM* (2015). PMID: 26962021 PMCID: PMC5149456
3. **Hardesty, JE**, Wahlang, B, Falkner, KC, Clair, HB, Clark, BJ, Ceresa, BP, Prough, RA, Cave, MC (2016) Polychlorinated biphenyls diminish Hepatic EGFR signaling *Xenobiotica* (2017). PMID: 27458090 PMCID: PMC5512701
4. **Hardesty JE**, Al-Eryani L, Wahlang B, Falkner KC, Shi H, Jin J, Vivace BJ, Ceresa BP, Prough RA, Cave MC. Epidermal Growth Factor Receptor Signaling Disruption by Endocrine and Metabolic Disrupting Chemicals. *Toxicol Sci*. 2018;162(2):622-34. Epub 2018/01/13. doi: 10.1093/toxsci/kfy004. PubMed PMID: 29329451; PMCID: PMC5888991.